Effects of Model Scales and Vegetations on Urban Hydrological Modeling

The effects of model scales and vegetation on urban hydrological modeling

A Dissertation Presented

by

Qing Chang

to

The Department of Civil and Environmental Engineering

in partial fulfillment of the requirements for the degree

of

Doctor of Philosophy

in the field of

Civil & Environmental Engineering

Tohoku University

Sendai, Japan

Committees

_____

Professor So Kazama

(Principle advisor)

_____

Professor Hitoshi Tanaka

(Examination committee member)

_____

Associate Professor Makoto Umeda

(Examination committee member)

_____

Associate Professor Daisuke Komori

(Examination committee member)

Abstract

Urban vegetation plays an important role in both ecological systems and hydrological circles. Selecting a proper spatial resolution for urban hydrological processes modeling was not a trivial issue because it could affect the model outputs. Recently, the development of remote sensing technology and increasingly available data source had enabled rainfall runoff process to be modeled at detailed and micro scales.

This study attempted to explore the impact of model scales on model performance as well as the effects of urban vegetation. A small urban catchment in Japan was used as the study site. Models with different discretization degree were built up on the basis of actual drainage networks, urban parcels and specific land use. Remotely sensed data were obtained and used for a distributed representation of vegetation growth information by converting to canopy storage abilities. The effects of the interception process modeling and the flood reduction of green infrastructures (GIs) were considered. The SWMM model and the Rutter model are coupled to simulate the urban vegetation interception process and the flow routing process.

The results showed that there was very little difference in the total runoff volumes while peak flows showed an obvious scale effects which could be up to 30%. Generally, model calibration could compensate the scale effect. The calibrated models with different resolution showed similar performances. The consideration of EIA (effective impervious area) as a calibration parameter marginally increased performance of calibration period but also slightly decreased performance in

validation period which indicated the importance of detailed EIA identification. The seasonal effect of the interception is very obvious. The seasonal difference in the interception ratio was as great as 12%. The rainfall characteristics also have a great influence on the interception. For tree species, deciduous trees have a higher annual interception ratio (16.62%), while the interception effect of evergreen trees is more stable with seasonal changes. The results of each GI indicate that the green roof has a relatively good flood-reduction effect (19% runoff reduction). The combination of green roof and urban canopy is a more effective response to flood reduction.

Key words: urban hydrology; modeling scale; hydrological process; interception; urban vegetation.

Acknowledgements

Time is running out, and I am about to enter a new era. My doctoral career, which is a little long and tortuous, is coming to an end. I chose to come to Tohoku University to continue my studies after graduating from master studies, and chose to pursue this path directly to realize my ideals and pursuits. I spent three and half years of my life at Tohoku University, and I also showed my youth and enthusiasm in this period. Along the way, there are too many things to say, and too many people to thank. Teachers, classmates, relatives and friends, it is your help and care in all aspects that have allowed me to stick along. With your companionship, my schooling career is becoming more colorful.

I am grateful for everything that I have received throughout these years and this is a great opportunity for me to thank everyone who made this thesis possible. I would like to express my deep and sincere gratitude to my supervisor Professor So KAZAMA for mentoring me in the area of urban hydrology. For these years, Prof. KAZAMA has given careful guidance in the studies and strict requirements in the work. He has given me meticulous care in life and provided me with a good and relaxed learning and working environment. For me, Prof. KAZAMA is not only an academic mentor, but also an elder in life. His extensive professional knowledge, rigorous academic attitude, selfless work spirit, and integrity in life style have benefited me a lot in my PhD career, and these wealth will certainly benefit me for life. I would also like to thank Professor Hitoshi TANAKA, Professor Daisuke KOMORI and Professor Makoto UMEDA for serving on my committee, and for their insightful questions and advice on my research. I gratefully acknowledge the China Scholarship Council for providing me the financial support

during my PhD studies.

I would like to express my sincere thanks to Dr. Yoshiya TOUGE and Mr. Shunsuke AITA. Their help are essential for the field measurements include the flow and LAI and thus make my PHD work possible. I am grateful for Dr. Nurul Fajar for his help of data processing in AcrGIS and for Ms. Grace Puyang Emang for her help to obtain the remote sensed data.

The time I spent at Tohoku University was especially enjoyable and unforgettable because of the many friends and colleagues. I would like to thank Mr. Henian BAO, Dr. Salem, Dr. Prem, Mr. Bou, Ms Uchida, Ms. Jaque and all other fellow graduate students in the Civil and Environmental Engineering department for the wonderful time that I spent with them.

Finally, I also want to thank dear parents. They unconditionally support any decision I make along the way, give me all you can love, and took most of the family responsibilities for me and what I could return was minimal. Thanks to all my family, you have made me realize the most important part of life. Learn to be content, tolerant, and keep an enterprising man in this difficult journey.

Qing Chang

Tohoku University

November 2019

Contents

List of figures

List of tables

List of symbols

UHE	Urban hydrological elements
EIA	Effective impervious area
TIA	Total impervious area
NDVI	Normalized difference vegetation index
LAI	Leaf area index
NIR	spectral reflectance measurements acquired in the near-infrared band
RED	spectral reflectance measurements acquired in the red band
V_{sub}	volume of water on the subcatchment (m^3)
t_c	computational time step (sec)
A_{sub}	area of the subcatchment (m^2)
i_e	effective inflow on sub-catchment area (m/sec)
Q_{sub}	outflow on subcatchment area (m/sec)
W_{sub}	subcatchment width (m)
k	conversion constant equal to 1.486 for U.S. metric units or 1.0 for SI units
n	Manning's roughness coefficient ($s/m^{1/3}$)
d_s	surface depression storage (m)
d	the depth of ponded water at the surface (m)
S_{sub}	subcatchment slope
x1	pipe distance (m)
t1	time elapsed (sec)
Ac	flow cross section area (m^2/s)
Qc	flow rate (m^3/s)
H_h	hydraulic head of water in the conduit (m)
fp	infiltration capacity into soil (m/hr)
Ks	saturated hydraulic conductivity (m/hr)
Ψs	suction head along the wetting front (m)
Ls	depth of the saturated layer below the surface (m)
R_p	mean rainfall rate (m/hr)
p_f	free throughfall coefficient
pt	stemflow coefficient
S_c	maximum canopy storage capacity (m)
S_t	trunk storage capacity (m)
t_r	rainfall duration time (hr)
C	actual canopy storage (m)
E_P	potential evapotranspiration (m/hr)
E_C	evaporation from the canopy (m/hr)
Et	evaporation from the trunk (m/hr)
ϵ	describes the evaporation from the trunk as a proportion of the evaporation from the saturated canopy
D_C	rate of water dripping from the canopy
D_S	rate of water dripping from the canopy when the canopy storage capacity has

	been reached
b_e	an empirical drainage parameter
I	interception
R_n	net radiation (W/m2)
G	soil heat flux density (W/m2)
T_C	air temperature (°C)
$u2$	wind speed at 2 m height (m/s)
e_s	saturation vapor pressure (Pa)
e_a	actual vapor pressure (Pa)
Hu	relative humidity (%)
c	psychometric constant
r	albedo of the surface (dimensionless)
$S\downarrow$	solar radiation incident on the surface (W/m2)
$L\downarrow$	longwave radiation incident on the surface (W/m2)
$L\uparrow$	longwave radiation emitted by the surface (W/m2)
H	sensible heat flux from thesurface (W/m2),
λE	latent heat flux from the surface (W/m2)
G_H	heat conducted away from the surface (W/m2).

Chapter 1. Introduction

1.1 Background

Urban hydrology is defined as the interdisciplinary science of water and its interrelationships within an urban watershed. An urban or urbanizing watershed may be defined as one in which impervious surfaces (e.g., roads, parking lots, buildings, etc.) cover or will soon cover a considerable area of the watershed, and where natural flow paths have been substituted by paved gutters, sewers, or other elements of artificial drainage. Consequently the land cover, the geomorphology characteristics and thus the hydrological processes in urbanized area were quite different and more complex compared with that in natural state. Due to the intense alteration of natural environmental processes by human activity, the watershed response to precipitation are also significantly altered (e.g. reduced infiltration, decreased travel time, higher runoff, etc.). Urban hydrology involves numerous interacting processes subsystems such as surface runoff, infiltration, conduit routing, groundwater discharge to receiving water, etc. (Salvadore et al., 2015).

In the past decades, driven by developments in computer capability and the availability of remote sensing data, the use of distributed hydrological models are becoming more and more a common practice. Hydrological modelling of urban catchments is highly challenging as urban catchments are strongly heterogeneous and have very specific hydrological processes. ‘The circulation of rainwater within urban areas has not yet been described in a detailed manner, as studies on this topic often remain limited to the runoff on impervious surfaces (Rodriguez et al., 2008). Developments in this direction

generally focus either on very specialized tools for a particular aspect of the urban hydrological cycle, or on generic software that combines and/or integrates several semi-specialized components to describe the total water cycle in urban areas. Bach et al. (2014) recognized the importance of integration in modelling the urban water system and proposed to classify models based on their degree of integration. However there is still insufficient agreement so far on a universal concept or methodology for simulating the urban water cycle at the catchment scale.

The fast urbanization processes had also impacted the local urban water systems. Several researches had reported that urbanization is considered to be the one major cause of pollution of water resources (Cronin et al., 2003). On the other hand, a more popular problem is the frequent flooding events which had increased the management costs. Urban areas have shown to be among the most vulnerable systems to the adverse impact of heavy rainfalls. Floods are becoming more frequent and more devastating than ever before as urban areas are enlarging and becoming denser (Schmitt et al., 2004; Chen et al., 2009). Society suffers yearly from the consequences of (flash) floods, with mortality nearly homogeneous over different continents (Jonkman and Vrijling, 2008).

Urban forests or urban vegetation is a kind of important urban infrastructure that has many environmental benefits. Vegetation plays an important role in preventing soil erosion and thus protecting soil structure and infiltration capacity by reducing raindrop energy by canopy interception. Also, urban forests had provided more green spaces for the city which could reduce urban heat island (UHI) effect and improve the air quality (Endreny et al., 2008; Nowak et al., 2018). The beneficial of urban vegetation on the aspect of hydrology or water resource management is also conspicuous. Different

kinds of green infrastructures (GIs) have improved the hydrological cycle and alleviated the burden of traditional drainage systems (Wang et al., 2018) by means of infiltration, storage and interception.

Traditionally, urban hydrological models have generally emphasized on the simulation of rainfalls of one event, so the interception process is often overlooked or simplified. But from the perspective of the whole year, the amount of intercepted/evaporated water usually accounts for a large proportion of the annual water balance. (Mitchell et al., 2009) had estimated the components of total water balance of an urban catchment and found that the actual evaporation rate usually exceeded 50%. (Berland et al., 2017) studied the function of trees as green infrastructure in urban storm water management and concluded that trees can play a substantial role in reducing storm water runoff by interception, infiltration and other methods. (Mullaney et al., 2017) generalized the benefits and challenges in growing streets trees in paved urban environments and emphasized the multi-perspective benefits of street trees. (Zabret et al., 2015) studied the possibility for urban trees to compensate the impact of climate change on storm runoff and suggested that urban green infrastructures mitigated the alterations caused by urbanization and also helped adapt to climate change. (Song XP et al., 2014) had reviewed the economic benefits and costs of urban forest management and concluded that the types of benefits were various and in most cases the benefits of urban trees outweigh the costs.

As stated above, urban catchments and urban water systems are naturally very complex: not only in the scales but also in the interactions of different hydrological process. As a result, complex mathematical models are needed to predict or simulate watershed response to rainfall events in urban areas and it was essential to make an accurate representation or characterization of urbanized catchment and

hydrological processes for hydrological modeling.

Reliable assessment of hydrological processes are crucial for human lives, environmental protection and infrastructures or goods safety. Water movement in urban areas is however not well understood, and so are the physical principles that regulate this movement as well as the interactions occurring between the hydrological processes. Scientific understanding can be supported by detailed and consistent measurements and by hydrological modelling. Those urban hydrology issues will become more and more important in the decades ahead (Praskievicz and Chang, 2009; Fletcher et al., 2013).

1.2 Literature review

1.2.1 Hydrological modeling scale issues

Modeling urban hydrological process at proper scale is not a trivial issue. However, increasing the modeling detail and reducing model uncertainty are two naturally conflicting goals. Thus, practically speaking, a compromise or tradeoff should be find between these targets (Petrucci and Bonhomme, 2014). In recent 10 years, both the computational capacity and the availability of high resolution distributed data had increased in a large degree. As a consequence, more and more researchers built up their model in high resolutions with detailed methods. Recently, hyper resolution input data obtained from multiple information source and urban features had already been used in flood modeling of urban area (Amaguchi and Kawamura, 2016; Noh et al., 2018). Schubert et al. (2008) emphasized the importance of rooftop footprints extraction and found that the rooftop representation in model could

better reproduce the inundation processes. Mannina and Viviani (2010) compared simplified and detailed integrated modelling approaches for urban water quality assessment and found the detailed model to be more robust and presented less uncertainty. Leandro et al. (2016) had pointed out the importance of identify heterogeneity urban key features (roof type and land surfaces) in successful urban flood modeling. Most recent efforts in this category focused on the impact of the inclusion of collecting inlets in urban flood simulation (Chang et al., 2018; Jang et al., 2018). Both studies claimed the necessity of inclusion of inlets for accurate flood extent and duration estimation because these inlets provided a more realistic representation of the actual drainage capacity between surface and sewer system.

All these researches modeled urban hydrological processes at very fine scales (single rooftop or urban blocks), and this method called for a lot of tedious work in delineating and data processing. Recent development, however, posed a possibility to effectively alleviate this problem. The public available database like the Open Street Map, could provide information like roof top footprint and detailed surface land use distribution which could be directly transferred to objects in GIS tools. On the other hand, (semi)automatic surface delineation tools had been developed and this could largely relieve the model building work. Sanzana et al. (2017) presented a semi-automatic tool Geo-PUMMA which could generate well-shaped vectorial meshes or Urban Hydrological Elements (UHEs). In order to avoid the tedious task of building the SWMM model, Warsta et al. (2017) developed a tool called GisToSWMM5 that could automatically generate raster based sub-catchments as well as their parameters values that can be directly used in model.

Although it is an irreversible trend to model urban hydrology at higher resolution with more detailed method, the benefits and drawbacks of doing so should be further discussed. One of the concerns was that the high resolution may lead to the increase of uncertainty or over-parameterization: When inappropriate selected or too many parameters were calibrated on limited data set, they would correspond well with the calibration data set but fail to fit additional data or predict future observations reliably (Petrucci and Bonhomme, 2014). The other concern was the existence of effective parameters. These effective parameters could representing a global hydrological behavior. This meant that some low resolution models could have same performances with more detailed model and the former could save more resources. Leitão et al. (2010) had assessed the influences of urban drainage network simplification and suggested that simplified models had less simulation time without compromising simulation results. What was more, although the high resolution model could simulate more detailed hydrological processes, most of the current calibration technology were focused on fitting the hydrograph data of one or few points. This raised an issue called equifinality which meant that the different parameter sets might produce equal model performance. This also reduced the fidelity of the simulated results at the local scale of a distributed model.

Therefore, the scale issue of distributed model is an important question to be understand. It is also a naturally concomitant problem in urban hydrology due to the nonlinear characteristics usually found in environmental hydrological systems (Jayawardena, 2014). The research of scale or resolution issues in urban hydrology had a long history. Zaghoul (1981) had examined the effect of spatial discretization and parameters in urban catchment. Goyen and O'Loughlin (1999) discuss the basic building blocks used for dividing urban hydrological modelling unit. A series of recent studies had also discussed this

issue with different model structures and catchments and got various results (Ghosh and Hellweger, 2012; Sun et al., 2014; Goldstein et al., 2016).

1.2.2 Vegetation and green infrastructures in urban area

The research about modeling the interception process had quite a long history. One of the earliest effort was (Rutter et al., 1971), who established a predictive forest intercept model, also known as the Rutter model. (Muzylo et al., 2009) had reviewed 15 physical based interception models and found majority of them were based on the original Gash models (Gash, 1979) or Rutter models, and the Mulder and Liu models also should be emphasized. (Bulcock et al., 2012) had modeled both canopy and litter interception in a commercial forest using a modified Gash model and idealized drying curve. The results showed that canopy and litter interception can account for 26% and 13% of the gross precipitation. (Huang et al., 2017) used sparse Gash model to model rainfall interception of four deciduous tree species in urban forest and suggested that the model performed well for all the tree species and the reason for differences between modelled and observed values should be the uncertainties in the measurements of different variables. (Mitchell et al, 2008) modeled the urban vegetation interception and evaporation for the purpose of urban water balance and found that interception and evaporation account for considerable proportion in urban water balance and also urban vegetation had potential to impact the urban microclimate. (Wang et al., 2008) evaluated the tree's effects and contributions for urban water balance consideration in several urban catchments and the results illustrated that trees can significantly reduce runoff for low intensity and short duration rainfall events. (F. Rodriguez et al., 2008) modeled the rainwater circulation within urban catchments with detailed manner and various

hydrological processes using a distributed hydrological model. The results highlighted the importance of evaluation of most hydrological fluxes on urban catchments.

On the other hand, there had also been many experimental based studies on the interception process. (Guevara-Escobar et al., 2007) studied the interception and distribution patterns of an isolated *Ficus benjamina* tree. This experiment had indicated many prominent rainfall partitioning parameters and those patterns were relatively stable to different rainfall events. (Armson et al., 2013) assessed the effect of street trees and amenity grass on the urban surface flow. The results suggested that the reduction caused by grass, tree and tree pit was more than interception alone could have produced. (Livesley et al., 2014) investigated the effect of canopy density and bark type on the interception and stem flow using direct measurement. It is suggested that tree canopy and bark characteristics should be considered before tree planting and street canopies is a cost-effective compliment method to urban design for stormwater reduction benefits. (Xiao et al., 2000) measured rainfall interception of 2 open-grown trees (one evergreen and one deciduous) during winter time and found that the interception ratio of gross precipitation were 15% and 27%, respectively.

Some researches integrated the monitoring and modeling of plant interception. (Bryant 2005) had compared the throughfall variability of 5 forest communities. The measurement results were compared with the simulated results using Gash model. (Herbst et al., 2006) studied the rainfall interception loss of hedgerows by comparing the modeled and monitored results and found that the interception loss predicted by Gash model had reasonable accuracy.

On the other hand, remote sensing technology has made great progress in recent years. This is also beneficial for the accuracy improvement of hydrological models. More and more researches are now taking advantage of the remote sensing data. (Kumar et al., 2015) analyzed remote sensing based indices for the purpose of improving urban water resources management. The results showed that the change of land use is the important reasons leading to increase in land surface temperature. (Elhag et al., 2014) assessed the remote sense based indices to improve water resources management using sensitivity analysis method and found that daily evapo-transpiration is the less sensitive and more certain index followed by draught vegetation index. (Sriwongsitanon et al., 2011) had used remote sensed data (band combinations of Landsat TM1/TM3) to assess the influence of atmospheric correction and the number of sampling points on the accuracy of lake water clarity and found out that the remote sensed data had improved the predicted average values of indices of clarity as well as their maximum and minimum values. (Udelhoven et al., 2009) analyzed the anomalies between climatic indices and Normalized Difference Vegetation Index (NDVI) data in ten years and suggested that the anomalies were good indicators of after drought biomass production. (Nourani et al., 2015) had utilized NDVI data to incorporate land cover variation effect with a rainfall runoff model in a small scale catchment and found that the models in which considered the land cover effects provided acceptable prediction results at both catchment and sub-catchments scale.

1.3 Research gap and problem statement

The above reviewed researches had addressed the important problems about the scale issues and vegetation in urban hydrological modeling. However, there are still lots of points that are not yet fully

discussed.

The previous research had discussed scale issues with different model structure in different catchments and obtained various results. However, these researches always lack detailed descriptions of how the parameter values were determined during the change of scale. Krebs et al. (2014) used the method of area weight average to determine the parameters across different resolutions but the value of one important parameter EIA (effective impervious area) was not maintained during the sub-catchment upscale process.

Also, there are lacking of the generalization of the calculated results: the scale effects may have some relationship with some other catchments characteristics. The finding and generalization of such relationships may reflect more fundamental logic of model scale and could be beneficial to other future modeling work (error estimation framework). What was more, most of these previous studies neglected a calibration process.

Finally, those who implemented calibration did not or failed to calibrate models with different resolutions to assess how calibration can compensate the scale non-linearity of the model. In such cases, several questions were worth to be asking: if the less complex models were calibrated to the available data and allowed to have alternative parameter values to those obtained for the most complex model, how would the parameter values change? Also, if the parameter values for the most complex model are better than those obtained for a less complex model? In other words, equifinality should be an issue in this discussion.

The research about urban vegetation have a lot of types. The monitoring studies had improved the understanding of the different components of rainfall partitioning and also provided helpful insight in determining the parameters of the interception models. But those researches were usually confined in one site during certain period of time and had not expanded to larger scale urban watersheds. For simulation studies, but most of them consider the interception as a separate process, lack of discussion on integration and interaction with other hydrological processes. The spatially variability were also lack of discussions, even though the computation capability and availability of remote sensing data had been developed in a large degree.

One of the obvious existing gaps is the lack of sufficient processed-based modeling of the hydrology of forests in urban areas with detailed information about the spatial distribution of vegetative areas as well as their seasonal variations to be considered. Coincident with the progress in remote sensing and GIS, it has been shown that in hydrological modeling, the use of remote sensing data to detect spatial values is more appropriate and efficient. Widely available earth observation data, such as Landsat images for detecting land cover changes via the normalized difference vegetation index (NDVI), have been demonstrated to be very beneficial for the successful evaluation, monitoring and depiction of landscape situations in many areas. The NDVI is functionally correlated with the leaf area index (LAI) and vegetation coverage; the higher the NDVI is, the larger the LAI, and the higher the vegetation coverage. Therefore, the NDVI can reflect the growth status of surface vegetation and act as an effective index for monitoring variations in vegetation. Some studies have considered the effect of vegetation cover using the NDVI on different hydrologic properties, such as inflow into reservoirs (Wang et al., 2012),

runoff coefficient (Sriwongsiatnon et al., 2011), runoff and sediment yield (Braud et al., 2001), rainfall and temperature (Wang et al., 2013) and evapotranspiration (Sun et al., 2008). The effects of variation in land cover over the watershed have not been explicitly incorporated into model formulation. However, such models may appropriately predict the output hydrographs in watersheds as well as reliably estimate interior sub-watershed outlet hydrographs in a watershed with extremely heterogeneous urban watersheds.

The logic relationship of those existing studies and the remaining gaps were shown in Fig 1.1.

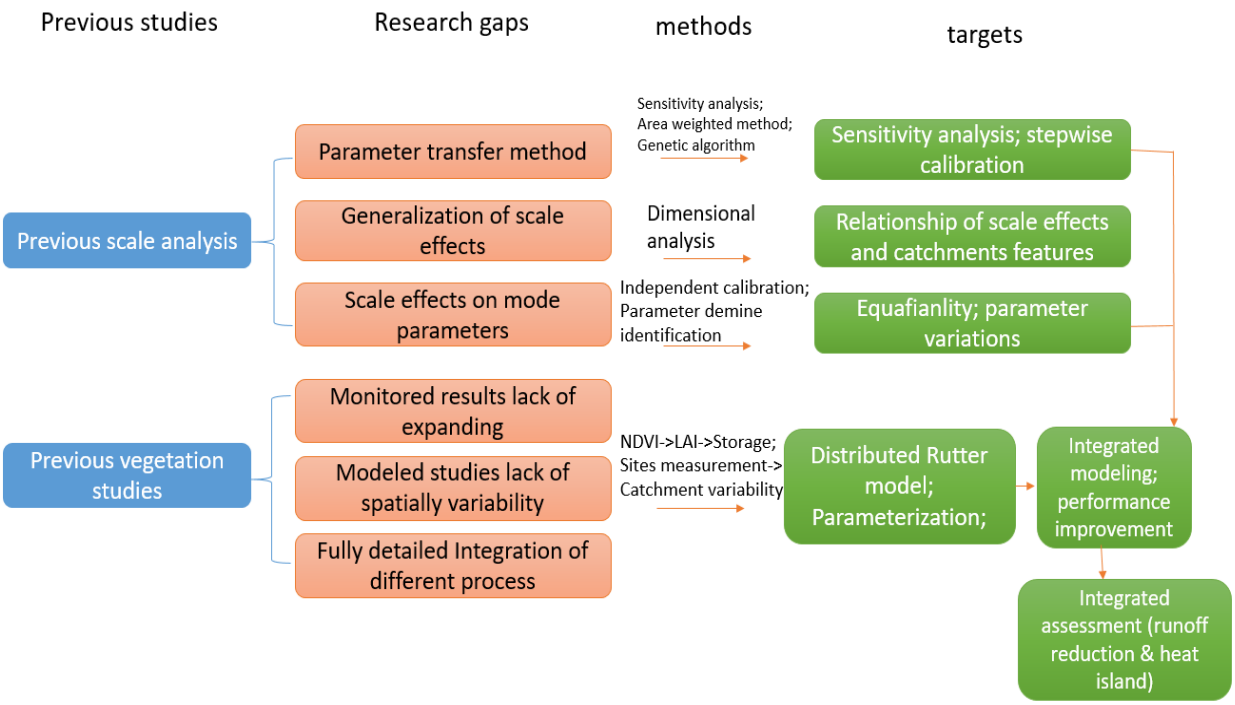

Fig 1.1 The conceptual representation of previous researches, research gaps and targets.

1.4 Research objectives

This study will address the following research questions:

(1) What are the impacts of spatial resolution change on model performance?

(2) If calibration can compensate the scale effects, how do the calibrated parameters change?

(3) How can remote sensing data contribute to a better hydrological parameterization of vegetation dynamics within the urban catchment scale?

(4) What is are the mitigation effects for runoff and urban heat for existing urban vegetation and/or with other potential green infrastructures?

The EPA Storm Water Management Model (SWMM) was used for rainfall runoff modeling. The Rutter model was used for interception modeling and a simple energy based model was used for heat island effect modeling.

1.5 Thesis organization

This section briefly describes the structure of the thesis (Fig 1.1). The description of study site and the data used were presented in Chapter 2. The general flow chart and methodology and the concept of the models used were also introduced in this chapter.

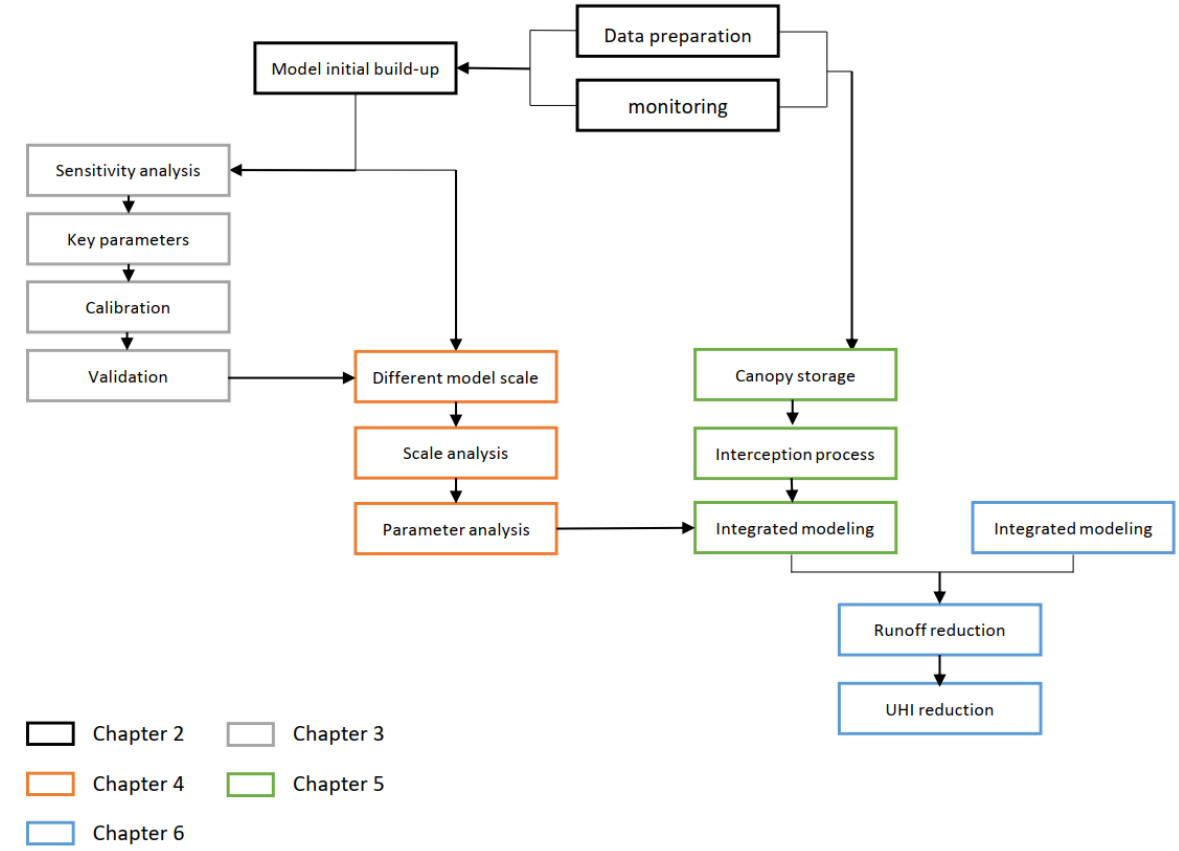

Fig 1.2 The structure and work flow chart of the thesis

Chapter 3 first discussed the initial build up and parameterization of the rainfall-runoff model. And then showed the results of sensitivity analysis and results of model calibration.

Chapter 4 firstly discusses the scale effects observed with respect to total outflow volume and peak flows for different storm events. These results were then compared and categorized with different indices (max rainfall intensity/total rainfall depth). Those scale effects were generalized using a dimensional analysis method. Independent calibration of different scale models were conducted after to find compensatory degree on scale effects. Parameter demines and equifinality degree were also discussed.

Chapter 5 showed the results of the interception model. The seasonal variation and were discussed. The integrated model results were compared with the previous model. The results of the energy balance model were also showed and compared with remote sensed data.

Chapter 6 discussed the effect of tree species and tree aging. The compare and combination with other potential green infrastructures (GIs) were also showed. Finally the effect of urban vegetation on urban heat island were discussed.

Chapter 7 generalized the important results and made the major conclusions of the work. The limitations and potential future directions were also discussed.

Chapter 2. Approach and methodology

2.1 Study site description

Sendai is the capital city of Miyagi Prefecture, Japan, the largest city in the Tohoku region of Japan. Sendai City is located around the center of the Tohoku region, at 38°16_05_N, 140°52_11_E. The city's borders are defined by the western Ou Mountains and the eastern Pacific Ocean. Its area is 786.30km2, and is 50.58km wide (east-west), and 31.20 km long (north-south). Approximately 60% of the city is covered by forests so it is nicknamed the City of Trees. There are zelkova trees lining many of the main streets and areas in the city. The Hirose-gawa River, the Natori-gawa River, and the Nanakita-gawa River flow through these hills into the Pacific Ocean.

According to the information of Japan Meteorology Agency (https://www.jma.go.jp/jma/indexe.html), Sendai has a humid continental climate, which features warm and wet summers, and cool and dry winters. Sendai summers are not as hot as Tokyo to the south, while the winters are much milder than Sapporo to the north, but retains significant seasonal differences in temperature and rainfall. Extremes range from −11.7 to +37.2 °C. Of Japan's prefectural capitals, Sendai experiences the fewest days of extreme temperatures (high temperature above 30° or below 0°) at 19.6 per year. Winters are cool and relatively dry, with January temperatures averaging 1.5 °C. Summers are very warm and much of the year's precipitation is delivered at this time, with an August average of 24.1 °C. The city is rarely hit by typhoons, and experiences only 6 days with more than 10 centimeters of rainfall on average. Sendai's rainy season usually begins in late June to early July, which is later than in most cities in Japan. The

city's average yearly temperature is 12.4 °C, and its yearly precipitation is 1,254.1 mm. 73% of Sendai's yearly precipitation falls in the six months from May to October (fig.2.1).

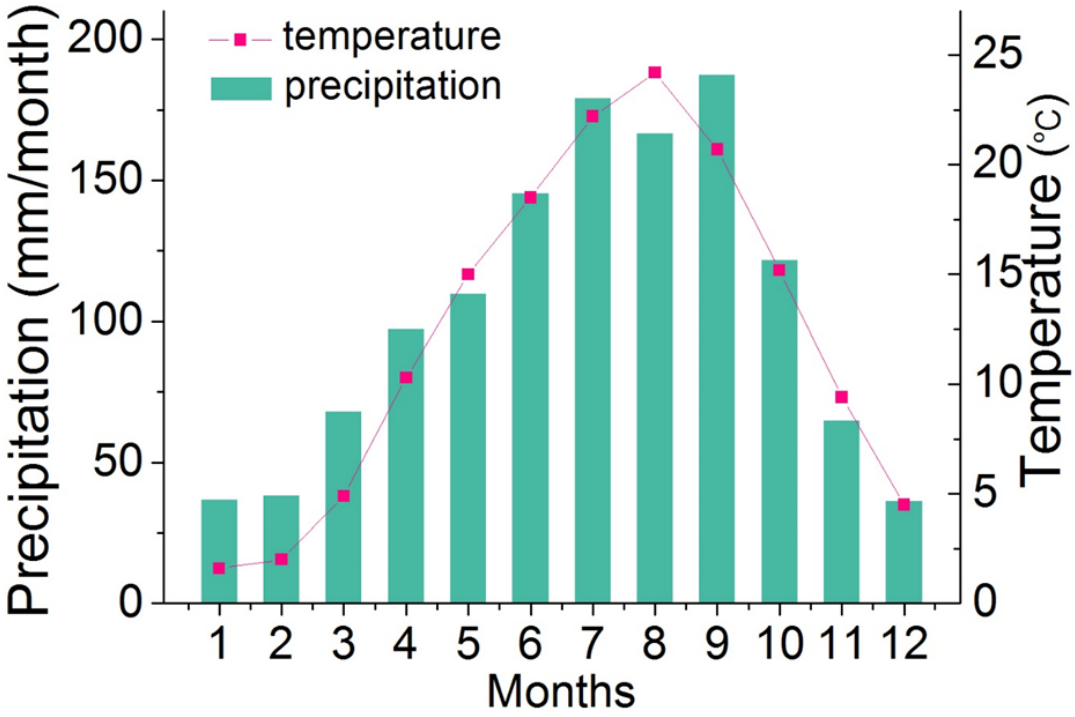

Fig 2.1. Average monthly temperature and monthly precipitation depth of Sendai City.

We chose the Kunimigaoka Area (KA) in Sendai City, Japan for the case study. KA is a residential dominated area located in the north-western part of Sendai City (Fig 2.2). This catchment covers approximately 46 ha with a medium gradient slope topography. The construction processes of KA mainly occurred in the 1990s. Currently the urbanization degree is rather complete and the land use showed little change after 2005. The surface runoff was firstly collected by the gutters which were built on both sides of the roads and then drained to storm water sewer conduits. At the outlet of the sewer system there is a regulation pond. The storm water firstly drains to this regulating pond and then to a downstream river.

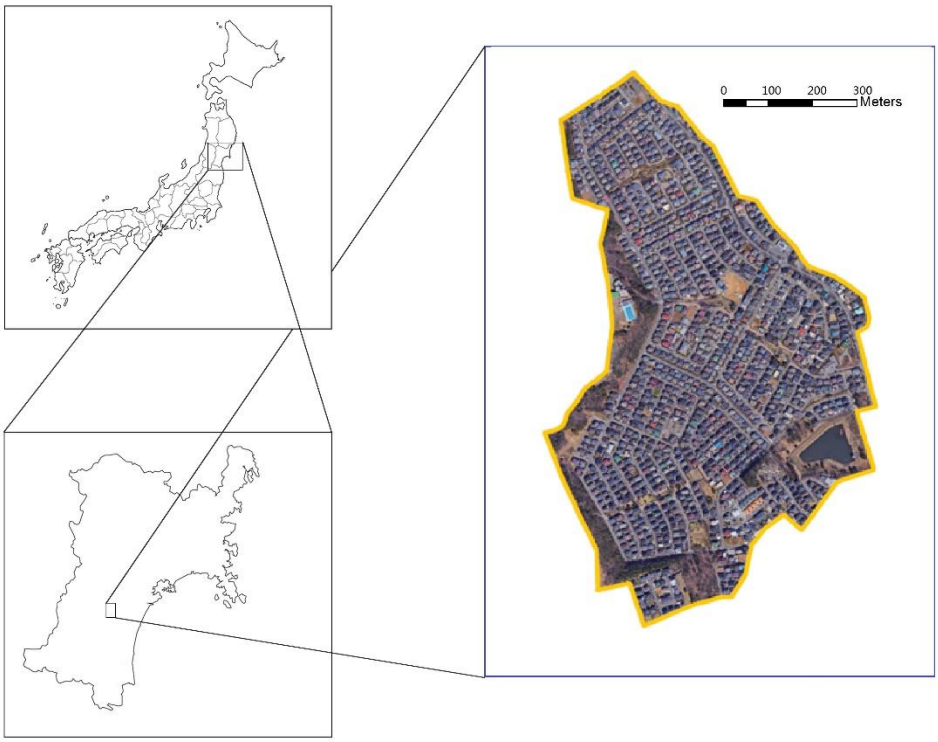

Fig 2.2. Location and aerial photo of the study catchment

2.2 Data preparation and processing

2.2.1 Topographic data

The DEM of KA was available in the form of a high-resolution (5 × 5 m) elevation data set (fig 2.3(a)), which was processed and quality controlled by the Ministry of Land, Infrastructure, Transport and Tourism of Japan (MLIT, https://www.mlit.go.jp/). In order to better represent the detailed path on surface flows, the building profiles as well as the shapes of streets and residential gardens were distinguished from the original DEM using a Google satellite image (the buildings foot prints can be seen in Fig. 2.3 (b)).

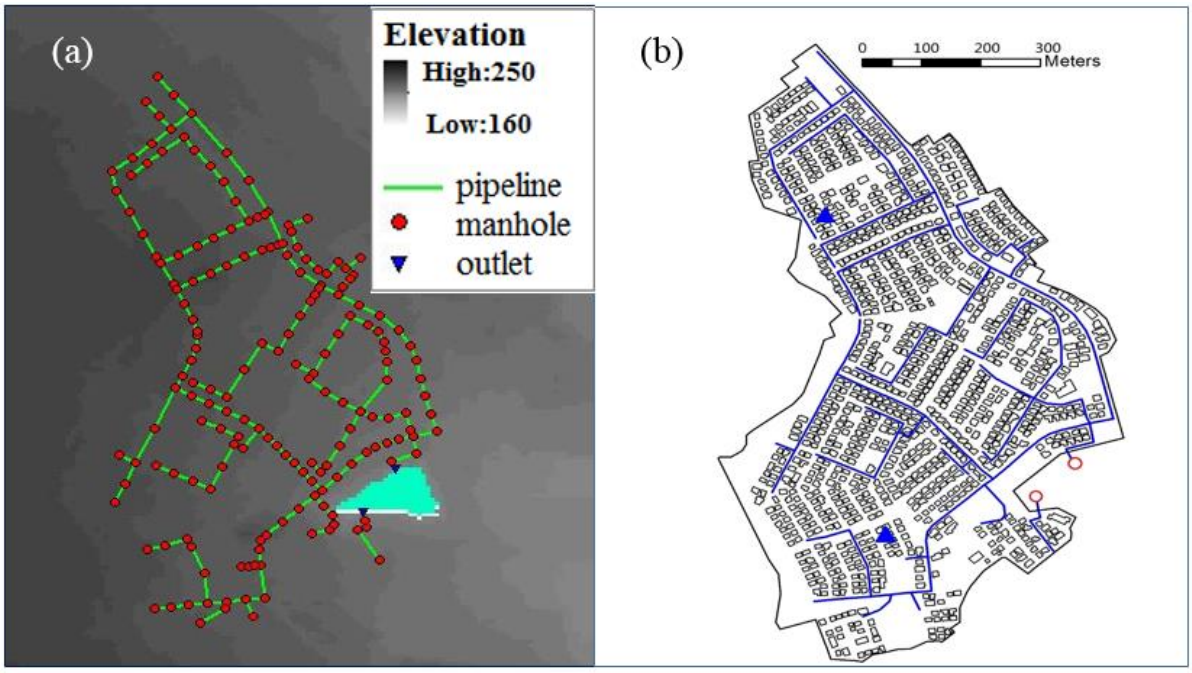

Fig 2.3. (a) Top view of the DEM of the study region and sewer network with 2 outlets and, (b) Scheme of the KA catchment: buildings footprints (black) pipe drainage network (blue), raingauges (blue triangle), and outlets (red circle).

2.2.2 Sewer network data

The underground pipeline data were provided by Sewer Administration Office of Sendai City which contained geographic and geometric information of more than 400 conduits and manholes (fig 2.3 (b)). Although some streets had quite steep slopes, the slope of underground conduits were no more than 3% while most of them had a slope of 0.5%. Most of the conduits were circular with diameters ranging from 0.3 to 2.4 m, while some pipes were rectangular whose widths and heights varied from 0.4 to 0.8 m. The drainage system of the study area also included street gutters mentioned before. The slopes and elevations of gutters were adopted from these values of adjacent roads. The slopes of gutters were ranged from 1.3% to 38%.

2.2.3 Precipitation monitoring

The rainfall was collected by two tipping-bucket rain gauges within the catchment from 26th February 2018 to the 29th July 2018 and include 23 individual events with a record resolution of 0.5mm. Those 23 rainfall events were used for model calibration and validation. The location of the two rain gauges were shown in Fig 2.3 (b). The data recorded by these 2 gauges were rather similar due to the limited catchment area. Some additional rainfall data got from the Japan Metrological Agency were also used in the simulation. These rainfall data included 39 rainfall events from July to October of 2017 and was collected by a metrological station at Sendai city which was around 4.2 km to the study site with 0.5 mm resolution. Those original rainfall data were processed into rainfall data with 5 minute temporal resolution that can be used in the hydrological models. All those rainfall data were used for simulation to observe the scale effect of model.

2.2.4 Flow monitoring

At the outlet, the water level was recorded at 5 min intervals. The water level–flow rate relationship (Fig 2.4) was obtained from several velocity measurement campaigns. There were some very small dry weather flow rate, which might be due to ground water exfiltration, was subtracted from records in order to obtain the storm water flow rate. Continuous flow measurements used for this study had a same period with the rain gauges in the catchment. The rainfall runoff data in this period were used for model calibration and validation.

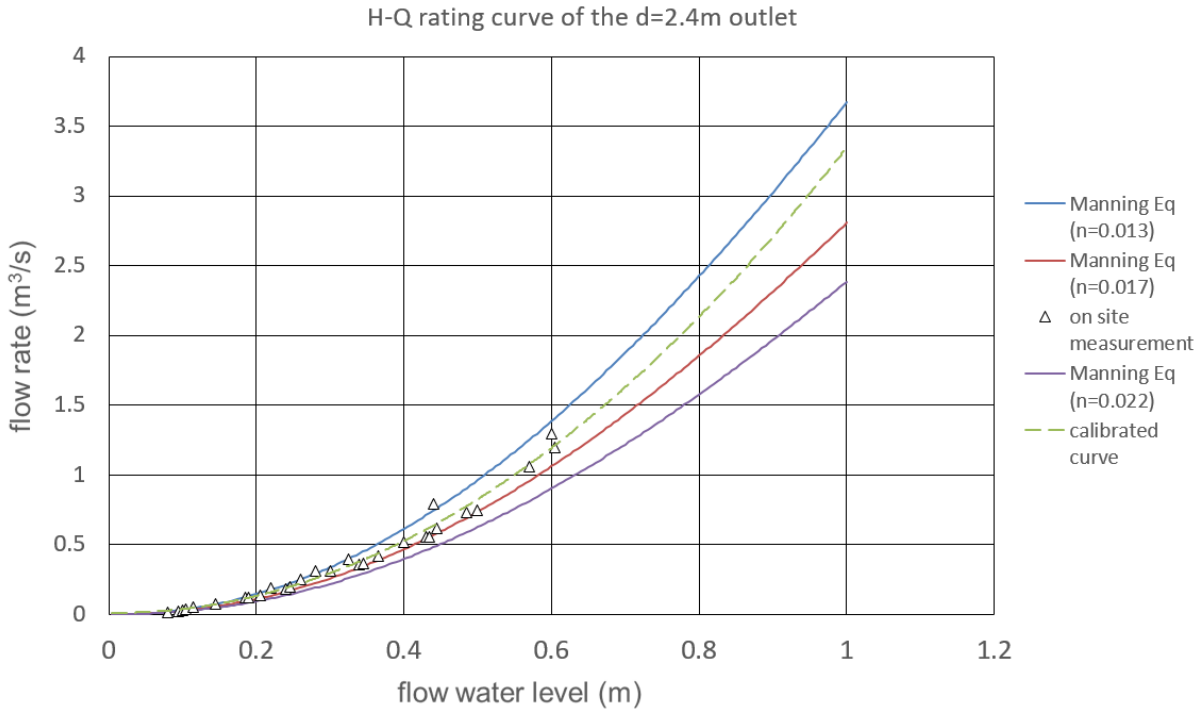

Fig 2.4. Calibrated rating curve used in calculation of flow rates in the KA catchment.

2.2.5 Remote sensing and climate data

Remote sensing provides a helpful tool for the precise detection of land cover changes over time and over relatively large areas. The effect of land cover changes on the proposed geomorphologic rainfall–runoff model was explored using Landsat 8 images as well as rainfall and runoff data. A well-developed global archive of Landsat images is available and is widely used to detect and monitor land-cover changes (Kepner et al., 2012). Landsat 8 data with a 30 m spatial resolution and 16 day temporal resolution were used to detect land use variation. The Landsat 8 satellite images of the studied area were downloaded from the USGS website (https://earthexplorer.usgs.gov/login/). As the urban subcatchments are approximately constant, the average vegetation index for the selected images could

be assigned for each sub-catchment. Cloud-free conditions over the watershed should be regarded for image selection.

The normalized difference vegetation index (NDVI) measures the photosynthetic activity indirectly and varies between -1 for low and +1 for high photosynthetic activity. The NDVI is a well-known vegetation index introduced by Rouse et al. (1974) as:

$$NDVI = \frac{NIR-RED}{NIR+RED} \quad (2\text{-}1)$$

The main concept behind the NDVI is that for vegetated surfaces, red (RED) and near-infrared (NIR) wavelengths are characterized by high and low absorptions, respectively (Chen et al., 2003). Chlorophyll reflects approximately 20% in the red (RED) and 60% in the near-infrared (NIR). The contrast among the responses of these bands is the quantified absorbed energy by chlorophyll, which indicates the level of different vegetated lands. The NDVI value for a specific pixel always varies from -1 to +1, and the NDVI value of a pixel with no green leaves will be close to zero. Water bodies are specified by extreme negative values, surfaces with no vegetation cover result in zero NDVIs, and the highest density of green leaves is indicated by NDVI values close to +1 (0.8–0.9). NDVI is related to the leaf area index (LAI) and vegetation coverage; the higher the NDVI is, the larger the LAI, and the higher the vegetation coverage. Therefore, the NDVI indicates the vegetation cover level and acts as a beneficial index for monitoring vegetation variations and land cover changes.

The aforementioned steps were applied to obtain the NDVI maps of the study area for 9 images. The 'Sum NDVI' values indicate the summation of the NDVIs in all pixels of each subwatershed land cover map. The NDVI of each subwatershed was calculated using GIS tools. The summation of the NDVIs

(over all pixels) in each subwatershed was calculated as:

$$NDVI_w = \sum_{i=1}^{l} NDVI_i \quad (2\text{-}2)$$

The climate data were used in the Penman-Montieth equation. Those data include net radiation (Rn), air temperature (Tc), wind speed (u2), saturation vapor pressure (es), and humidity (H). The time series data of these parameters were obtained from Japan meteorological agency with a time step of 1 hour.

2.3 Description of models and methods

2.3.1 Storm Water Management Model (SWMM)

SWMM is a physically based, spatially distributed model for simulating all aspects of hydrologic and water quality cycles primarily within urban areas (Huber et al. 1988; Rossman 2010) (Fig 2.5 (a)). SWMM treats each catchment as a nonlinear reservoir (Fig 2.5(b)) and employs the combined continuity Eq. and Manning's Eq. on each subcatchment (Huber et al. 1988). Usually, a subcatchment is defined as an area of land containing its own fraction of pervious and impervious surfaces whose runoff drains to an outlet point, which could be either a storm drain or another subcatchment (Rossman 2010)

$$\frac{dV_{sub}}{dt_c} = (A \times i_e) - Q_{sub} \quad (2\text{-}3)$$

Where V_{sub} = volume of water on the subcatchment; t_c = computational time step; A_{sub} denotes the area

of the subcatchment; i_e =effective inflow; and Q_{sub} = subcatchment outflow, derived as follows:

$$Q_{sub} = W_{sub}\frac{k}{n}(d \quad - d_s)^{5/3} - S_{sub}{}^{1/2} \tag{2-4}$$

Where W_{sub} denotes the subcatchment width; k = conversion constant equal to 1.486 for U.S. metric units or 1.0 for SI units; n = Manning's roughness coefficient; d = the depth of ponded water on the subcatchment surface; d_s = surface depression storage; and S_{sub} = subcatchment slope.

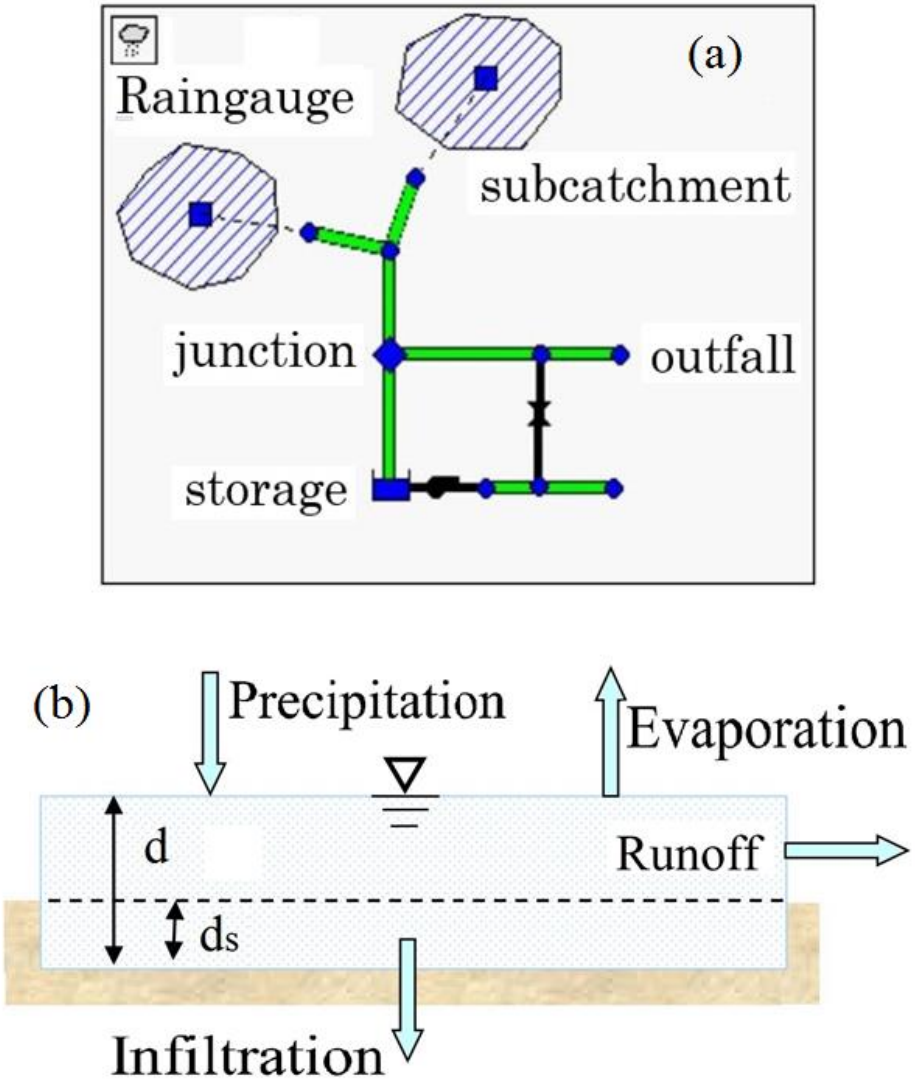

Fig 2.5. (a) Conceptual representation of the SWMM drainage system (Rossman, 2010), (b) Nonlinear reservoir model used to calculate surface runoff of a subcatchment.

Runoff routing in the pipe or channel was calculated by the one dimensional the St. Venant equations which include the Continuity equation and Momentum equation. They can be expressed as:

$$\frac{\partial Ac}{\partial t1} + \frac{\partial Qc}{\partial x1} = 0 \tag{2-5}$$

$$\frac{\partial Qc}{\partial t1} + \frac{\partial (Qc^2/Ac\ )}{\partial x1} + gAc\frac{H_h}{\partial x1} + gAcSf\ = 0 \tag{2-6}$$

Here, x1 = pipe distance (m); t1 = time elapsed (sec); Ac = flow cross section area (m2); Qc = flow rate (m3/s); H_h = hydraulic head of water in the conduit (m);

The SWMM model can use different method to calculate the infiltration process within a subcatchment. The possible method include: Horton's method, Green-Ampt method, modified Horton's method, modified Green-Ampt method, and curve number method. In this study, the Green Ampt method (Fig 2.6) was adopted to calculate the infiltration, so this method is introduced here. The governing equation of Green-Ampt model is:

$$f_p = K_s\left[\frac{d + L_s + \psi_s}{L_s}\right] \tag{2-7}$$

Where,

f_p = infiltration capacity into soil (m/hr)

K_s = saturated hydraulic conductivity (m/hr)

ψ_s = suction head along the wetting front (m)

d = the depth of ponded water at the surface (m)

L_s = depth of the saturated layer below the surface (m)

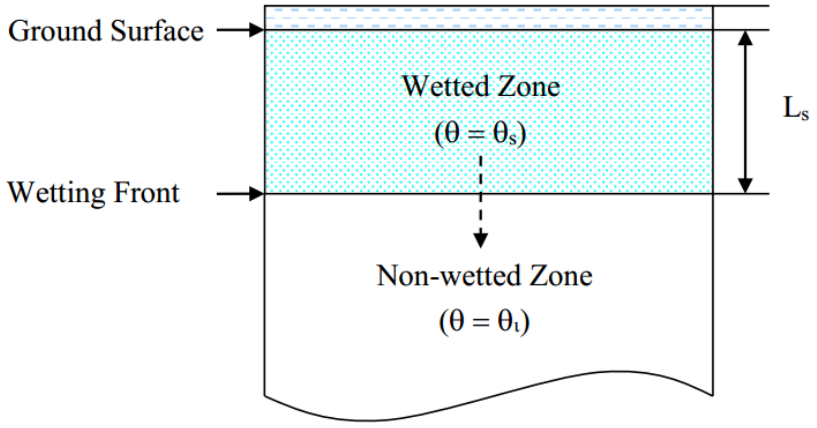

Fig 2.6. Conceptual representation of the two-zone in the Green-Ampt infiltration model

2.3.2 Interception model- the Rutter model

The Rutter model was used here. It is one of the foundations of modern interception modeling (Rutter et al., 1971; Rutter and Morton, 1977). It is a numerical model that uses continuous running equations describing the canopy water balance, trunk water balance, the rate of drainage from the canopy, evaporation from the canopy, stemflow and evaporation from the trunks:

Canopy water balance:

$$(1 - p - p_t) \int_0^{t_r} R\, dt = \int_0^{t_r} D_c\, dt + \int_0^{t_r} E_c\, dt + \Delta C \tag{2-8}$$

Trunk water balance:

$$p_t \int_0^{t_r} R\, dt = Sf + \int_0^{t_r} E_t\, dt + \Delta C_t \tag{2-9}$$

Canopy drainage:

$$D_c = \begin{cases} D_s \exp[b(C - S_c)] & C \geq S_c \\ 0 & C < S_c \end{cases} \tag{2-10}$$

Evaporation from canopy:

$$E_c = \begin{cases} E_P \frac{C}{S_c} & C < S_c \\ E_P & C \geq S_c \end{cases} \quad (2\text{-}11)$$

Stemflow:

$$Sf = \begin{cases} C_t - S_t & C_t \geqslant S_t \\ 0 & C_t < S_t \end{cases} \quad (2\text{-}12)$$

Evaporation from trunks:

$$E_t = \begin{cases} \epsilon E_P \frac{C}{S} & C_t < S_t \\ \epsilon E_P & C_t \geqslant S_t \end{cases} \quad (2\text{-}13)$$

Here, R is the mean rainfall rate, p is the free throughfall coefficient, p_t is the stemflow coefficient, S_c is the maximum canopy storage capacity, t_r is rainfall duration time, S_t is the trunk storage capacity, C is the actual canopy storage, E_P is potential evaporation, E_C is evaporation from the canopy, E_t is evaporation from the trunk, ϵ describes the evaporation from the trunk as a proportion of the evaporation from the saturated canopy, D_C is the rate of water dripping from the canopy, D_S is the rate of water dripping from the canopy when the canopy storage capacity has been reached, b is an empirical drainage parameter, and I is interception. The conceptual representation of the relationships among these equations were shown in Fig 2.7.

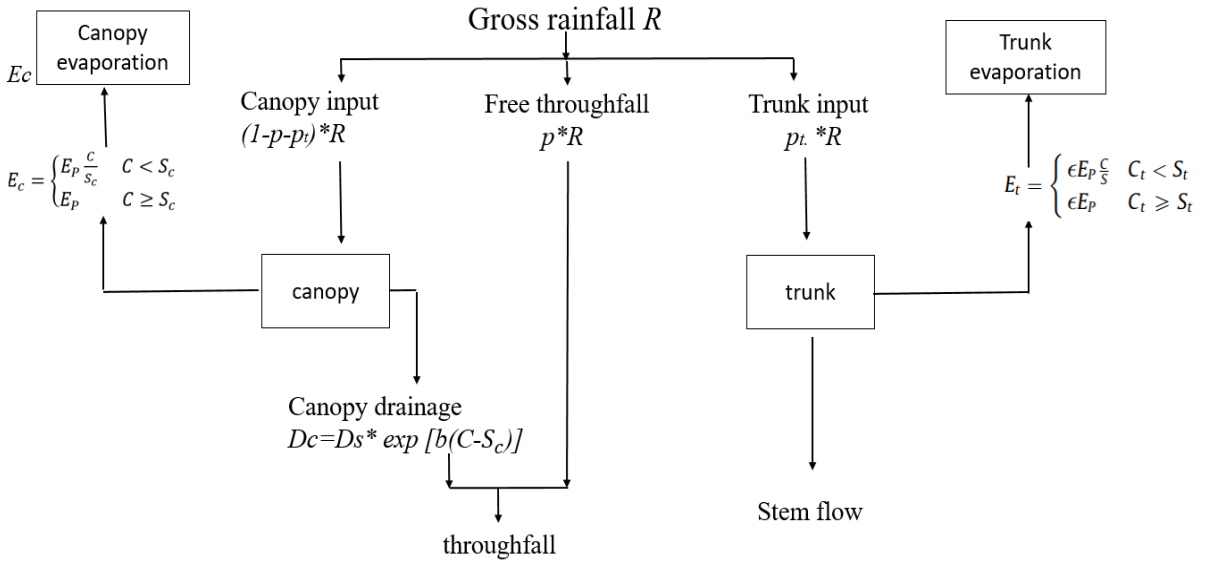

Fig 2.7. The conceptual framework of Rutter model (adopted from Rutter et al, 1971)

The Penman-Montieth reference evaporation equation was used to calculate hourly potential evaporation [E_P] in the interception models. The Penman-Montieth equation requires observational measurements of maximum and minimum temperature, maximum and minimum relative humidity, solar radiation, and wind speed. Here, R_n is net radiation, G_S is the soil heat flux density, T_C is the air temperature, *u2* is wind speed at 2 m height, e_s is saturation vapor pressure, e_a is actual vapor pressure, *H* is humidity and γ is the psychometric constant.

$$E_P = \frac{0.408\Delta(R_n - G_S) + \gamma \frac{900}{T_C + 273} u_2 (e_s - e_a)}{\Delta + \gamma(1 + 0.34u_2)} \quad (2\text{-}14)$$

2.3.3 Energy Balance model

Solar radiation and atmospheric longwave radiation warm the surface and provide energy to drive

weather and climate. The energy is expended as follows：

• Some of it is stored in the ground (or the oceans);

• Some of it is returned to the atmosphere, warming the air;

• The rest is used to evaporate water.

These are the surface energy fluxes which we will be discussing in this Section. The surface energy balance equation is:

$$(1-r)S_{\downarrow} + L_{\downarrow} = L_{\uparrow} + H + \lambda E + G_H \quad (2\text{-}15)$$

where r is the albedo of the surface (dimensionless), S ↓ is the solar radiation incident on the surface (W/m^2), L ↓ is the longwave radiation incident on the surface (W/m^2), L ↑ is longwave radiation emitted by the surface (W/m^2), H is sensible heat flux from thesurface (W/m^2), λE is latent heat flux from the surface (W/m^2) and G_H is heat conducted away from the surface (W/m^2).

The left hand side of the equation denotes the energy inputs to the surface – gain terms - (also called the radiative forcing term). The right hand side of the equation denotes energy outputs from the surface (loss terms). The net radiation can be defined as follows:

$$R_n = (1-r)S_{\downarrow} + (L_{\downarrow} - L_{\uparrow}) \quad (2\text{-}16)$$

The surface energy balance equation can be rewritten as,

$$(1-r)S_{\downarrow} + (L_{\downarrow} - L_{\uparrow}) = H + \lambda E + G_H \quad (2\text{-}17)$$

Thus, the energy balance equation is a statement of how net radiation is balanced by sensible, latent and conduction heat fluxes.

Albedo (r): Aledo is the fraction of incident solar radiation reflected by a surface. It varies between 0 and 1. The albedo of natural surfaces varies from about 0.1 (vegetated surfaces) to greater than 0.9 (fresh snow). The albedo of a surface depends on the solar zenith angle, that is, it changes during the day time.

Solar Radiation: Electromagnetic radiation from the sun is contained approximately between 0.3 and 4 microns. The energy is inversely proportional to the wavelength. The total solar radiation at the surface can be as high as 1000 W/m^2 at midday on a sunny day. A surface receives both direct and diffuse solar radiation. The amount of direct solar radiation incident on a surface varies with the solar zenith angle. Diffuse solar radiation is radiant energy that has interacted with the constituents of the atmosphere and thus has no directionality. The fraction of diffuse radiation depends on the cloud conditions. On clear days, the diffuse fraction is about 10-20% and varies with the solar zenith angle.

Longwave Radiation: Terrestrial objects emit electromagnetic radiation in the wavelength range of 4 to 100 microns. The amount emitted is given by the Boltzmann's law as

$$L\uparrow = \varepsilon\sigma(T_s + 273.15)^4 \tag{2-18}$$

Where (T_S + 273.15) is absolute temperature in degrees Kelvin, σ is Boltzmann's constant (5.67 x 10-8 $W/m^2/K^4$) and ε is the emissivity of the surface (between 0.95 and 1).

Sensible Heat Flux: Movement of air carries heat and mass (water and carbon dioxide molecules, for example) away from an object. This is called convection or sensible heat transport. The heat flux can be represented as being directly proportional to the temperature difference between the object and the air surrounding it and inversely proportional to the transfer resistance (in analogy to Ohm's law in electricity),

$$H = [-\rho C_p \ (T_a - T_s)] / (r_H) \tag{2-19}$$

Where ρ is density of air (about 1.2 kg/m^3), C_P is heat capacity of the air (about 1010 J/kg/K), T_a and T_s are temperature of the air and the surface, respectively, and r_H is the transfer resistance (s/m), which depends on wind speed and surface characteristics.

Latent Heat Flux: Heat is also lost from an object through evaporation and/or transpiration. This process involves transfer of mass and heat to the atmosphere from the object. Clearly, a significant amount of energy is required to change the state of water from liquid to gas. Importantly, this exchange does not involve temperature changes, that is, as energy from the surface is released into the atmosphere, it does not result in an increase in the temperature of the air surrounding the object. This latent heat of vaporization varies with temperature (about 2.43×10^6 J/kg at 30 °C). This latent heat is released when water vapor condenses back to liquid. The values of this item were calculated based on Penman-Montieth equation mentioned in previous Section.

Conduction: Conduction is transfer of energy in solids, that is, transfer of heat along a temperature

gradient due to direct contact. The rate at which an object gains or loses heat via conduction depends on the temperature gradient and thermal conductivity as:

$$G_H = \kappa(\Delta T/\Delta Z) \quad (2\text{-}20)$$

Where κ is thermal conductivity (W/m/K) – which is a measure of the ability of an object to conduct heat.

2.3.4 Sensitivity analysis and calibration methods

The water management of urban system have become an important issue which increased the need of enhancing the modeling for the hydrological and the water quality processes in both the overland flow and the flow in sewer systems. Nowadays many researchers and practitioners studying and managing stormwater sewer systems in urban catchments use semi-distributed models like SWMM, CANOE or MOUSE (Zoppou, 2001; Elliott and Trowsdale, 2007). These models are based on a description of the catchment as a set of subcatchments linked by a drainage network. The runoff generation processes are simulated for each subcatchment, and the network is used to simulate the routing of water to the catchment outlet. Due to the natural complexity, the number of parameters of these models are so large that the calibration and validation of such models require a huge amount of data and computation.

In order to discern which parameters have the most influence over model performance and to identify what are the most appropriate parameter values, we need to find a way to screen out sensitive parameters and quantitatively evaluate the influence of each parameter on model performance. Sensitivity analysis

(SA) has been used by many people for this purpose. SA can identify parameters of which a reduction in uncertainty specification will have the most significant impact on improving model performance measures. Thus, if some non-influential parameters can be identified and fixed reasonably at given values over their ranges, the computational cost may decrease without reducing model performance.

SA approaches based on design of experiment (DOE) have gained popularity recently because they offer sensitivity measures while maintaining computational efficiency. A typical DOE-based SA method involves two steps: first, generating a sample set of parameters within the feasible parameter spaces using a chosen design; and then, obtaining a quantitative attribution of model output variation due to the variation of different parameters. There are many sampling techniques, such as MC, Latin Hypercube (LH), Orthogonal Array (OA) and Orthogonal Array based Latin Hypercube (OALH), which are commonly used for DOE-based SA. Some DOE based SA methods, such as Morris One-At-a-Time (MOAT), Fourier Amplitude Sensitivity Test (FAST), and extended Sobol method, require special sampling techniques. More recently, along with the development of response surface methods (RSM), SA based on RSM makes it cheaper for estimating parameter effects.

In this study, 2 methods of sensitivity analysis were used. One is a Morris One-At-a-Time (MOAT) method:

$$Se = \sum_{i=0}^{n-1} \frac{(Y_{i+1} - Y_i)/Y_0}{(P_{i+1} - P_i)/100} / n \qquad (2\text{-}21)$$

Where: Se: Morris sensitivity

Yi: Model output of the i th run (output refers to peak flow (m3/s) or total flow (m3)),

Y0: Model output of initial parameter values,

Pi: Variation degree of a certain parameter in the i th run,

n: times of model run.

In this study, the fluctuation range of parameters were set to [70%, 130%] with a step of 5%.

Another method is the Variance based Global Sensitivity Analysis (GSA) methods. Variance GSA methods explore the entire parametric space of a model by simultaneously using different combinations of values for each uncertain parameter. The Sobol method is an example of a variance based GSA method. Sobol uses a quasi-Monte-Carlo based method to decompose the model variance (Saltelli et al., 2004). The total variance of the model is partitioned in terms of increasing dimension, which represents the contribution of single, paired, tripled, etc. parameters to the overall model sensitivity:

$$V(y) = \sum_i V_i + \sum_i \sum_{j>i} V_{ij} + \ldots + V_{12\ldots z} \tag{2-22}$$

Here, y is the model output, z is the total number of parameters, Vi is the first order effect for each parameter, Vij is the second order interaction between two parameters, etc.

The first order sensitivity index [Ni] and the second order sensitivity index [Nij] for each parameter is given by the following equations:

$$N_i = \frac{V_i}{V(y)} \tag{2-23}$$

$$N_{ij} = \frac{V_{ij}}{V(y)} \tag{2-24}$$

Thus, the total sensitivity index [N_{Ti}], which is given below, represents the total contribution to the output variance by a single parameter from first and higher order interactions. The complete description of this method could be found in (Sobol, 1993) and (Saltelli et al., 2004)

$$N_{T_i} = N_i + \sum_{1 \neq j} N_{i,j} + \sum_{1 \neq j \neq k} N_{i,j,k} + \dots \tag{2-25}$$

Chapter 3. Sensitivity analysis and model calibration

3.1 Runoff model build up

Subatchments for the SWMM model were delineated using available sewer network data maintained by the local water supply office, complemented with catchment information acquired through on-site observations in wet and dry conditions. The catchment surface was categorized using different surface types and further subdivided based on the land-use type. The high-resolution discretization based on surface types results in subcatchments covered by a single surface type and homogenous surface properties (e.g. green area, asphalt surface, roof surface). Thus, the vast majority of subcatchments are either 100% impervious or pervious. Consequently, these subcatchments are conceptionally not subdivided into pervious and impervious sub-areas. The remaining subcatchments are areas covered with stone pavers, cobble stone, or asphalt. The corresponding pervious fraction of 5% for these surface types represents cracks in the asphalt surface and seams for stone paver and cobble stone surfaces and allow for infiltration of surface water. However, as the pervious sub-area of these surface types is very small, they were assigned the same parameter value applied to both the pervious and impervious sub-areas (i.e. the subcatchment depression storage D include Di (impervious), Dp (pervious) and the subcatchment Manning's n include ni and np). This simplification allows the reduction of the number of calibration parameters and the potentially larger depression storage and Manning's n of surface cracks and seams are accounted for in the parameter values for the entire surface. Thus, in this study, the annotation ‘‘pervious’’ refers to pervious surface types (e.g. vegetation, lawn, etc.) and the annotation ‘‘impervious’’ refers to impervious surface types (e.g. asphalt, metal sheeted roofs, etc.),

rather than subcatchment sub-areas. The created surfaces were then further subdivided to assign stormwater sewer network inlets and to describe flow paths of overland flow between subcatchments before runoff enters the drainage network. Each sub-catchment was built upon small urban structures like a single rooftop, a single garden or a short part of road. This made each sub-catchment to be occupied by a single land use type. The routing between sub-catchments could better represent the actual flow path at micro scale. In this model, not only the drainage conduits underground, but also the street gutters (small trench) with fixed cross section beside the road were considered and modeled explicitly.

3.2 Sensitivity analysis method and results

Five rainfall event were selected for sensitivity analysis. These rainfall included 3 single rainfall events recorded in 2017, a designed extreme rainfall and a long series rainfall for the entire year of 2016. The snow events of 2016 were picked out and then removed from the series. The shape of the three single rainfalls were single peak, double peak and non-peak flat rainfall with similar total rainfall amount. Their characteristics were shown in Table 3.1. We developed models with 2 different resolution, the ordinary and high resolution (Fig 3.1). The ordinary model was delineated based on urban block. Each block was treat as a homogenous area and the flow with the block was neglected. While the high resolution model was delineated based on each roof, garden and road. The flow direction between different components were modeled explicitly. The considered parameters were listed in Table 3.2.

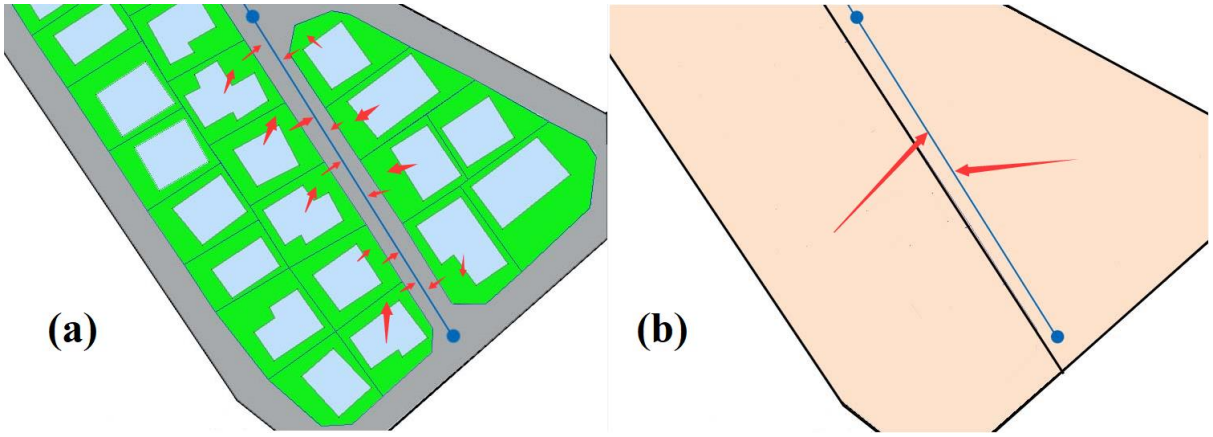

Fig 3.1 Surface discretization and flow routing for the high (a) and ordinary (b) resolution model

Table 3.1 The characteristics of rainfall events used in sensitivity analysis

	Rainfall depth (mm)	Rainfall duration
Single peak rainfall	24.5	3.2 h
Double peak rainfall	27.5	4.5 h
Flat rainfall	21	12 h
Extreme rainfall	199	6 h
Long series rainfall	1117	1 year

Table 3.2 Parameter abbreviations and descriptions. OR=ordinary resolution, HR=high resolution, LS=local sensitivity, GS=global sensitivity. The "x" indicates that the parameter is considered in sensitivity analysis

ABBREVIATION	DESCRIPTION	OR		HR	
		LS	GS	LS	GS
%Imperv	Impervious ratio	X		X	
Min-inf	Hydraulic conductivity	X		X	
Max-inf	Initial infiltration rate	X	X	X	X
N-imp	Manning's roughness at imperv surface	X	X	X	X
N-perv	Manning's roughness at perv surface	X	X	X	X
N-con	Manning's roughness of pipe	X	X	X	X
D-imp	Depression storage at imperv surface	X	X	X	X
D-perv	Depression storage at perv surface	X	X	X	X

The results of global and local sensitivity analysis were shown in this section (Fig 3.2, Fig 3.3 and Fig 3.4). The sensitivity analysis had identified the most and least important parameters in the model. Overall, the parameters behaved similarly in different precipitation and with different objective function, with the most and the least important parameters fairly consistent across scenarios. For local sensitivity (Fig 3.2), the ranks of parameters were similar in different rainfall, resolution and criteria. Imperviousness was the most sensitive parameter, and its sensitivity was much larger than other parameters. The secondary important parameters were N-imp and D-imp. Relatively, infiltration parameters, the infiltration parameters, were not sensitive. The sensitivity performance of annual rainfall and single rainfall were different in some degree. In the annual rainfall, the Imperviousness

impact was less than that in the single rainfall while the depression storage parameters impacts were larger than that in single rainfall.

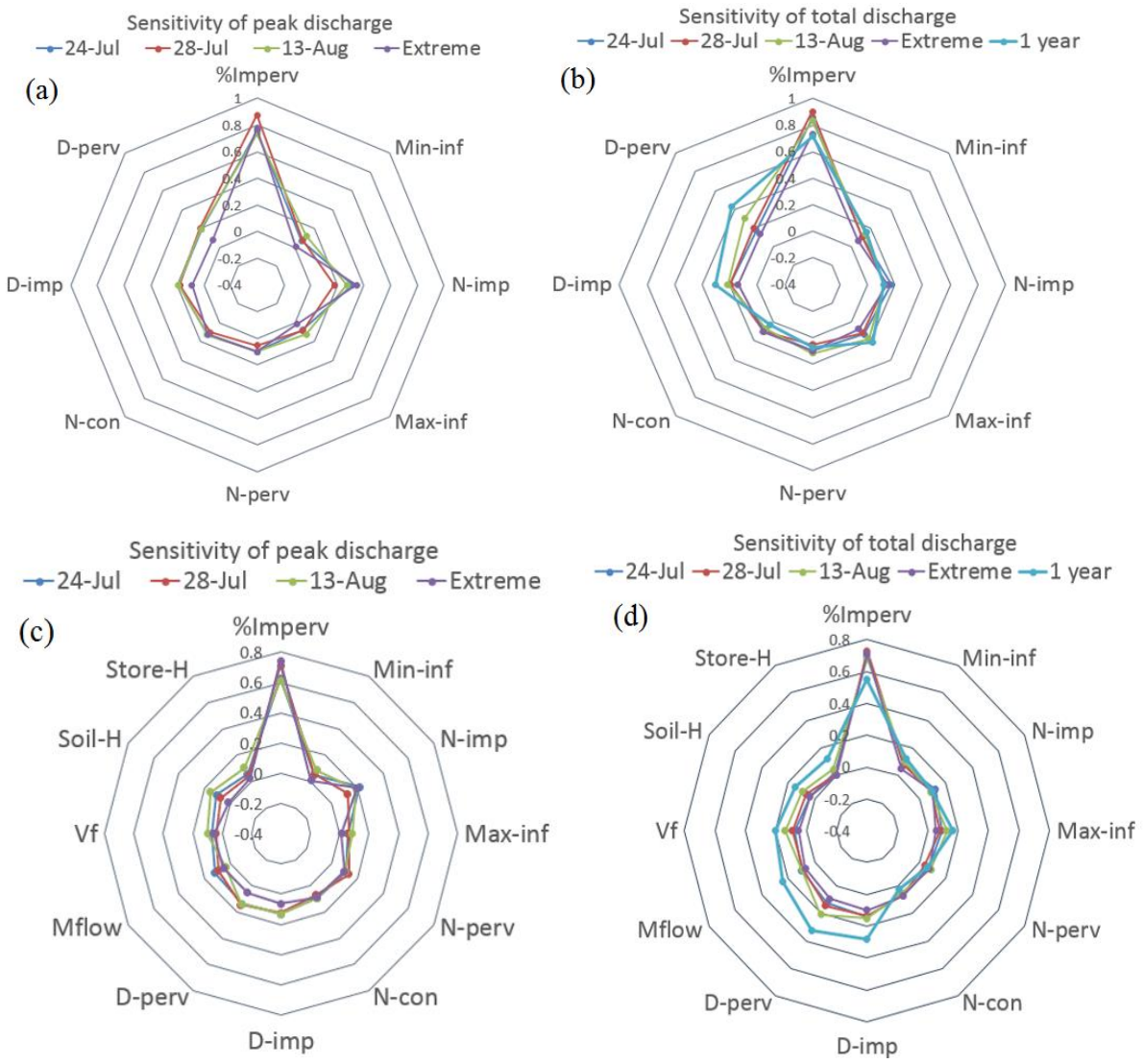

Fig 3.2 Local sensitivity results of (a) ordinary resolution, peak flow (b) ordinary resolution, total flow (c) high resolution, peak flow (d) ordinary resolution, total flow.

For the global sensitivity analysis (Fig 3.3), the results were generally similar with the local sensitivity analysis. As the imperviousness was not taken into consideration, generally the most important model parameters were depression storage and roughness parameters. For total flow, D-imp accounted for

15%-24% of the total model sensitivity and followed was the N-imp accounted for 16-30%. For peak flow, N-imp was the most sensitive parameter which accounted for 15% of the total, D-imp was followed by an occupation of 15% of total sensitivity. The specific ranking of the top most important parameters varied between different rainfall events and evaluations criteria. There were a number of parameters that were relatively unimportant in all of the models. The infiltration parameters max-inf, min-inf, and the appended parameters in the high resolution model, also showed unimportant characters. The sensitivity occupations of these parameters were usually less than 10%.

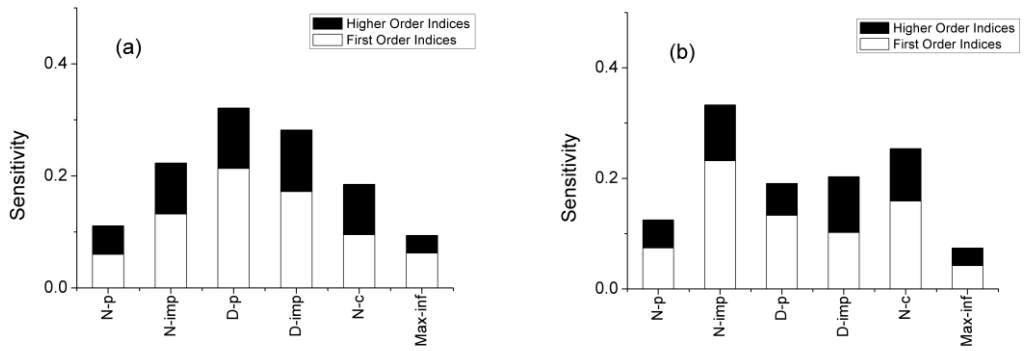

Fig 3.3 Global sensitivity results of (a) total flow (b) peak flow.

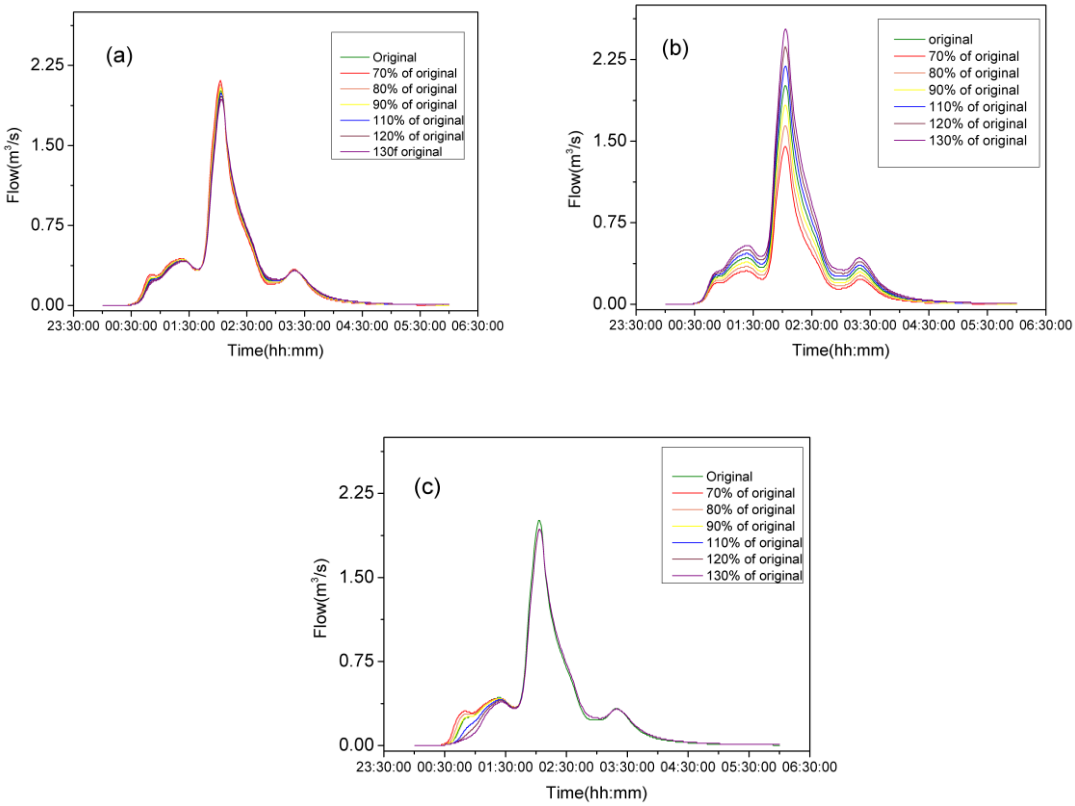

Fig 3.4 The hydrograph comparison with different parameter perturbations, (a) Manning's roughness, (b) Impervious ratio, and (c) Depression storage depth.

For the long series annual rainfall event, the importance of depression storage and infiltration parameters were increased obviously (Fig 3.2). The main reason of this was the distribution characteristics of the rainfall in the entire year. Among the 1117 mm rainfall of 2016, the small rainfall events occupied a large proportion of the total rainfall. These small rainfall event usually generated only little amount or completely no runoff. The large proportion of the rainfall was intercepted by the canopy and shrubs and stored by the depression on the land surface. The intercepted or stored water was then evaporated. Infiltration process in this situation was relative significant because the infiltration capacity was considerable compared with the small rainfall depth. Thus, on the scale of the entire year, the interception and infiltration were actually important processes. Meanwhile, from the same reason, the

roughness parameters like N-imp or N-conduit were less important compared with single events.

We considered several different rainfall types of single event, including the typical single peak event, double peak event, mild flat rainfall event and designed extreme event. We found that when the total amount of rainfalls were similar, the temporal distribution characteristics of rainfall had an impact on the results. The results of single peak and double peak rainfall were quite similar. The result of mild flat rainfall had some differences compared with peak rainfalls while the infiltration parameters became more important. The reason might be that the small intensity allowed more amount of infiltration, which made the infiltration a more important process. And for the extreme rainfall, the parameter sensitivities showed a large difference compared with other rainfalls. The importance of infiltration and depression storage decreased a lot. The roughness parameters were decreasing as well. As an only exception, the sensitivities of impervious ratio did not change much, which was still an important parameter. This was because that this designed rainfall was with very strong intensity and very large rainfall amount. The infiltration and depression storage capacities were soon overwhelmed by the vast amount of rainfall water. Also a very fast routing process occurred. At this situation, the importance of roughness also decreased.

For different resolutions of the model, the differences were relatively small, which might indicate that the model spatial resolution did not have a large impact on the sensitivity. Fig 3.5 showed a comparison between OR and HR. We can see that the sensitivity changes for most parameters are not significant. The conduit roughness was an exception. The sensitivity of this parameter increased in the high resolution model. Also the N-imp decreased slightly compared with the ordinary resolution model. This

was mainly because of that different modeling way of high and ordinary resolution model. In high resolution model every underground pipe and gutter beside the road were modeled explicitly. The change of resolution had altered the form of surface routing process in some degree. Even though, the differences of sensitivity were not significant.

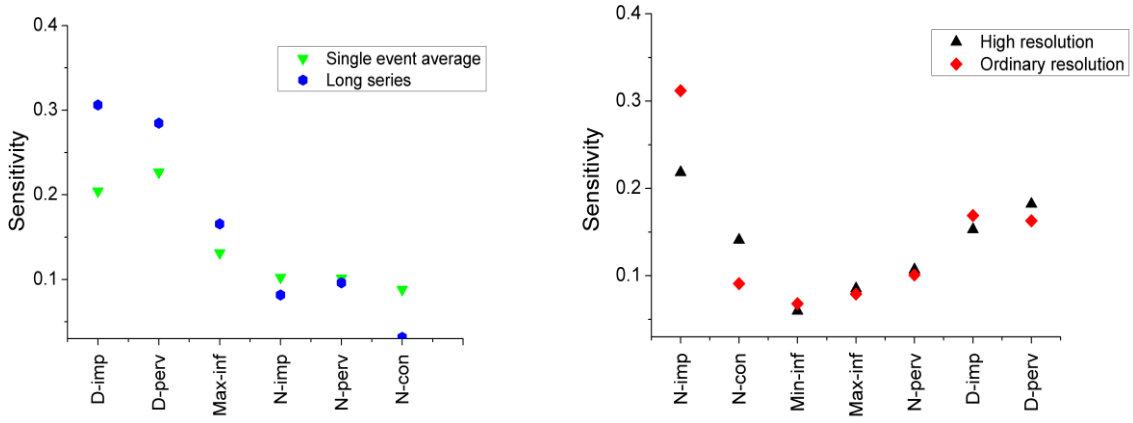

Fig 3.5 Cross comparison of sensitivity results (a) between different rainfalls (b) between different resolutions.

3.3 Calibration method and results

The model was optimized by using an automatic calibration method based on genetic algorithms. Genetic algorithms (GA) is a meta-heuristic that belongs to the larger class of evolutionary algorithms. In recent years, it has been widely used in the optimization of hydrological modeling. The detailed description of genetic algorithm were shown in Section 2.3.4. In this study, the monitored rainfall runoff data were divided into the calibration period (from 26th February to 31st May of 2018, and from 1st Mar to 30th Jun of 2019) and validation period (from 1st June to 30th Oct 2018). The Nash–Sutcliffe efficiency (NSE) was selected as the objective function for the optimization:

$$NSE = 1 - \frac{\sum_{t=1}^{T}(Q_m^t - Q_o^t)^2}{\sum_{t=1}^{T}(Q_o^t - \bar{Q}_o)^2} \quad (3\text{-}1)$$

Where $\bar{Q}_o$ is the mean of observed discharges, and Q_m^t is modeled discharge while Q_o^t is observed discharge at time t. The higher values of NSE represent more accurate models. After simulation, the NSE values in calibration period and validation period were calculated. All the rainfall events in certain period were connected into one longer series and the monitored and modeled data of this longer series were used for calculating. Thus, the calculated NSE values represented the general performance in the period and the irrelevant part (base flows) was effectively avoided.

For S1 model, due to its highly detailed representation method and the single land use type on each sub-catchment, the information like the imperviousness land surface or the flow path length could be all identified. The soil type in the study area was dominated by clay loam, thus the corresponding infiltration parameter values in the SWMM manual were used here. Even though, the depression storage parameters (di/dp: depression depth on impervious/pervious surface) and the roughness parameters (ni, np and nc: the manning's roughness of impervious/pervious surface and of conduits) remained unknown. Thus the values of these parameters were obtained through model calibration. Fig 3.6 had shown the hydrographs of several calibration and validation events.

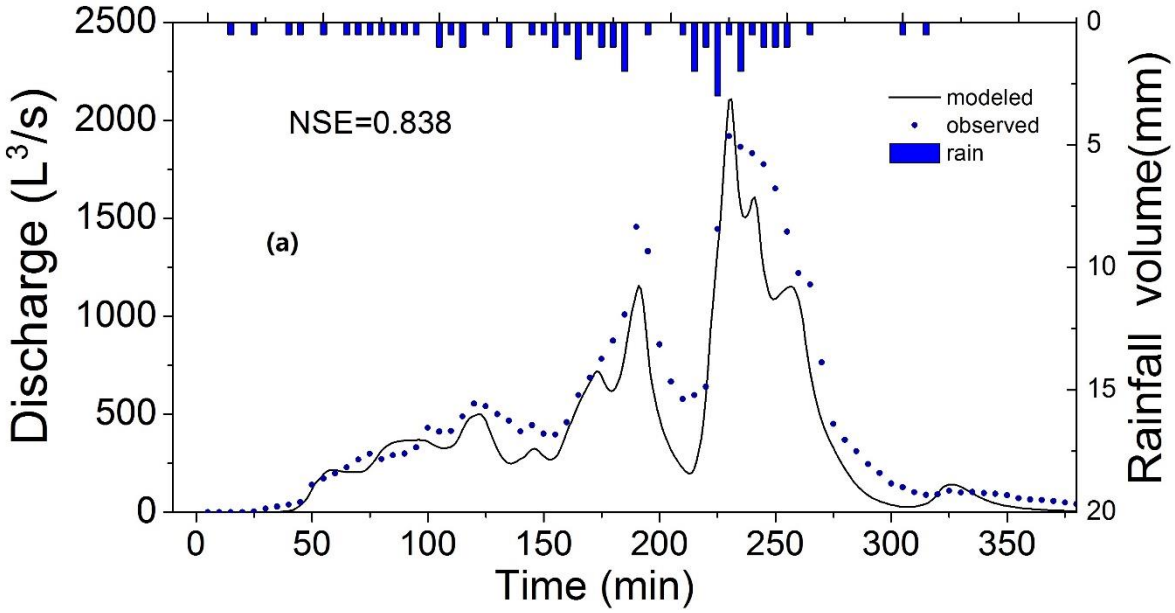

(a) Hydrograph of 1st Mar 2018 event for calibration;

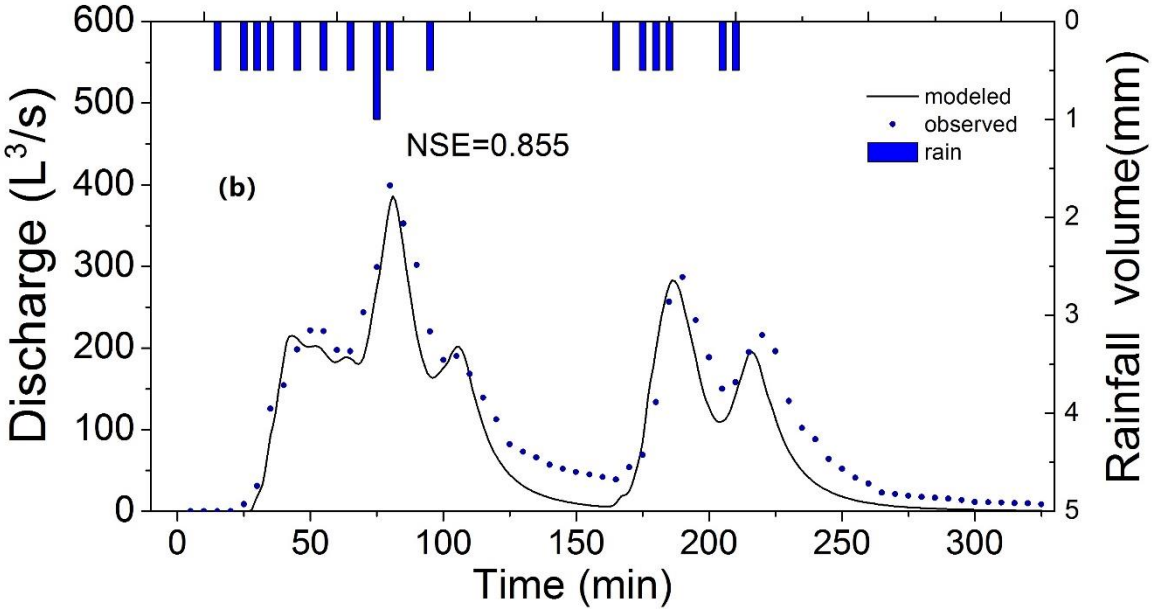

(b) Hydrograph of 17th May 2018 event for calibration;

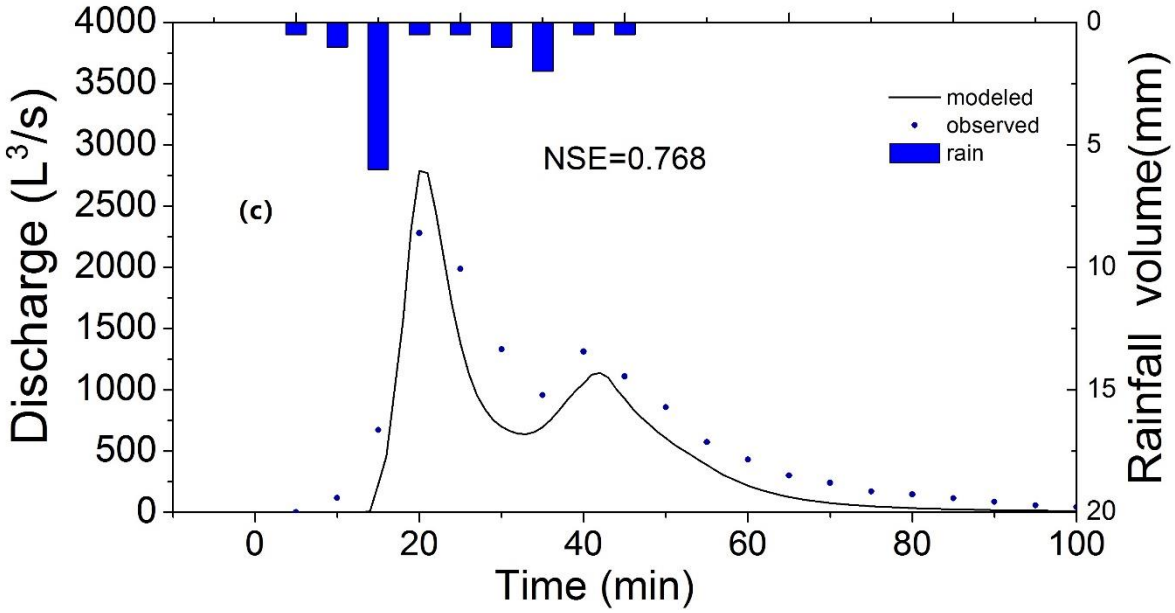

(c) Hydrograph of 29th Jun 2018 event for validation;

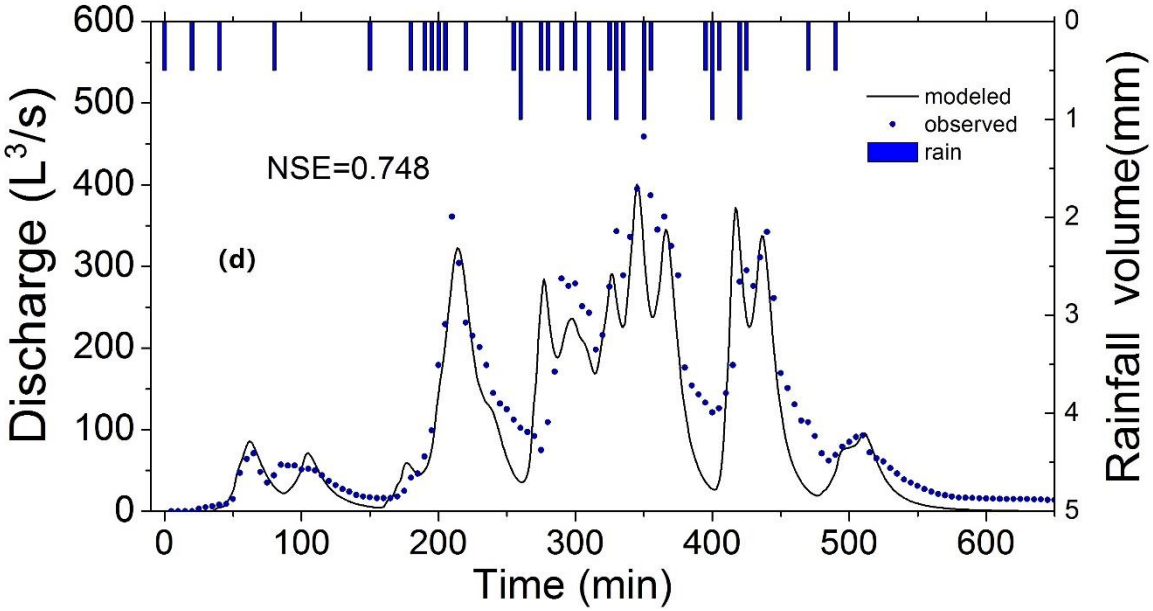

(d) Hydrograph of 5th Jul 2018 event for validation.

Fig 3.6 Hydrographs of calibration and validation events (a~d).

3.4 Discussion

This sensitivity analysis had identified the most and least important model parameters. The impervious

ratio, the depression storage and surface roughness parameters were important parameters. The infiltration related parameter were unimportant. The impervious ratio was a very important parameter. Its sensitivity was much larger than any other parameters. Nevertheless, the development of GIS and remote sensing technology allowed users to get higher quality impervious information. Actually currently the modeler could determine the impervious area in a very high accuracy. (Krebs et al., 2014) had built a high resolution model of an urban catchment and only N-conduit and depression storage parameters were calibrated, the model showed good performance during validation. On the other hand, although the accurate impervious area can be got, they are lack of a further classification such as the determination of EIA (directly connected impervious area), which was reported to play an important role in the rainfall runoff modeling (Yao et al, 2016).

For roughness parameters, the result showed that they were important parameter. What was more, it was usually difficult to measure these parameters directly. Even though some measurement could be done, it was hard to deal with the spatial differences of the parameter. Thus these parameter were usually regarded as calibration parameter. And based on our analysis, the peak flow was suitable to use for calibrating roughness parameter.

For depression storage parameters, they were quite important in some certain situation. Actually in SWMM model these parameters were effective parameter that represent a general behavior. In our case the entire interception process including not only the interception of the land surface but also the interception of different layers plants like the canopy, shrubs and grass. Therefore, on the one hand, the total runoff amount should be used to calibrate there parameters. On the other hand, these parameters

had the potential to be further divided. One way to do this was the integrated modeling method which explicitly modeled the plant interception process. The spatial distributed remote sensing data like NDVI could be used to reduce parameter uncertainty. This will be the future work after sensitivity analysis.

3.5 Brief summary

The key parameters for calibration found in this study were the depression storage parameters and the Manning's roughness parameters. All other potential calibration parameters were found to have no or little effect on the simulation results. The high spatial resolution in this study, resulting in detailed catchment disaggregation into individual homogenous surfaces, allows very accurate initial estimates and narrow boundaries for surface properties. The chosen approach limits both the number of calibration parameters and individual parameter ranges. (Ghosh and Hellweger, 2012) showed that the scale effect of catchment disaggregation is partly induced by the effects of conduit routing on runoff dynamics for smaller storms in the range explored in this study. Conduit length decreases when the sewer network becomes less dense with coarser catchment resolution.

The calibrated model performed well in terms of the Nash-Sutcliffe efficiency with the E values of more than 0.8 and 0.7 for the calibration and the validation, respectively. The quality of high frequency rainfall-runoff data is a critical issue in a successful calibration and validation of an urban hydrological model. The calibration, addressing only the identified key parameters and hence drastically reducing the number of calibration parameters, produced good results throughout the investigated statistical

measures for both calibration and validation.

Chapter 4. Effects of model spatial resolution

4.1 Different model scales

The models of the study area were build up at 4 levels of spatial resolution (S1, S2, S3, and S4). The S1 model which had the highest resolution was build up firstly. The principles of establishing S1 model referred to some previous research about high resolution or hyper resolution urban hydrologic model (Krebs et al., 2014; Amaguchi and Kawamura, 2016; Noh et al., 2018). Each sub-catchment was built upon small urban structures like a single rooftop, a single garden or a short part of road. This made each sub-catchment to be occupied by a single land use type. The routing between sub-catchments could better represent the actual flow path at micro scale. In S1 model, not only the drainage conduits underground, but also the street gutters (small trench) with fixed cross section beside the road were considered and modeled explicitly.

The sub-catchments of S2 model was discretized based on the urban blocks. The idea was similar to the concept of Urban Hydrological Elements (UHEs) proposed by Rodriguez et al., (2008). In S2 model a sub-catchment included a single residential block and the road surrounding them. All the gutters was neglected in this level but all underground conduits were remained.

S4 model was delineated by the partitioning information of pipelines system provided by Sewer Administration Office. The whole catchment was divided to 6 sub-catchments. Those sub-catchment drains directly to a most downstream inlet within the sub-catchment and the pipes located at upstream

of that inlet was neglected.

S3 was a transitional scale between S2 and S4. Several adjacent blocks in S2 were aggregated to form larger UHEs than S2 model according to the drainage directions. Similar with S4, the pipes within each sub-catchment was omitted. The spatial representations of models were shown in Fig 4.1and a brief summary of these 4 levels of models was listed in Tab 4.1.

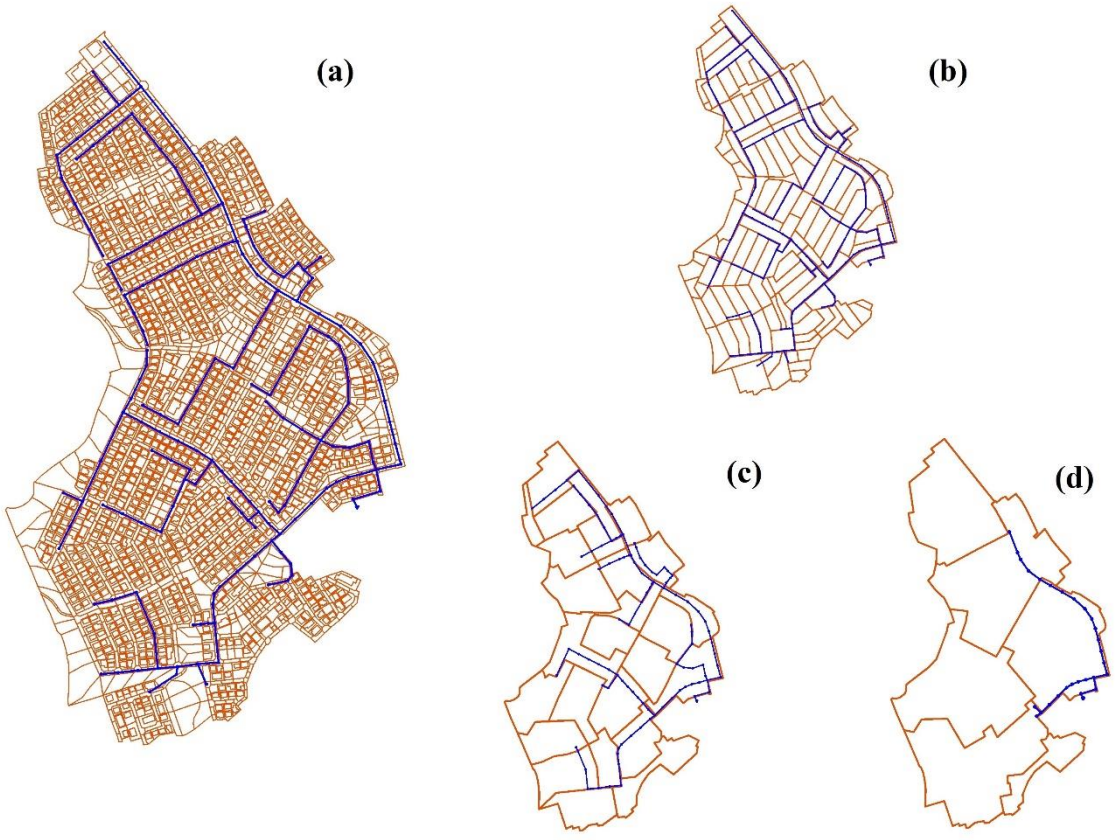

Fig 4.1 The spatial resolutions representations of different model scales: (a) S1 model; (b) S2 model; (c) S3 model; and (d) S4 model. The orange lines showed the boundaries of the subcatchments; the blue lines showed the underground pipes modeled. The gutters in S1 model were not showed here.

Table 4.1 Characteristics of 4 models with different level of detail.

Model	Sub-catchment number	Average sub-catchment area (m^2)	Modeled conduits	Total conduits length (m)
S1	3216	143.4	All Pipes and street gutters	18331.1
S2	147	3138.1	All pipes	6400.9
S3	26	17742.2	Partial pipes	3642.3
S4	6	76883.3	Partial pipes	1033.8

Area weighted average of parameter values. After the calibration of S1 model, the parameters values of S2, S3 and S4 model were derived from S1 model by parameter upscale. Most of the parameters including the imperviousness, slope, depression storage and roughness were calculated by area weighted average method during upscale process. Dominant parameters like the proportion of EIA (Effective Impervious Area: the impervious area which were directly connected to drainage sewer) and TIA (Total Impervious Area) within particular area were conserved during upscale. In the SWMM model, the pervious sub-area routing was set as the routing mode in order to represent the EIA proportion within sub-catchments by adjusting the sub-area routing ratio (Kong et al., 2017). The width parameter were determined using the method proposed by (Guo et al., 2011) because it took sufficient consideration of the impact of surface flow convergence pattern on width parameters.

4.2 Results and comparison

After the parameterization, these models would run under different rainfall events to find how the model

spatial discretization degree affected the simulation results. The rainfall used for simulation here include the events which was collected by two tipping-bucket rain gauges within the catchment from 26th February 2018 to the 29th July 2018 and include 23 individual events with a record resolution of 0.5mm. Those measured rainfall events were also used for model calibration and validation. Some additional rainfall data got from the Japan Metrological Agency were also used in the simulation. These rainfall data included 39 rainfall events from July to October of 2017 and was collected by a metrological station at Sendai city which was around 4.2 km to the study site with 0.5 mm resolution. Those original rainfall data were processed into rainfall data with 5 minute temporal resolution that can be used in the hydrological models. All those rainfall data were used for simulation to observe the scale effect of model.

The S1 model was firstly calibrated. The detailed information were mentioned in Section 3.2. Afterward, the parameters of S2-S4 models were determined by area weighted average method in upscale process. And those models with different resolutions were run under all the 62 rainfall events. Fig 4.2 showed the hydrographs of two rainfall events: 5th Mar 2018 and 17th Sept 2017. It can be seen that the model's response to rainfall was weakened with the decrease of resolution with the most obvious phenomenon to be the deceasing of peak discharge. The decreasing trend of peak discharge was more distinct in the 17th Sept 2017 event.

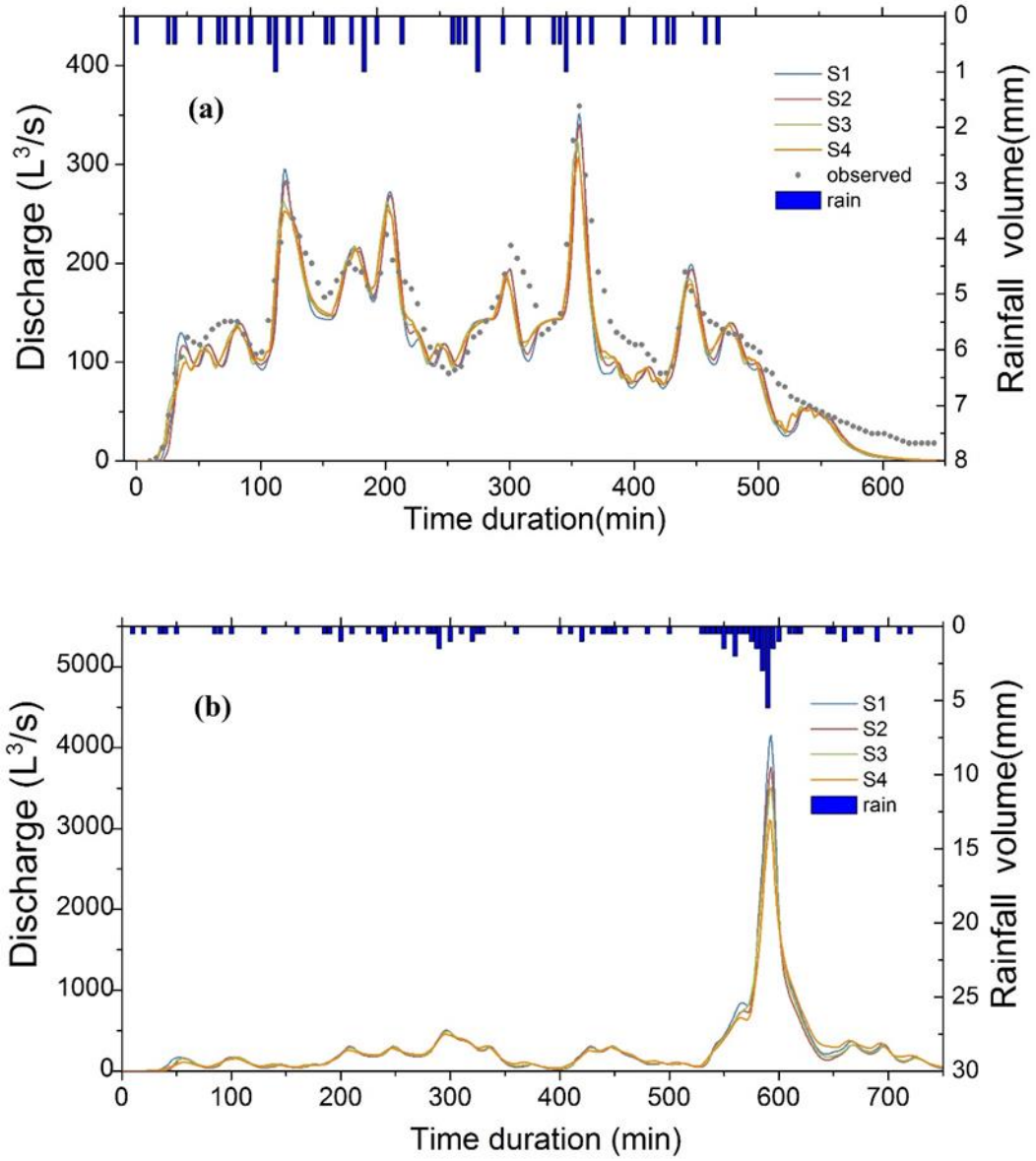

Fig 4.2 Hydrographs comparing of models with different resolutions. (a) Rainfall event of 5th Mar 2018; (b) rainfall event of 17th Sept 2017.

In order to compare the results of all the rainfall events, the general trends observed in the hydrologic outputs should be identified. The S1 model with the highest resolution was used as reference model. Hydrological modelling outputs were analyzed based upon these statistics: relative peak flows and relative total flows. The peak flows and total flows were normalized to those results of the S1 model.

Fig 4.3 had generalized the results of all the rainfall events simulated. It can be seen that as the spatial scale of the model decreased, the total flow and peak flow tended to decrease as well. While the variations of total flow were very slight, and the peak flows of different resolution showed a distinct variation.

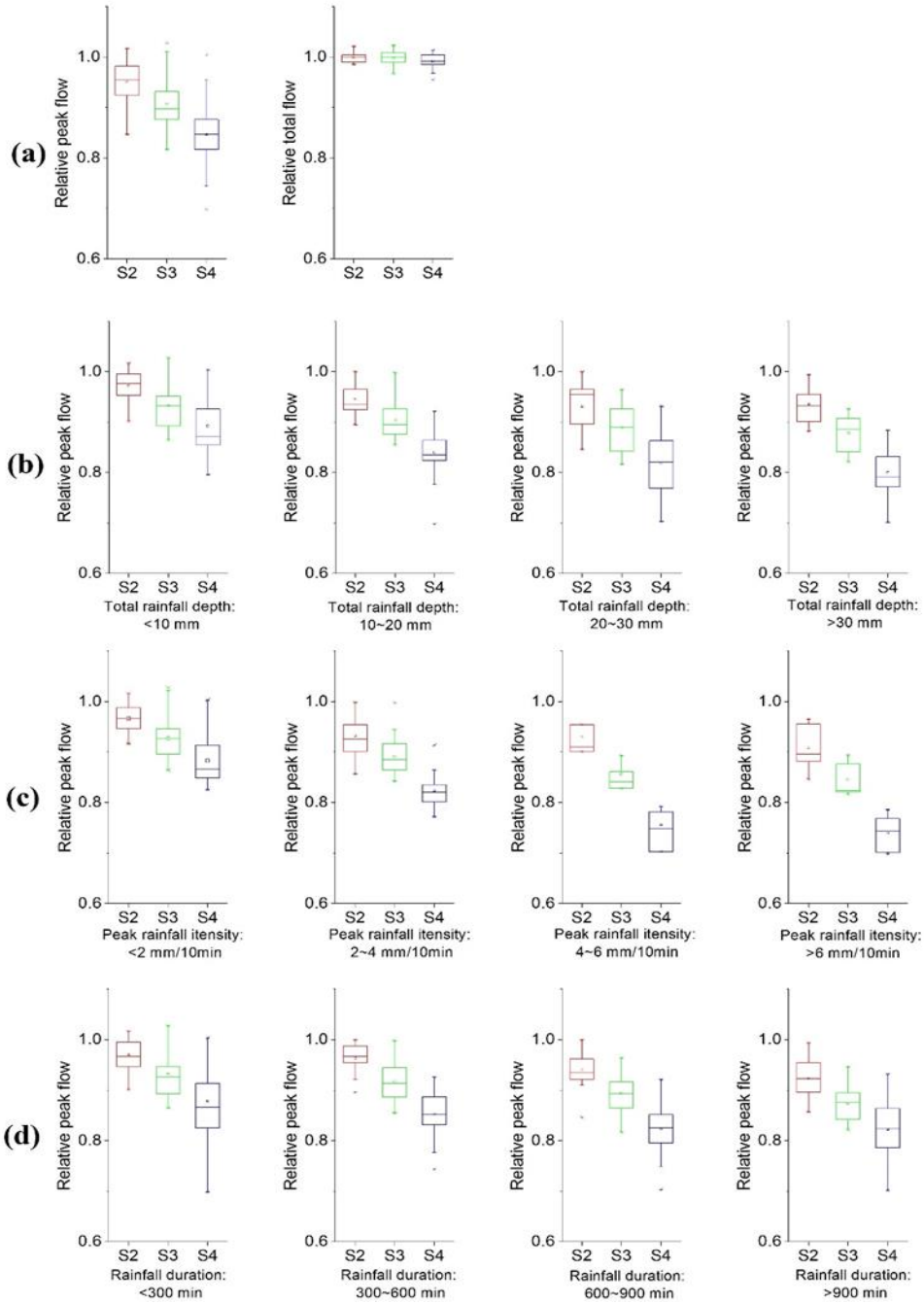

Fig 4.3 Boxplots of relative peak and total runoff (S1 results as the reference value). (a) relative peak and total runoff for all rainfall events; (b) relative peak flow for different rainfall depths; (c) relative peak flow for different peak rainfall intensities; (d) relative peak flow for different rainfall durations.

4.3 Analysis of scale effects

Generally speaking, the coarsening of model spatial resolution lead to a decreasing of both peak runoff and total runoff. It should be pointed out that not all simulation scenarios strictly follow this trend, and actually there were exceptions in the results. However, from the larger point of view, this general trend was clear. At the same time, rainfall characteristics had an impact on the degree of models' scale effect. The larger the peak intensity and total depth, the more obvious the scale effect (fig.3 (b) and fig.3 (c)). Thus the impacts of rainfall should be considered simultaneously. In order to quantify those scale effects, the method of dimensional analysis (Legendre et al., 2012) was used here.

Since the total flow rate showed little variation with different spatial resolutions while the variation on the peak flow rate was more obvious, only the results of the peak flow rate was quantified. The sub-catchment average size dx (square of average sub-catchment area) and drainage density dd (total conduits length divided by catchment area) was used to represent the level of discretization degree of different models. The peak 10 minutes rainfall intensity Ipk was used to represent the rainfall characteristic. The relative peak flow was selected as the independent variable, and the other factors were selected as the dependent variable. Then a scatter plot of the independent variable and the dependent variable were made. After several round of trial and error, an empirical relationships were obtained.

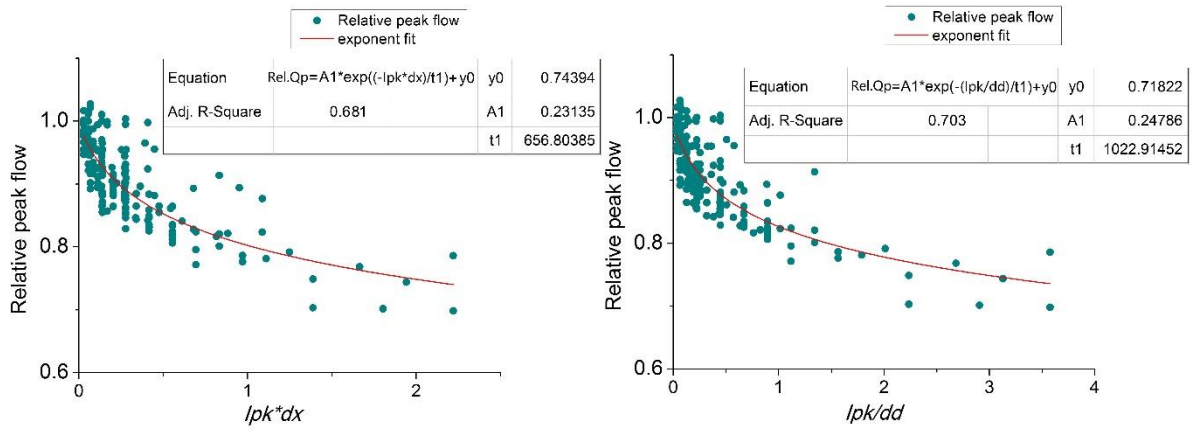

Fig 4.4 Scatterplots of relative peak flow versus combinations of rainfall intensity (Ipk) and resolution index (dx, dd).

In Fig 4.4, the relative peak flow were plotted as a function for different resolution and rainfall intensity combinations. An exponent function was fitted to the resulting plots. The function structure was defined as:

$$Rel.Qp=A1*exp((-Ipk*dx)/t1)+y0 \quad (4\text{-}1)$$

$$Rel.Qp=A1*exp((-Ipk/dd)/t1)+y0 \quad (4\text{-}2)$$

The obtained A1, t1 and y0 parameters and the associated coefficient of determination (R2) of the fitting were summarized in Fig.4. The exponent functions provided a rough estimate of what hydrodynamic modelling performance could be expected for a given input resolution and rainfall peak intensity.

After obtaining these results, another question was how to use these results. Fig 4.4 had showed the relationship between relative peak flow and resolution with rainfall intensity. My opinion is that these results could be used as an error estimation framework in practical situation. In practical usage of hydrological models in a new area without observed flow data. In such a situation, the determination of the parameter will refer some manual or previous studies. In such a case, the scale differences should

be noted. If there were scale differences, there will be errors in modeled results. Also the impact of rainfall will be considered because rainfall intensity is one major factor that can affect the peak flow estimation which is one of the most important purpose of modeling. The results showed in Fig 4.4 can help determine the peak flow estimation errors for certain model scale under certain rainfall intensity.

4.4 Parameters variation analysis

S2, S3 and S4 models were calibrated independently to find if calibration overcome the scale effect and how the parameters will change. Following the calibration of S1 model, here 5 calibration parameters were selected: The depression storage parameters (di and dp) and the roughness parameters (ni, np and nc). Other parameters like Slope, TIA and EIA were obtained by area weighted average. As stated in section “Model parameterization and simulation design”, due to its importance and particularity, EIA was necessary to be considered as calibration parameter. So this generated a secondary calibration scenario in which EIA was regarded as unknown and thus 6 parameters were calibrated (5 above parameters and EIA). The models performance during calibration and validation period were shown in Fig 4.5.

It was clear that the performance of S2-S4 models were similar with S1 model after independent calibration. The NSE value of all the model exceeded 0.83 for calibration sequence and 0.71 for validation period. This indicated that calibration process could compensate the differences caused by scale effect. The calibration performance of models were almost the same, while the prediction ability had small difference. For the NSE during validation period, of S1, S2 and S3 were slightly higher than

that of S4.

When EIA was regarded as calibrated parameter, the models performances in calibration period was quite good and NES value were equal to or slightly better than the previous calibration that did not taken EIA into consideration. However, the NSE values during validation period were relatively lower than previous results. Among them the NSE of S4 model had an obvious declining. This phenomenon indicated that the calibration method had caused over-parameterization in a certain degree. The above analysis demonstrated that it was better to use the detailed spatial distributed EIA parameter in model application when this information was available.

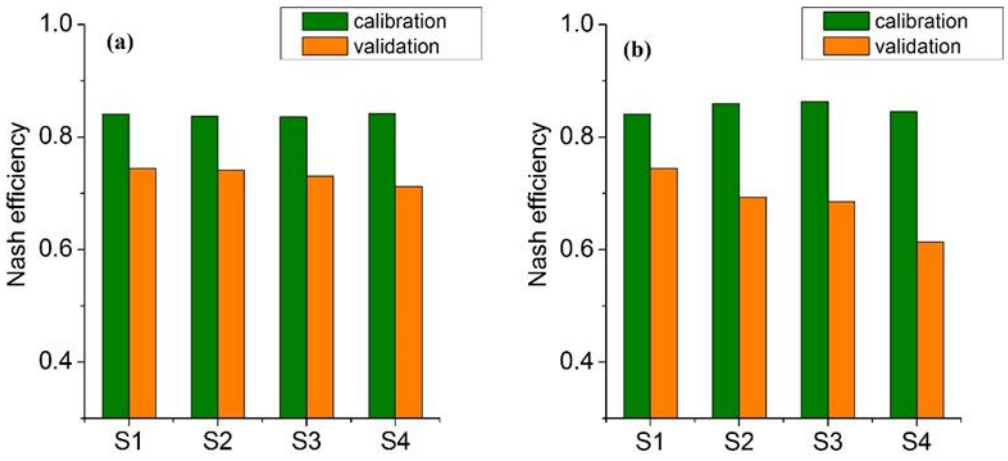

Fig 4.5 Performance of models for independent calibration. (a) Roughness and depression storage were calibrated parameters; (b) roughness, depression storage and EIA were calibrated parameters.

In order to better represent the spatial resolution effect on model calibration, the NSE response surface of certain parameters were analyzed. Fig.6 showed a certain slice of objective function surface for ni vs nc, EIA vs ni and EIA nc bi-variance parameter domain while other parameters remained at their optimal values. It was obvious that the domain of ni and nc showed a long strip structure. This indicated that

those 2 parameter interact with each other. This kind of dependence between parameters was harmful to model build up and parameterization. The reason for this phenomenon was that the model structure and certain assumptions in which all the runoff was firstly in the form of overland flow and then all the runoff drained into an inlet and became conduit flow. This assumption simplified the complex runoff process and the interactions between different flow pattern and may be had large differences with real world process and thus caused conceptual error (Leandro et al., 2016; Salvadore et al., 2015).

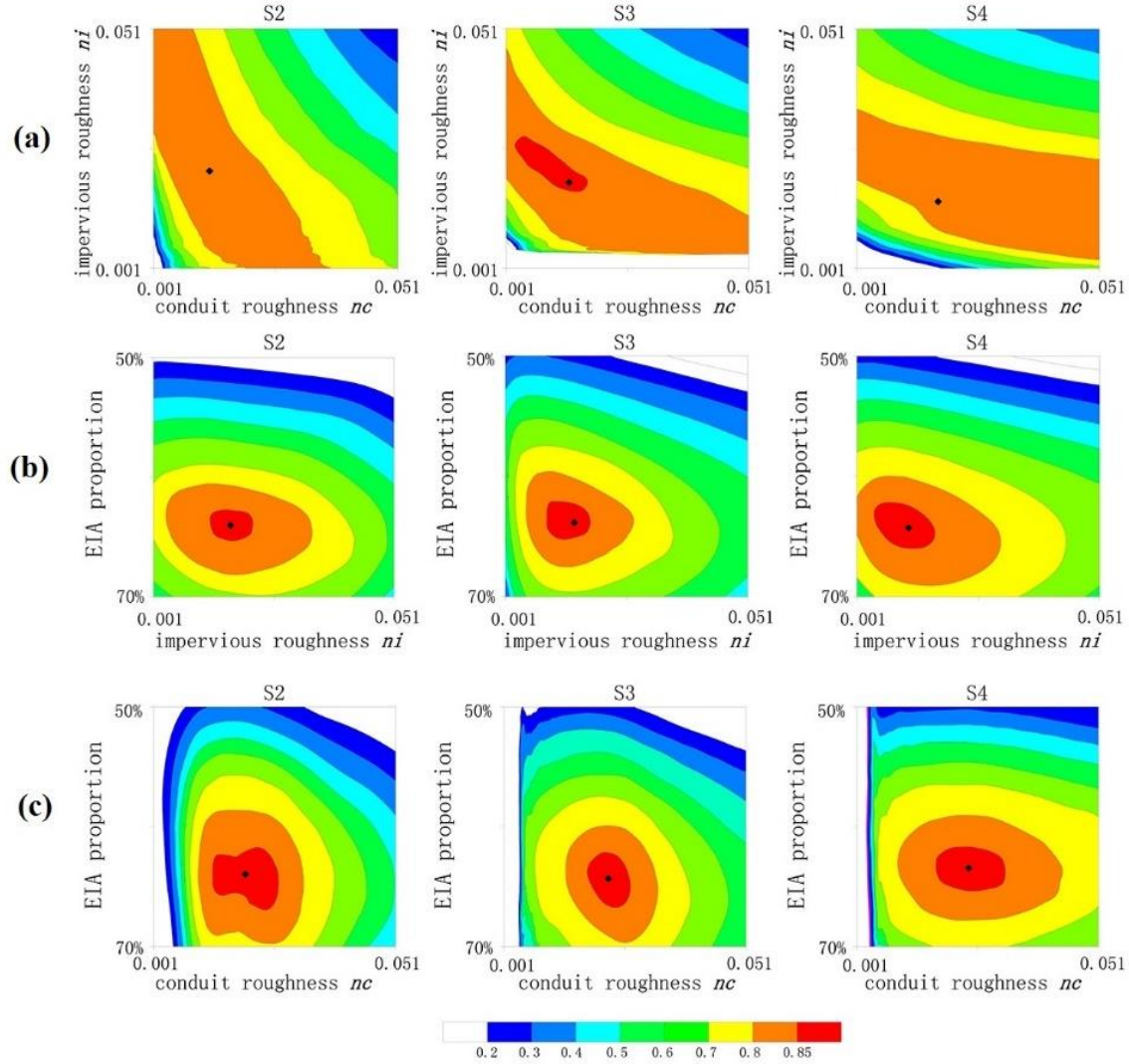

Fig 4.6 Impacts of model spatial resolution on the response surface of performance objective function (NSE). Several principle parameters conbinations were considered: (a) ni vs nc, (b) EIA vs ni and (c) EIA vs nc. The black dot represent the calibrated optimal value.

When EIA was introduced, the NSE response surface showed large difference with that of the ni vs nc. Firstly, as EIA had a relative large impact on model, the shape of NSE contour had a big change with the direction of EIA. And relatively, the impact of ni and nc parameter were weakened. Different from previous, the EIA did not show clear interaction or dependence with ni and nc parameter. The shapes of the NSE contour were no longer a strip but oval. All the scenarios had a similar macroscale shape with different microscale features.

The optimal calibrated parameter values were also showed in Fig.6. It could be seen that the values of impervious surface roughness (ni) had a declining trend with the increase of model resolution. The calibrated ni parameter values of S2 to S4 models were 0.022, 0.019 and 0.015 (fig.6 (a)). It is mainly because that the peak flow variations of different models were compensated by this parameter. The values of conduits roughness (nc) did not show a clear pattern after calibration. The calibrated EIA ratio were quite similar among different model scales and this emphasized the importance of correctly determining EIA value in model applications. The area of the orange region (NSE>0.8) and red region (NSE>0.85) indicated the degree of equifinality of the models. It can been seen that the equifinality existed not only in different parameter sets of the same model but also among different models.

As stated in Section 2.1, the drainage system divides the study area into 2 drainage catchments: a larger one of 41 ha and a smaller one of 5.1 ha. Previously calibration and validation were based on the runoff data observed at outlet of the larger catchment (OT1). For models with different scales, the corresponding optimal parameters values were determined by model calibration. In order to evaluate

the universality of those calibrated parameter sets. The calibrated parameters values of the larger catchment models were used in the small catchment models of corresponding spatial resolution.

The results were shown in fig.5. In the aspect of NSE value, the performance of all the scales had a declining compared with catchment alpha. Among them, S1 and S2 model had a relative low declining and S3 model had a larger decrease in NSE performance. This indicated that the best solution found by calibration could be the optimal at entire catchment scale but not at local scale. The reason could be that the equifinality effect was difficult to eliminate and this hampered the small scale performance. Also, there could be errors on model structure and parameterization and global optimal is a result of errors compensating with each other which lead to poorer performance at local scale. The actual reason was probably the combination of above possible explanations.

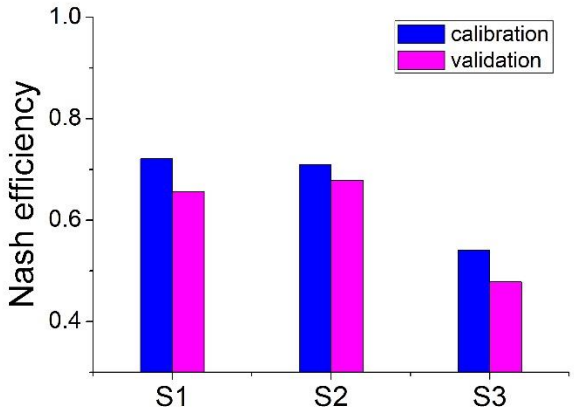

Fig 4.7 Performance of models for regionalization of the OT2 outlet during calibration and validation period.

This kind of performance declining at local scale manifest that there were disadvantages of current used single point data calibration method. Thus, the distributed calibration or process based calibration should be advocated in order to improve local scale performance of distributed model. The error

identification or reduction of model structure is also important. For example, a model sub-catchment can represent a very small area like single roof top and it can also represent a relative large catchment which main contain hundreds of roof tops and conduits. But we actually expect them to have a same performance pattern. Thus the improvement of model theory is still essential. A detailed distinguish and quantification is beyond the scope of this research but is an interesting topic in future research.

4.5 Discussion

There had been some previous studies on model scales issues but the conclusions are not the same. (Ghosh and Hellweger, 2012) found that the total discharge was not affected by the model resolution while the peak flow rate showed a dual scale effect. (Guo et al., 2011) concluded that that a model with more drainage details results in higher peak flows. However, in these studies, the method to determine or maintain the parameters at different spatial resolution modes was ambiguous. (Krebs et al., 2014) had found that model aggregation increased peak flow rates but this could be due to that the EIA parameter was not maintained: all the imperviousness area in high resolution model became EIA in low resolution model. In this study we found that the model aggregation led to a decrease in peak flow while the total runoff was not affected. By summarizing the above studies, it could be found that, in general, the total outflow was less affected by the resolution of the model, while the peak flow was affected more greatly with different variation trends. This could be because of that total outflow were controlled by several important factors: The infiltration rate, the pervious ratio and the EIA ratio. All these factors were kept constant at catchment scale using areal weighted average method during the upscale. So the infiltration process and infiltrated amount were quite similar in different models, this is why the total

flow changed little. While the peak flow is quite different. Although the factors responsible for peak flow rate (the roughness parameters, the slope and depression storage parameters) were obtained using area weighted averaged method, the surface runoff routing process itself was non-linear. Also different EIA distribution may have an impact on peak flow. So the peak flow rate cannot be maintained across scales.

Meanwhile, our results show that rainfall characteristics also have an effect on the scale effect of the model. Then the scale effect caused by spatial resolution and rainfall intensity was quantified. The quantification results showed that a exponent function can well represent the scale effect and this can be used as an error estimation method in practical application. Those quantification had provided useful insights into the impacts and interactions of model resolution and rainfall characteristics but should be applied with caution in practical use.

While discussing the impact of model spatial resolution on the results, the calibration of models with different resolution is also worth mentioning, which include the performance of the model after calibration, and the comparison of the calibrated parameter values (Merz et al., 2009; Wildemeersch et al., 2014). When considering only the roughness and depression storage parameter, the models can always have satisfied performance with respect to resolution. When the EIA is considered, the predictive ability showed a decline. This indicated that EIA and its distribution were key information for the model. Therefore, when then benefit of high resolution data were removed (EIA considered as unknown parameter), a coarse model resolution may lead to a relatively poor EIA identification and performance. The selection of model scale should be related to the data obtained and purpose of the model. In our

case, the scale of S2 and S1 were both considered satisfying while the S3 and S4 model had the potential of performance declining. Thus it is suggested that in such small urban areas the urban block scale is recommended in hydrological modeling.

Also, the response surface analysis suggested that equifinality existed among different models and parameter sets, and the scale of the model had a certain influence on the parameter domain and the corresponding surface. Among them, the parameter ni, nc has an interaction relationship, and its response surface shape was greatly affected by the accuracy of the model. The corresponding surface associated with EIA was more stable in shape. On a large scale, the reduction in accuracy did not destroy the shape of the corresponding surface, nor does it led to mathematical artifacts. The distribution information of EIA only affected the performance of the model to a small extent although several previous research suggested that EIA distribution had a great impact. This would be a topic worthy of further discussion.

4.6 Brief summary

This Chapter attempted to analyze how the model performance and parameter optimization were affected by model grid resolution for a given model structure, SWMM. The performances of models with different resolution were compared. The parameterization and prediction capacities were discussed during and after the calibration. The conclusions are as follows:

Although weighted average method was used, there were obvious scale effect across models due to the non-linearity nature of model structure. With the coarsening of grid, both the total and peak runoff tend to decrease while the variations of peak runoff rate was quite obvious while the relative differences can be larger than 30%. The effect of spatial resolution on simulated peak flows is also influenced by storm characteristics. The impact of these factors was quantified by dimensional analysis and a exponent function was fitted to the resulting scatter plots. This provide useful insights into the impact and interaction of spatial resolutions and other factors as well as a practical estimation of the performance that can be expected for a given model input resolution.

After independent calibration, all the models showed satisfying performances. The performance of the calibrated models were similar to the S1 model (NSES2=0.837, NSES3=0.836 and NSES4=0.841). This meant that calibration could completely compensate models' scale effect. When EIA was considered as a calibrated parameter, the NSE value of S2, S3 and S4 model during calibrated period were 0.859, 0.863 and 0.845, while the performance of validation period hold the line or decreased (NSES2=0.744, NSES3=0.685 and NSES4=0.613). The objective function surface of the models were analyzed. It could be found that the grid resolution led to the change of the overall shape of the surface and deviation of the best performance area.

Chapter 5. Interception process and energy balance modeling

5.1 Interception modeling and integration

There were a lot of parameters (Table 5.1) in Rutter model and one of the most important one is the canopy storage capacity. The initial steps were to obtain the NDVI maps within the study area for different seasons.

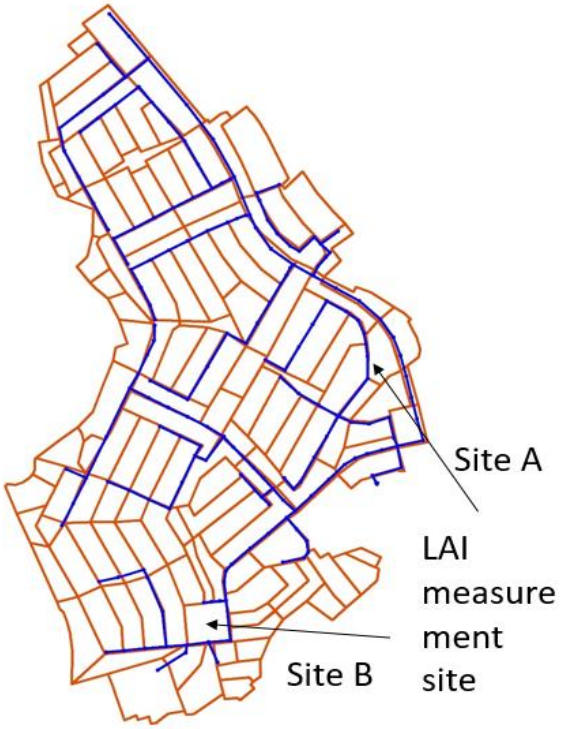

Fig 5.1 The LAI measure locations in the study area

At the same time, the LAI were measured at 2 locations within the catchments (Fig 5.1). Those 2 locations were both covered by urban forest and could be considered homogenous in a relatively larger

scale. The LAI-2200C Plant Canopy Analyzer were used to measure LAI values.

Many previously research had showed that the NDVI and LAI had a statistical effective relationship although those relationships were not exactly same. Several representative relationships from previous studies were generalized in Table 5.2 as well as their study site information. The relationships of NDVI and LAI calculated from these equations were shown in Fig 5.2.

Table 5.1 Parameters used for Rutter model. Reference values adopted from (Linhoss et al.2016)

Abb.	description	Parameterization
R_P	Precipitation (mm)	Data
P_f	free throughfall coefficient (%)	Reference U(0.06, 0.55)
p_t	stemflow coefficient (%)	Reference U(0.0031, 0.0600)
S_c	canopy storage capacity (mm)	Calculated from NDVI
C	Current storage (mm)	Calculated real-time
S_t	trunk storage capacity (mm)	Reference U(0.0037, 0.9800)
E_P	potential evaporation	Calculated from P-M eq.
E_C	Canopy evaporation	Calculated from Ep
E_t	Trunk evaporation	Calculated from Ep and ϵ
ϵ	proportion coefficient	Reference U(0.022, 0.024)
D_C	water dripping from the canopy	Calculated from Ds
b_e	empirical drainage parameter	Reference U(3.0, 4.6)
D_S	water dripping from the canopy when C=S	Reference U(0.024, 0.740)

Table 5.2 Relationships between NDVI and LAI adopted from previous research

	equation	reference	country	forest type	scale	area
1	LAI=0.57*exp(2.33* NDVI)	Sato et al,2001	Japan	peri-urban/natural forest	watershed scale	
2	LAI =5.19*(NDVI ^2.138)	Alexandre et al,2004	Brazil	natural forest	watershed scale	5973 ha
3	LAI =5.36* NDVI -0.617	Stenberg et al,2004	Finland	artifical forest		2000 ha
4	LAI =0.44+3.69* NDVI	L.Fan et al,2009	China	natural forest	site scale	
5	LAI =0.228*exp(NDVI /0.311)	L.Fan et al,2009	China	natural forest	site scale	
6	LAI =0.0459*exp(4.7955* NDVI)	Santounu et al,2015	US	natural forest	watershed scale	

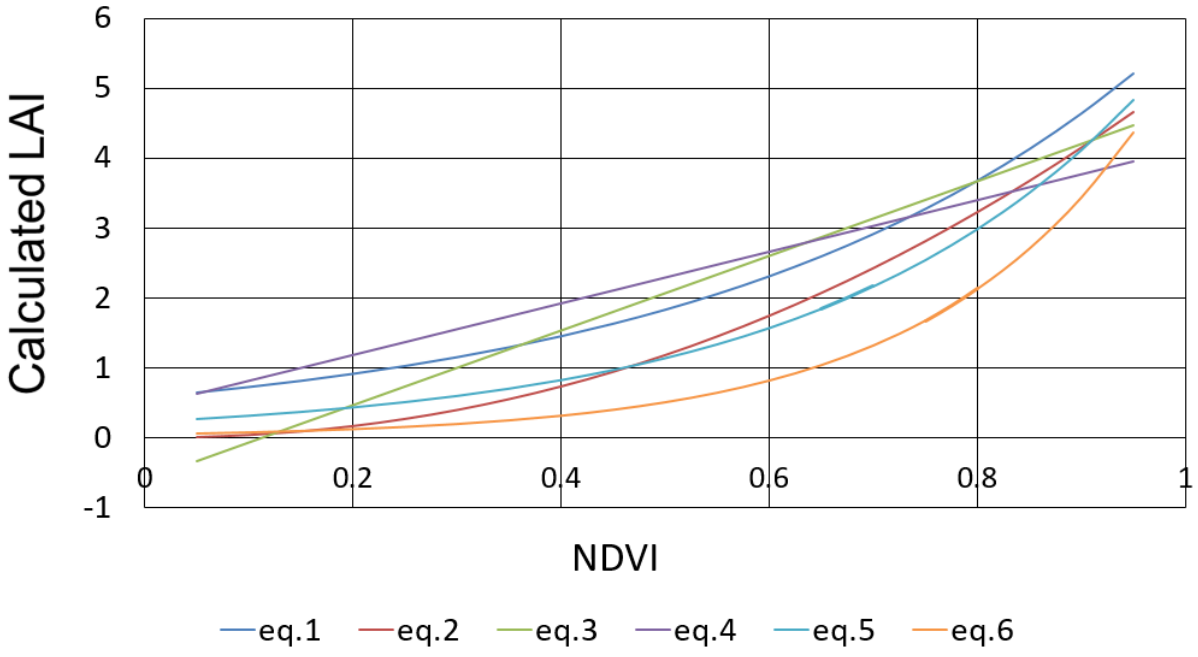

Fig 5.2 A comparison of different LAI calculate equations

Because the amount of the observed LAI data were limited, those data were used for only equations validation but not for fitting new relationships. Fig 5.3 had showed the comparison of the calculated LAI values and the measured ones. The results from Fig 5.3 suggested that the Equation.1 outperformed other equations and thus this equation were used in our calculation.

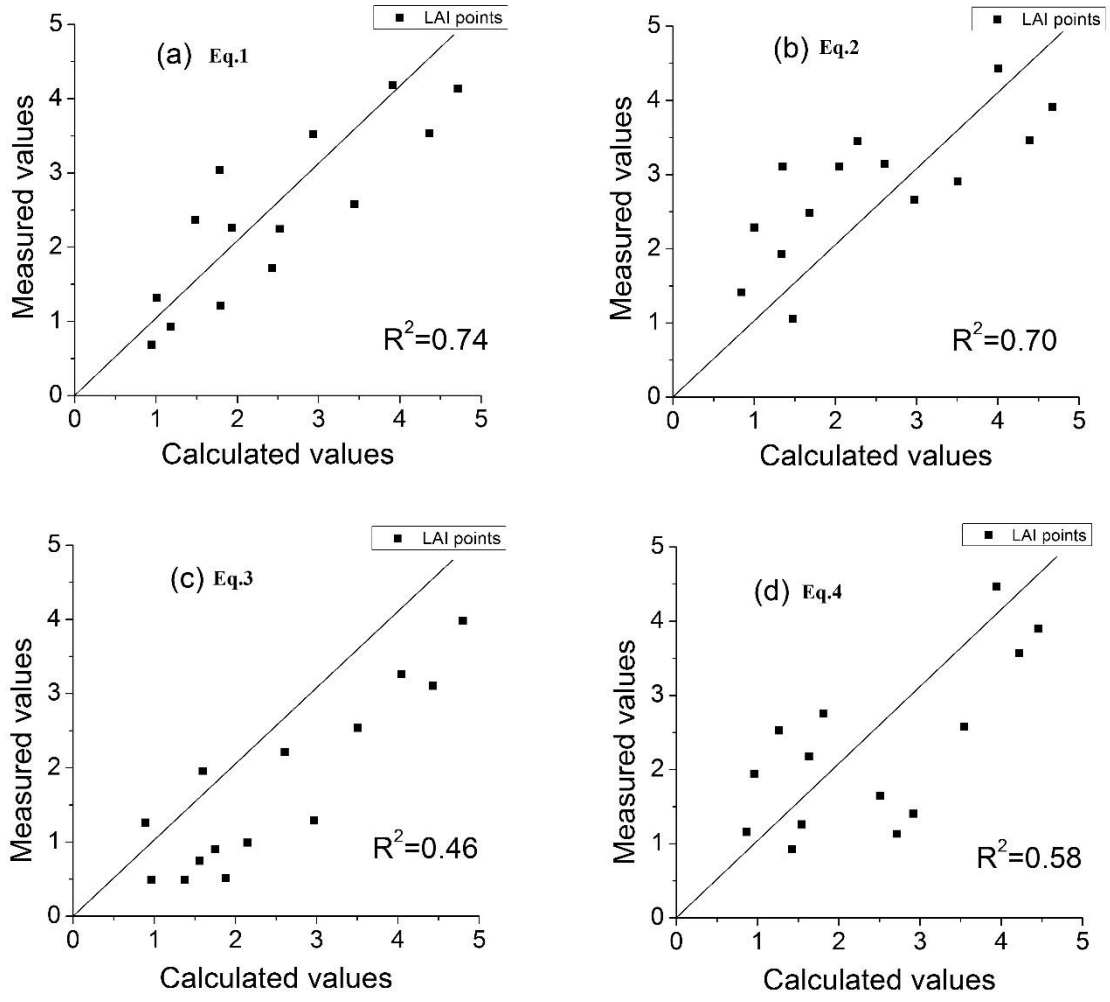

Fig 5.3 The Measured LAI value were compared with the calculated LAI value. The results showed that eq.1 had the best performance, so eq.1 was adopted to calculate LAI.

5.2 Annually variation and rainfall partitioning results

The seasonal effects of rainfall itself (Fig 5.4) are very obvious. The total precipitation from April to September accounted for more than 90% of the annual precipitation. Most of the precipitation in December, January, and February is snowfall. From the perspective of the ratio of interception, from March to July there was a clear upward trend. The proportion of interception increased from 6.7% to 19.1%, and from July to November interception showed a downward trend, dropping to approximately 12%. In proportion, this difference does not seem to be particularly large because the precipitation itself is seasonal. If the absolute intercept flow is considered, then the intercept flow in March is 2 mm, the intercept flow in April is 23 mm, the intercept flow in June reaches 29 mm, and in November it drops to 2.5 mm.

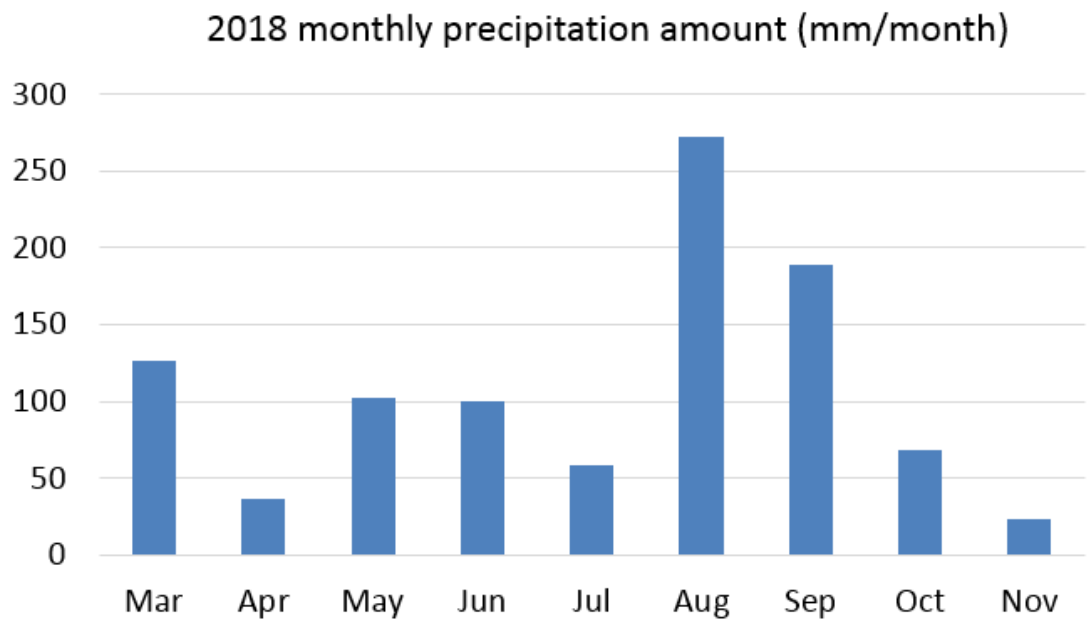

Fig 5.4 Monthly rainfall amount of 2018, with snow season excluded

During the summer seasons (May to August), net precipitation (NP) (rainwater that reached the ground surface) was 79.5% of gross precipitation (GP), whereas interception and tree surface storage was 21.5% of total precipitation. However, during the winter event, 94.5% of GP reached the ground surface as NP, and interception accounted for only 5.5% of GP. Evaporation after summer storms reduced tree surface storage, thereby increasing interception during subsequent rainfall. Evaporation and infiltration rates, seen as declining surface storage rates in Fig 5.5, were higher during the winter storms than during the summer storms.

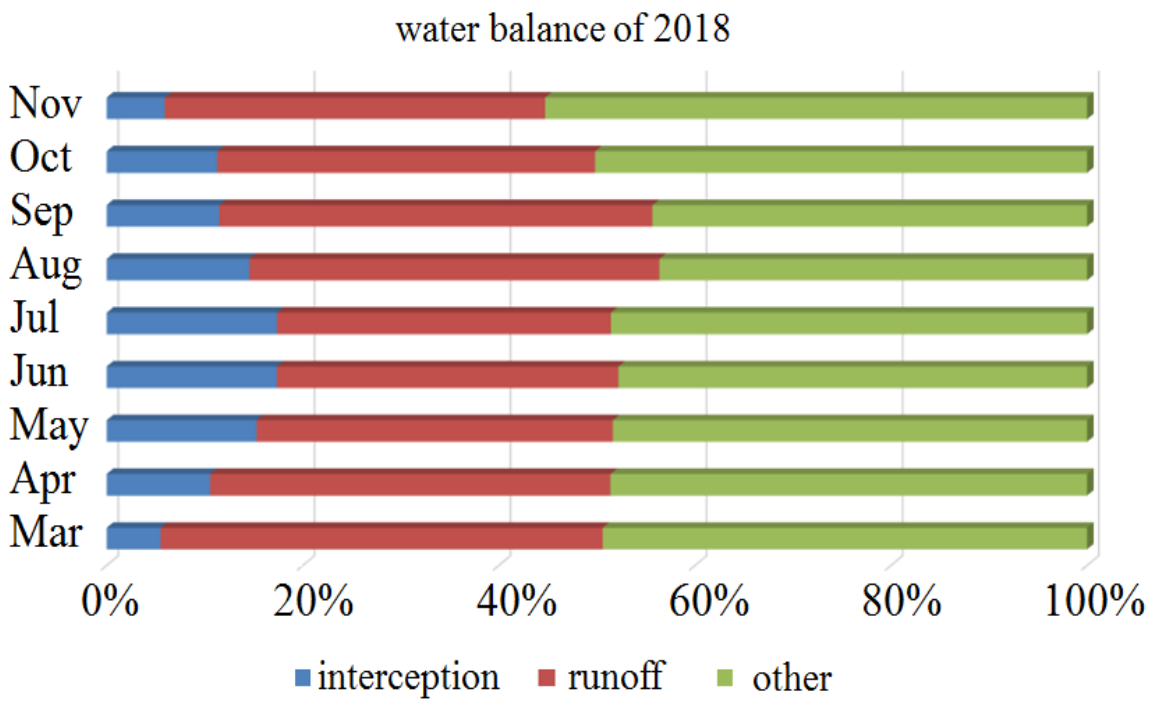

Fig 5.5 Monthly water balance of the year 2018.

5.3 Energy balance modeling method and results

For energy balance model, in this study it is relied upon not only the climate data but also the evapotranspiration time series calculated from the interception model. The calculation unit of energy balance was on the sub-catchment scale. Because of the modeling theory, the scale used and the data required, this model would have a relatively larger uncertainty.

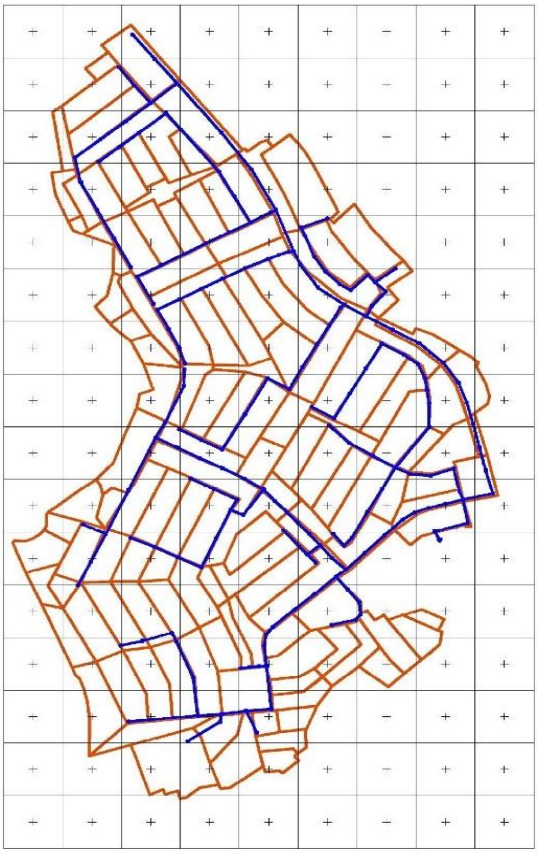

Fig 5.6 The sub-catchment (orange boundary) and the land surface temperature grid (grey grid)

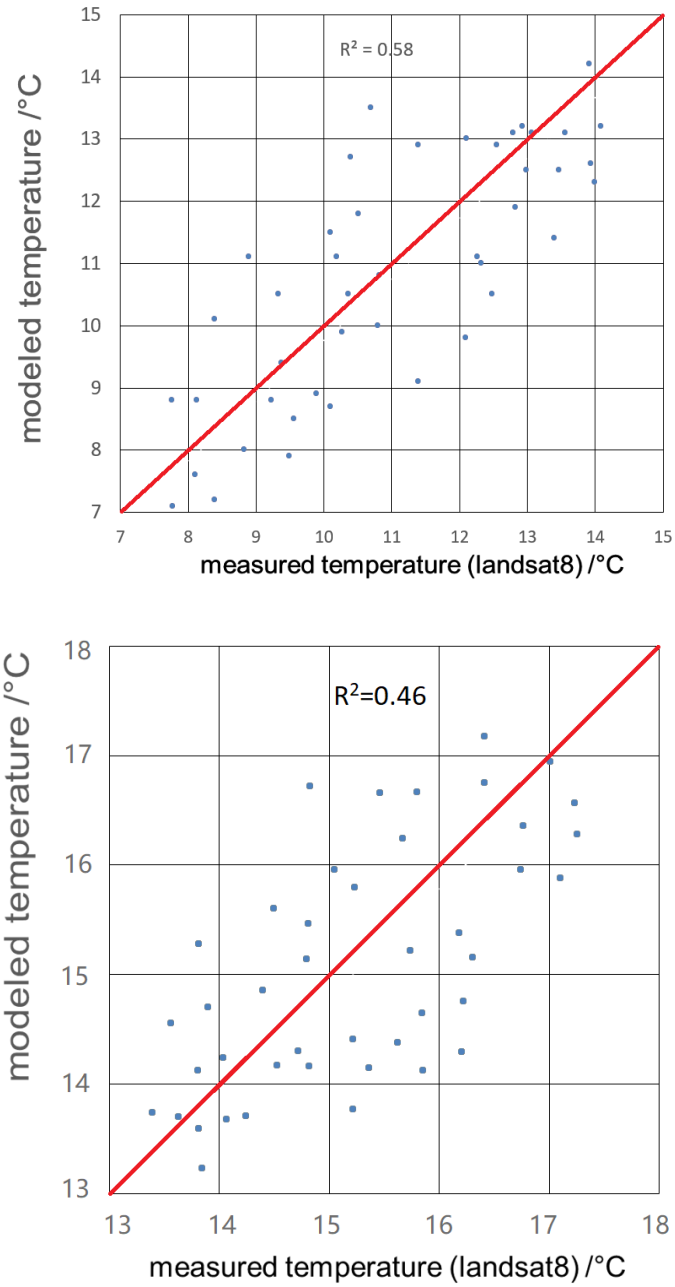

Fig 5.7 The validation of calculated surface temperature and measured temperature with landsat 8 (up: 2018-04-08, 1 am; down: 2018-05-26, 1 am).

However, due to the current technology there are difficulties for measuring the validation data (surface temperature on site), there are larger uncertainties and errors relatively. Our result showed that the correlations were neither so good nor too bad, the energy balance model performance in this study is

within a reasonable range.

5.4 Discussion

Spatio-temporal gaps exist between the physical scales of hydrological processes and the resolution of applied models. Many approaches target very specific objectives and the level of detail in representing physical processes is not consistent.

Simulations are one option to evaluate the performance and cost effectiveness of GIs. Nowadays majority of the study is focusing on relative smaller area, with the resolutions as high as possible. With higher resolutions the characteristics of greenings were easy to catch up. However, the evaluation of GI performance for large scales (i.e., an entire city) remains a challenge (Kahder and Montalto, 2008). Building the high spatial resolution model required for GI scenario evaluation is time consuming and can only be applied to small watersheds covering subareas of cities. In such a case the scale problem, both the scale on land surface and the scale of vegetation, is an important question to discuss.

In this study, the interception model is integrated to the hydrological model like and add-on, so the scale of the ground surface is the base of the scale of the interception layer. The NDVI data had fixed resolutions but the resolutions of ground surface can be variable, it is better that the scales of these two calculation unit to be matched. The higher resolution is better for descripting the process, the effect of scale changing should be discussed in advance.

Urban forest management and planning requires knowledge of optimal tree species for maximizing canopy interception when developing strategies for mitigating stormwater runoff and flooding. Forest types and structures have a direct impact on rainfall partitioning in forest ecosystems (Brauman et al. 2010). To maximize canopy interception, appropriate forest species and structure should be established and then maintained with silvicultural measures. Urban forest management activities alter the composition of forests, which can be expected to influence rainfall partitioning in canopies. The impacts of managing the forest composition were evident, and the effects of logging on rainfall partitioning have been observed in many studies (Dietz et al. 2006). Dietz et al. (2006) reported lower canopy interception in forest plots under management than in natural or unmanaged forest (18–20% versus 30% of bulk precipitation, respectively).

When canopy interception by urban forest is a priority in forest management goals, several general aspects should be considered. First, species composition should contain deciduous and coniferous trees, forming mixed forest stands. Forests containing species that are adopted to a particular site are also more biologically resilient and prone to sudden environmental (climate) changes (Beniston et al. 2007). Second, continuous canopy cover should be maintained, and larger canopy gaps need to be avoided. Finally, the deciduous trees have a relatively larger interception capability all year because their leafed period overlaps with the study area rainy season, while evergreen tree species with larger dimensions are desired due to their ability to intercept precipitation in the leafless period. In our study, all deciduous scenarios and the current scenario (majority of deciduous species with less proportion of evergreen trees) exhibited many of these features, while all evergreen forests and mixed forests had larger interception

capabilities during the leafless season, but in leafed seasons, the interception was considered to be lesser. Key findings of this study indicate that for the maximized canopy interception, urban forest structures should have mixed tree species compositions with mostly broad leaf deciduous trees. This may be useful for urban forest management and planning and could contribute to the implementation of hydrology-oriented measures in urban forests, aiming at mitigating stormwater runoff and flooding (Kirnbauer et al. 2013; Livesley et al. 2014).

5.5 Brief summary

In this Chapter, remotely sensed NDVI data were obtained and used for a distributed representation of vegetation growth information. The SWMM model and the Rutter model are coupled to simulate the urban vegetation interception process and the flow routing process. The rainfall data for 2018 were used for simulation. The NDVI data are first converted to LAI and then converted to canopy storage ability. The NDVI to LAI equations was validated using the on-site monitoring data and the equation with the highest performance (R^2=0.74) was used in this study. After the interception model, a simple energy balance model were adopted to model the heat and temperatures in the area

The results showed that the use of NDVI data is helpful in obtaining distributed vegetation information, and the interception process is simulated separately, making the model more process-based. Due to the seasonality of the vegetation, interception, as a hydrological process, also has a strong seasonality. The interception ratio during the leafed season is more than 85% of the annual interception. This is mainly

due to the increase in the degree of vegetation and the intensity of rainfall during this season. At the same time, the rainfall characteristics have a greater impact on the interception process. The smaller the rainfall is, the greater the rate of interception. The energy balance modeling results of the current situation had showed a reasonable performance compared with other studies.

Chapter 6. The mitigation of runoff and heat island by urban vegetation

6.1 Effects of plant species and aging

The average estimated stemflow was 5.33% of bulk precipitation in the all deciduous scenario, 4.98% in the all evergreen scenario, 5.48% in the current scenario and 5.56% in the mixed forest (50% deciduous + 50% evergreen). In all scenarios, the estimated leafed-period stemflow was higher than the estimated leafless-period stemflow. In the mixed forest, the leafed-period stemflow was 5.65% of the bulk precipitation, and stemflow in the leafless period was 5.2%. In the current scenario, the leafed-period stemflow was 5.8% of bulk precipitation, and the leafless period stemflow was estimated as 2.98%. In all evergreen forests, the leafed-period stemflow was estimated to represent 4.99% of bulk precipitation, and stemflow values in the leafless period accounted for 4.68%. In all deciduous scenarios, the leafed-period stemflow was 5.65% of bulk precipitation, and the stemflow in the leafless period was 4.31%.

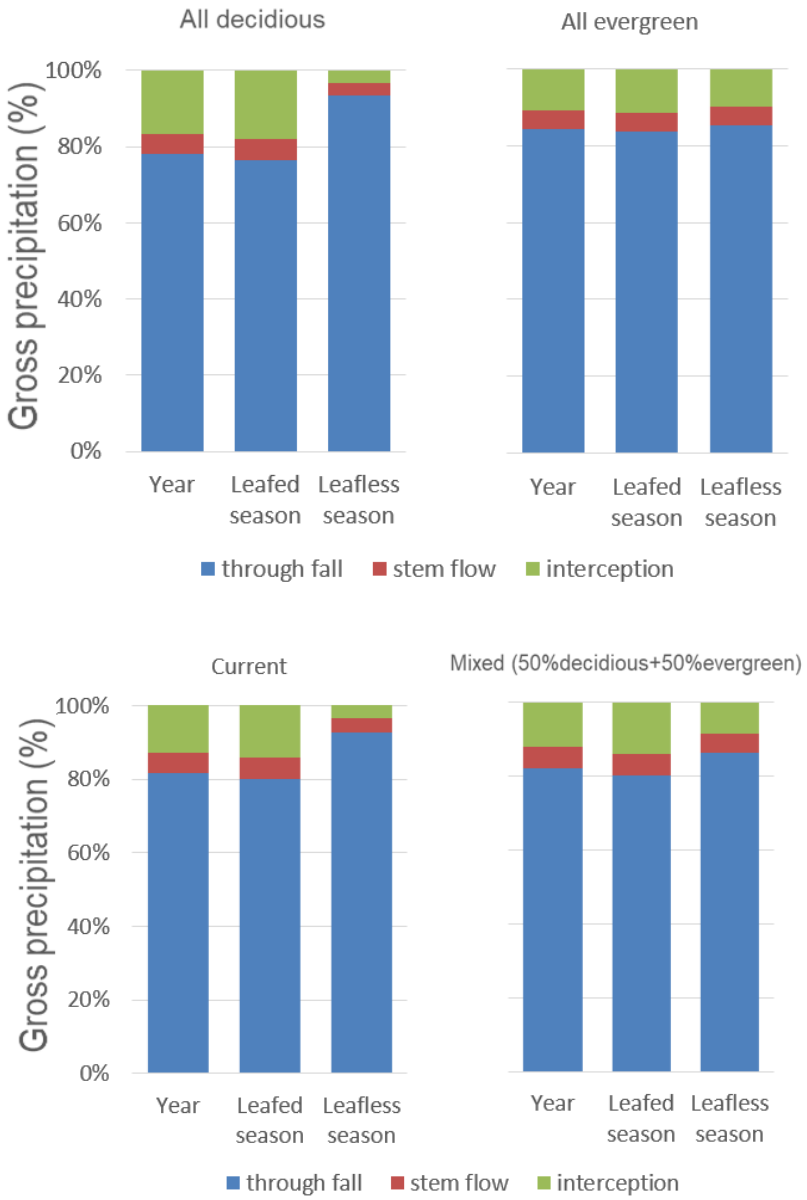

Fig 6.1 Average throughfall, stemflow and canopy interception (% of gross precipitation) for all deciduous scenarios; all evergreen scenarios; current scenarios; and mixed forest scenarios for the leafed period (from April to Sept), the leafless period (Mar, Oct and Nov), and all year.

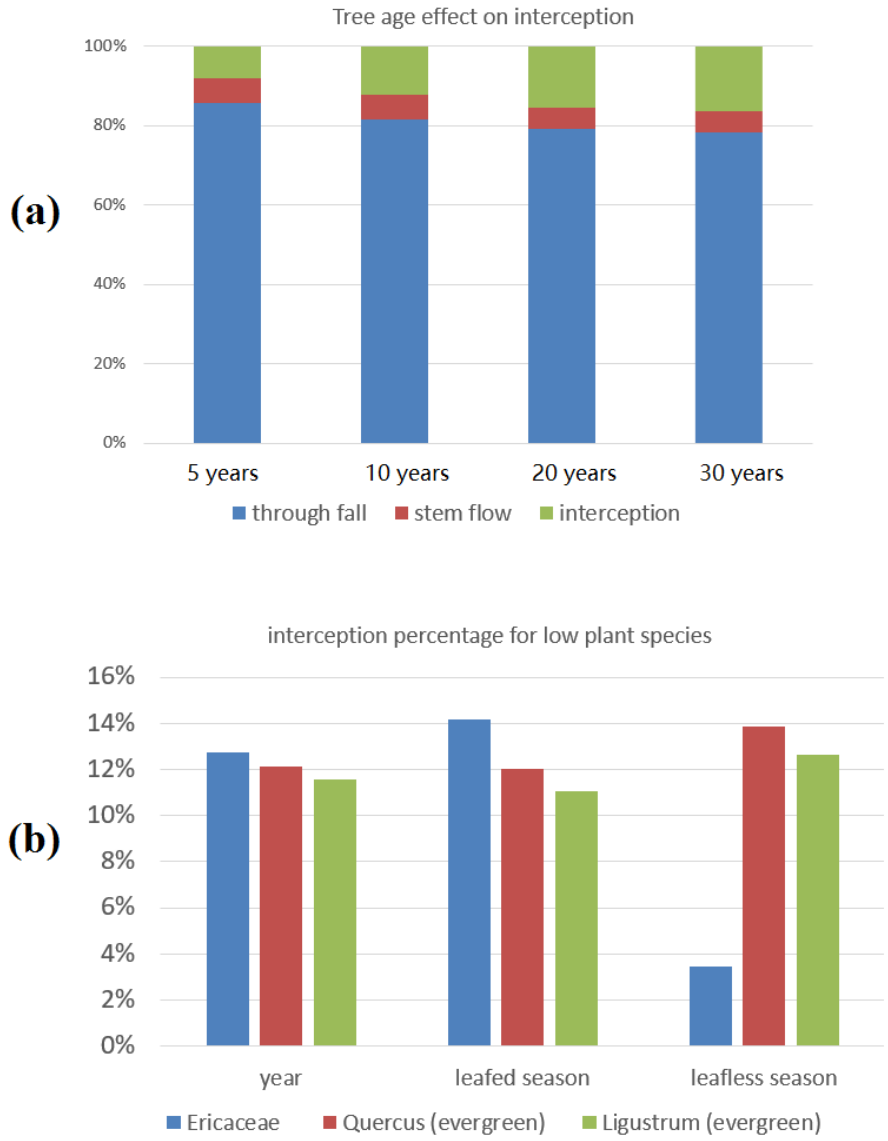

Fig 6.2 (a) The effect of canopy age on interception; (b) the effect of low plant species on interception.

Annual canopy interception was highest in all deciduous forests (16.62% of bulk precipitation) and lowest in all evergreen forests (10.85%), followed by mixed forests (12.12%) and current scenarios (12.72%) (See Fig 6.2). Seasonally, the all deciduous forest exhibited the largest seasonal differences in canopy interception, followed by the current scenario forest, which had considerably higher leafed-period canopy interception compared to that in the leafless period. In the mixed forest, where the leafed-period canopy interception was higher compared to that in the all evergreen forest, seasonal canopy

interception partitioning was nearly identical. In addition, the leafed-period canopy interception in the mixed forest was only 0.4% lower compared to that during the leafless period. The age of the trees also has a certain impact on the interception. As the age of trees increases, the proportion of interception shows a more obvious increasing trend. At the same time, the proportion of the stem flow decreases with the increase in the age of the tree, which may be due to the effect of the increase in the leaf area being significantly greater than the increase in the trunk. Low plants also have an effect on the overall intercept ratio, but the magnitude of the impact is relatively small. This may be because the low biomass has a relatively small biomass and thus has a weaker impact on the overall ratio. In general, the situation of Ericaceae species has the largest interception ratio throughout the year.

6.2 Combination of other green infrastructures

The results (Fig 6.3) showed that GI is effective in reducing flooding within the study area. Three different possible green infrastructures were considered: the green roof, permeable pavement and permeable trench. Urban canopy (UC) was also considered a green infrastructure here. The effects of each GI were evaluated separately. After that, evaluation of flood reduction was performed using combinations of the three types of GIs and the UC. For example, the peak flow reduction rate of the UC+GR scenario was as high as 28% under the whole year rainfall average. However, flooding cannot be eliminated under the different GI scenarios for all rainfall events, and the effectiveness of the various GI practices was diminished under scenarios of heavier rainfall. Therefore, combinations of green and gray infrastructure will result in improved flood mitigation effects. Because of the high densities of

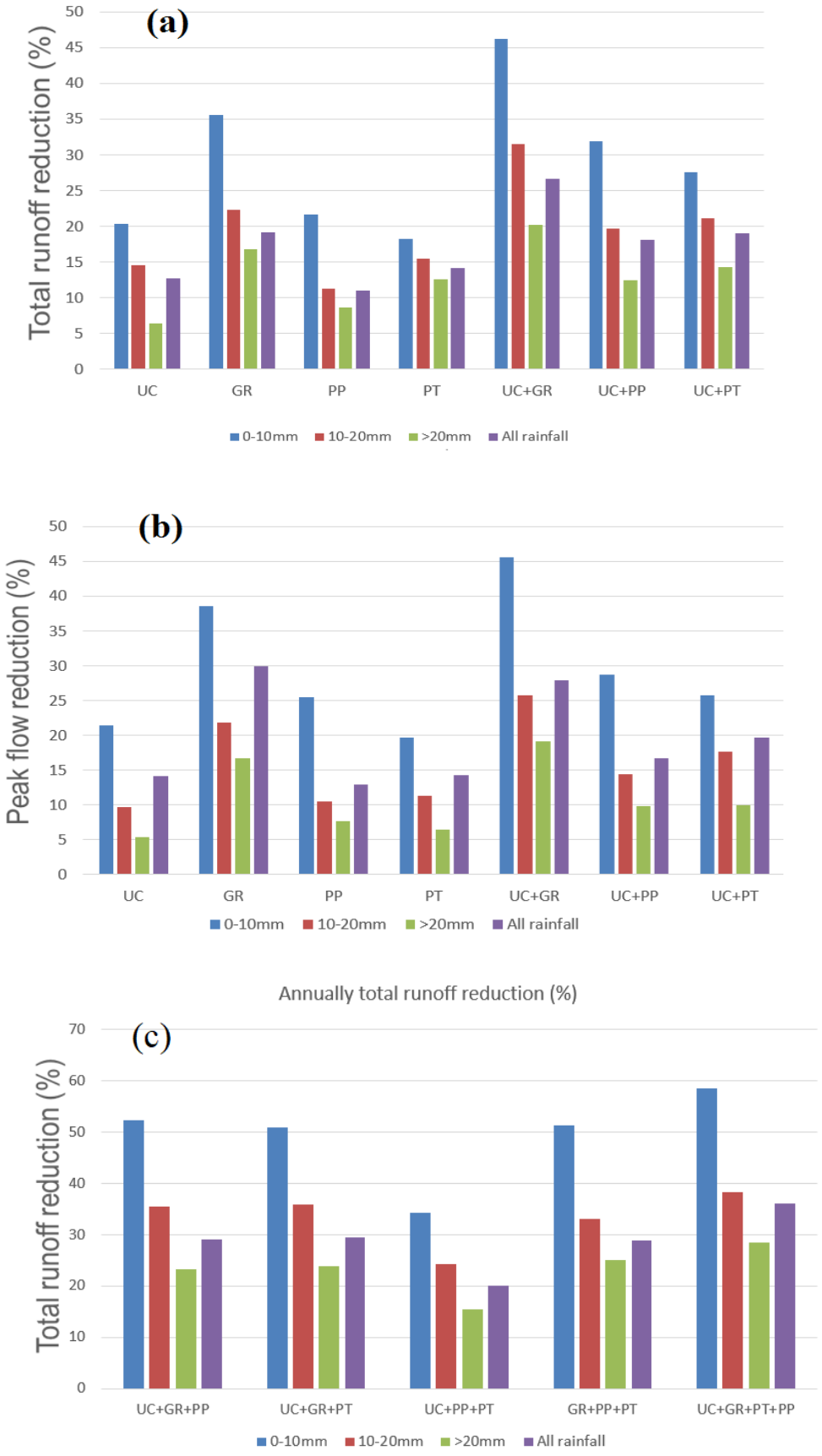

Fig 6.3 Runoff reduction effect with different green infrastructures.

buildings and populations in urban areas, the implementation of GI often involves many stakeholders. However, the implementation of gray infrastructure reduces land occupation, indicating that the combined development of green and gray infrastructure could be practical, even in megacities.

The GI performance varies with the variations in rainfall scenarios, and the effectiveness decreased with increasing rainfall amount because the GIs are interception or infiltration-based flood control measures, and under heavy rainfall events, the GIs are easier to saturate. In summary, this study confirms the effectiveness of both urban canopy (UC) and other GIs on flood mitigation.

SWMM represents GI practices at the watershed scale. First, the estimation of the potential areas of GI practices in this study could be considered optimistic given that the methodology presented in Table 2 probably overestimates the real potential. It was assumed that all space belonging to the selected land use categories could effectively implement GI practices, meaning that the implementation of GI practices was technically possible. Second, different GI areas were considered unique entities at the subcatchment scale without taking into account the spatial distribution of the specified land use and GI operations. Thus, we considered this representation suitable to assess the hydrological impacts of GI strategies at the watershed scale but not at the subcatchment scale. In general, the combination of green roofs and urban canopy had good performance in flood mitigation. Thus, this combination was recommended for similar urban catchments.

In this situation, the water will firstly going through the urban canopy. Then the throughfall and stemflow will go through green infrastructures (PP, PT and GR) and then to the surface runoff or

conduits runoff of the hydrological model. But in the actual situation, even though there are vegetation and urban trees in the study area, there are few trees that were growing above the rooftop. In this case, the calculation method will have “conceptual errors” and might have mistakenly estimated the rainfall amount intercepted by trees and green roofs.

In order to overcome this conceptual error, the roof area and non-roof area were divided. In all the calculations in the dissertation about the “current situation”, the throughfall and stemflow of the urban canopy layer will only going to the non-roof area. The rainfall will go directly to the roof area. This is shown in below.

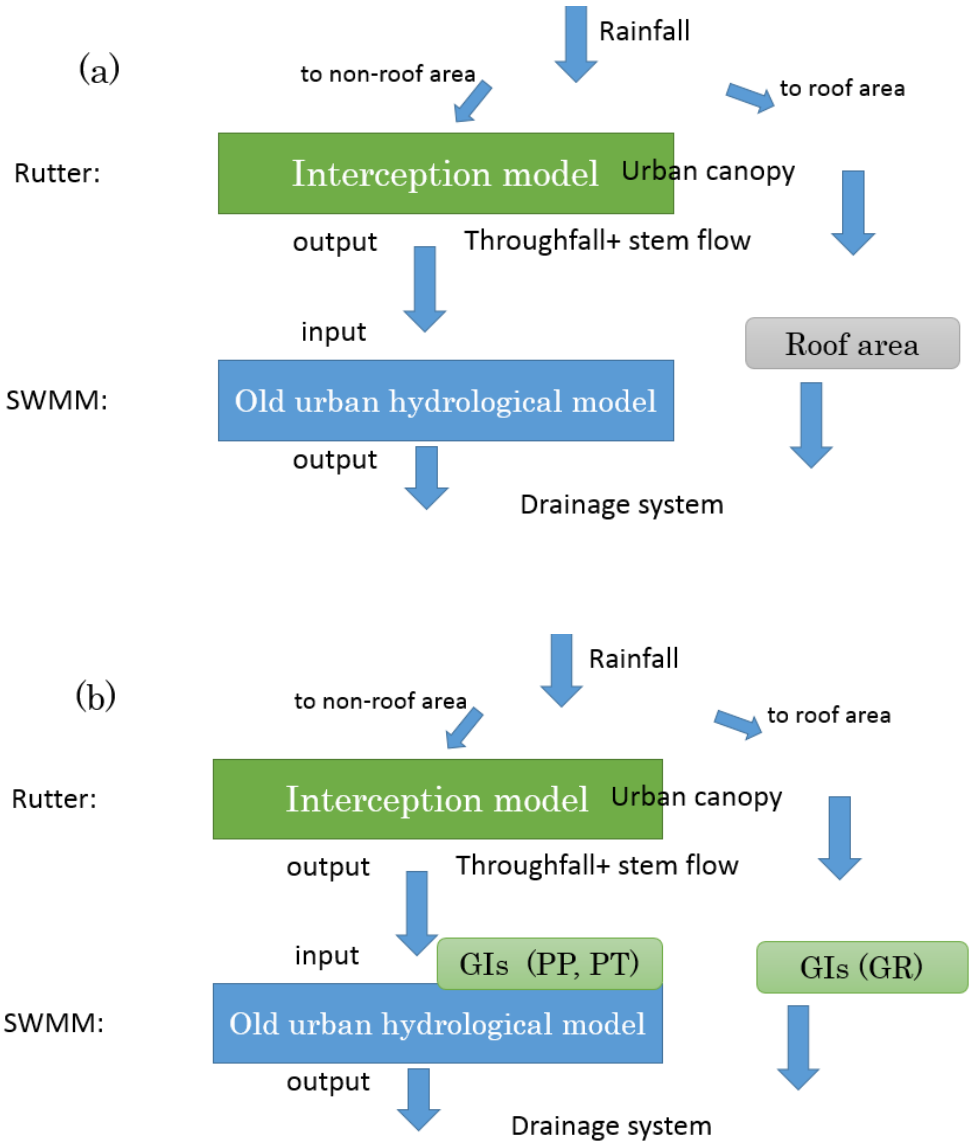

Fig 6.4 the conceptual representation of water flow. (a) without other green infrastructures; (b) in combination with other green infrastructures (PP, PT and GR).

On the other hand, for some future-based scenarios, I will consider that the growth of plants will increase the plant area, which will cause a part of the canopy area to overlap with the roof area. Therefore, in several future scenarios, the water flow of the model will consider the overlap. Such scenarios include calculations that take into account tree age and calculations that consider the increase of LAI in section 6.3. In these calculations, the schematic diagram of the water flow is shown in the figure.

6.3 The effect of urban heat island

The calculation of surface temperature depends on the ET (evapotranspiration) time series calculated in the previous interception model. ET is an important component of heat balance (latent heat), and in order to keep the consistency of scales with the interception model, the S2 scale mentioned in Chapter 4 is adopted in this part. Each urban block/urban parcel is considered a sub-catchment.

Figures 6.5 to 6.10 show the results of the spatial distribution of the calculated surface temperature of the energy balance model. To account for seasonal changes in temperature, three seasons are defined: spring (March, April), summer (June, July) and winter (October-November). Figures 6.5, 6.6, and 6.7 show the average LST in different seasons under current actual vegetation conditions, respectively. The difference in values between small areas can be seen by the color shade. The darker the colors, the higher the values will be.

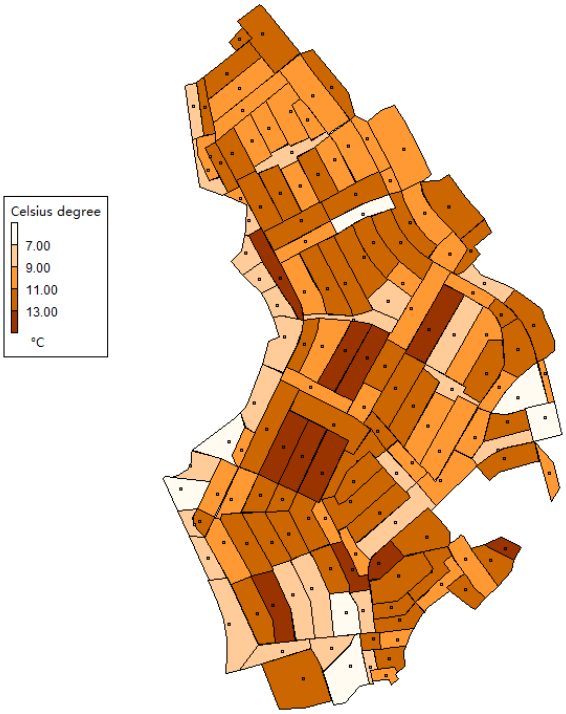

Fig 6.5 Spatial distribution of the simulated surface temperature (LST) (Celsius degree in each sub-catchment area) between Mar, 2018 and April, 2018 (spring season) on catchment KA. Dark parcels are characterized by high values.

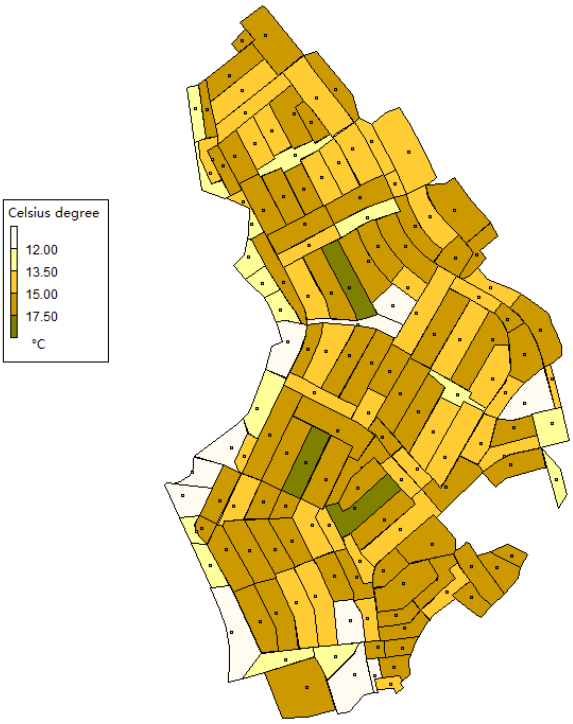

Fig 6.6 Spatial distribution of the simulated surface temperature (LST) (Celsius degree in each sub-catchment area) between Oct, 2018 and Nov, 2018 (autumn season) on catchment KA. Dark parcels are characterized by high values.

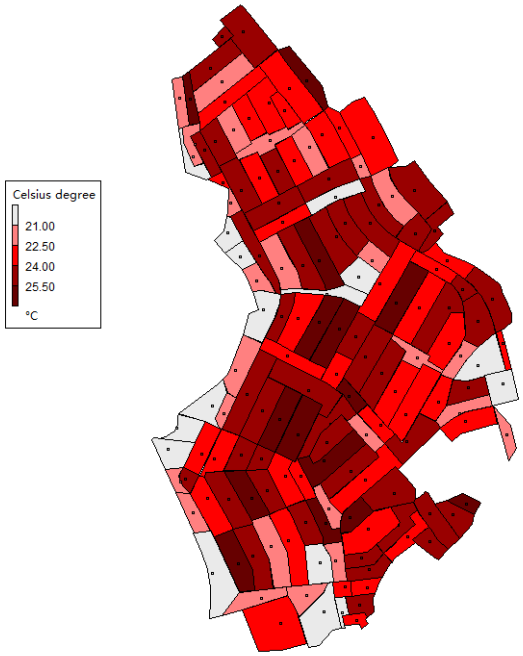

Fig 6.7 Spatial distribution of the simulated surface temperature (LST) (Celsius degree in each sub-catchment area) between June, 2018 and Jul, 2018 (summer season) on catchment KA. Dark parcels are characterized by high values.

On the other hand, because LAI is a very important vegetation factor, the change in LAI can represent the amount of vegetation. In order to explore the difference in the amount of urban vegetation, the existing LAI distribution values were adjusted by multiples. Figure 6.8, Figure 6.9, and Figure 6.10 show the surface temperature distribution of the study area in summer when the LAI values are 80%, 120%, and 140% of the actual values, respectively. It can be seen that as the LAI index increases, the surface temperature in the study area tends to decrease accordingly.

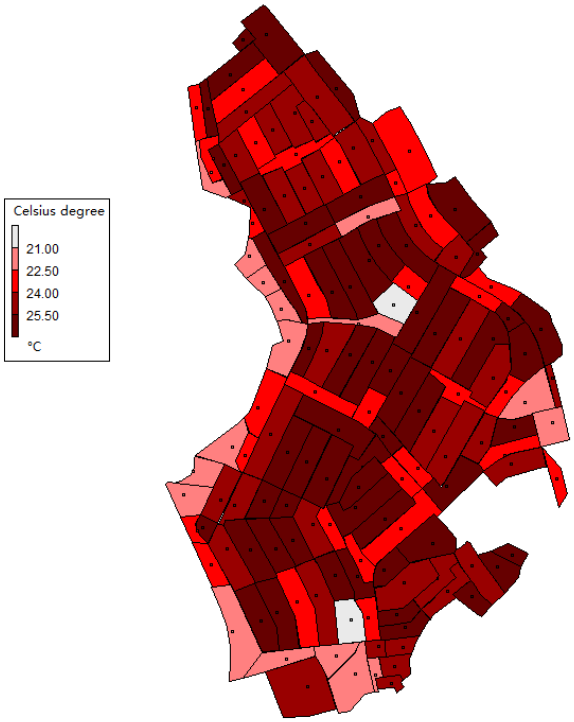

Fig 6.8 Spatial distribution of the simulated surface temperature (LST) with 80% of current LAI (Celsius degree in each sub-catchment area) between June, 2018 and Jul, 2018 (summer season) on catchment KA. Dark parcels are characterized by high values.

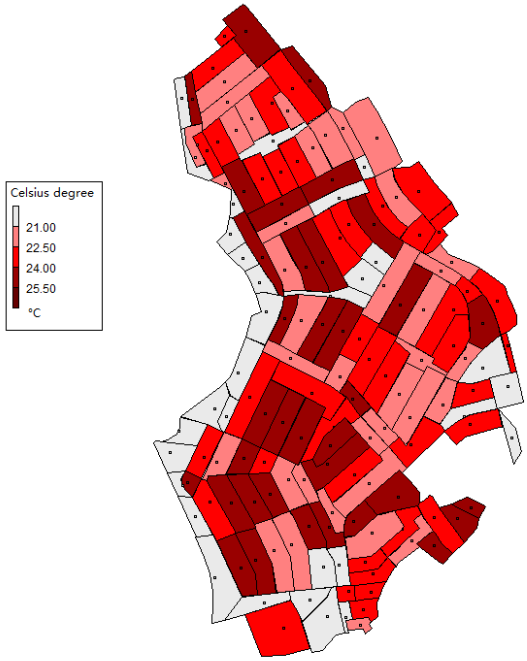

Fig 6.9 Spatial distribution of the simulated surface temperature (LST) with 120% of current LAI (Celsius degree in each sub-catchment area) between June, 2018 and Jul, 2018 (summer season) on catchment KA. Dark parcels are characterized by high values.

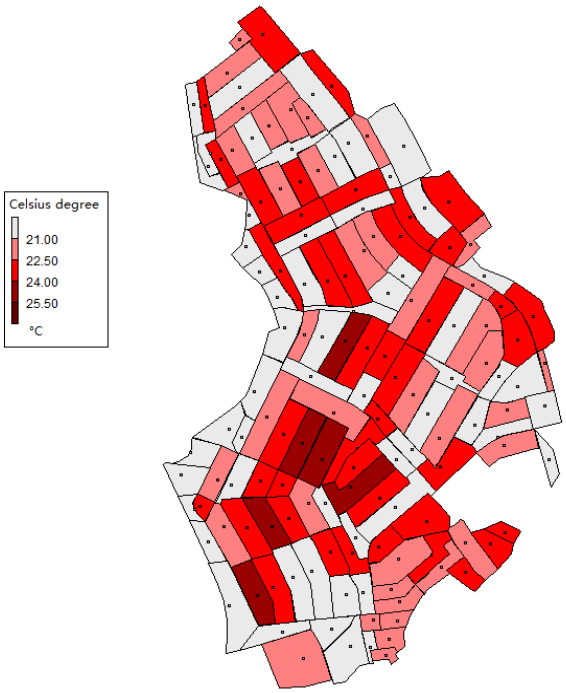

Fig 6.10 Spatial distribution of the simulated surface temperature (LST) with 140% of current LAI (Celsius degree in each sub-catchment area) between June, 2018 and Jul, 2018 (summer season) on catchment KA. Dark parcels are characterized by high values.

Figure 6.11 summarizes changes in urban vegetation (changes in LAI) for surface temperature and reductions in total runoff. With the increase of urban vegetation, the surface temperature and total runoff have decreased, indicating that urban vegetation has the ability to reduce runoff and urban heat island effect.

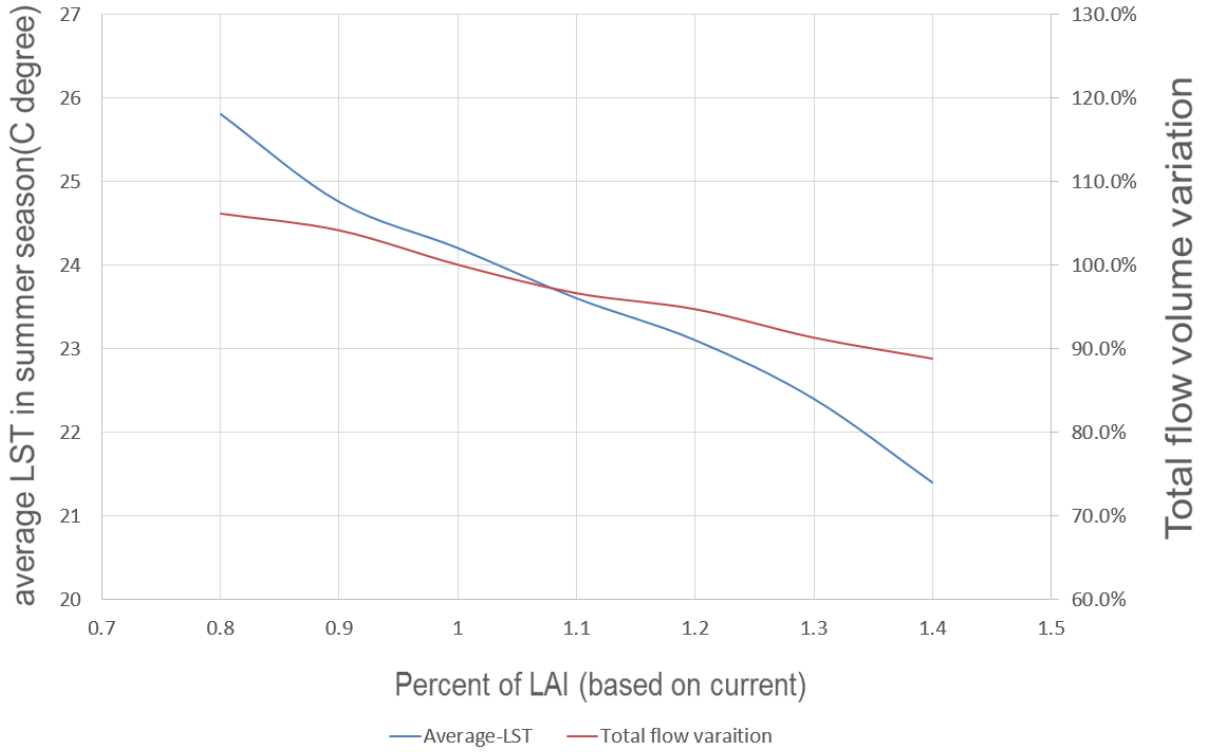

Fig 6.11 The relationship of different LAI with catchment average LSTs (Celsius degree) and the total flow volume (percentage) between June, 2018 and Jul, 2018 (summer season).

There are several schemes of planning or projects about the greening of the city. There are description about the current greening situation or the future planning. Several documents were referred, they are listed below.

Table 6.1 The generalization of Sendai's greening policy

Name	Link
Development of Sendai City Road Tree Manual	http://www.city.sendai.jp/shisetsukanri/kurashi/shizen/midori/mesho/manual.html
Realization of a beautiful green city-Sendai	http://www.city.sendai.jp/hyakunen-chose/kurashi/shizen/midori/midori/saise.html
Sendai City Green Basic Plan	http://www.city.sendai.jp/hyakunen-chose/kurashi/shizen/midori/midori/kekaku/index.html
The current state of greening in Sendai	http://www.city.sendai.jp/shisetsukanri/kurashi/shizen/midori/mesho/genjo.html
City park barrier-free specific business plan	http://www.city.sendai.jp/koen-kensetsu/kurashi/shizen/midori/midori/jigyo.html

The specific policies can be various, but there are general ideas can be generalized:

1. Keep and protect the current greening.

2. Increasing the city's greening in a mild and steady way.

The increasing were mainly focused in 3 aspects: street trees (main avenues and community streets), the greening in parks and the greening along the river.

In the file "Development of Sendai City Road Tree Manual"

The expected beneficial of city greening can be generalized as:

1. Maintenance of living environment (purification of air, reduction of noise);

2. Ensuring comfort by forming green shade (inhibiting temperature rise);

3. Ensuring traffic safety (Gaze guidance, separation of walking paths);

4. Disaster prevention functions such as fire prevention, wind prevention, and evacuation routes;

5. Conserving the natural environment (green corridor connecting park green spaces and existing forests);

In this study, several topics were closely related to the Sendai City's policy. The results could have the evaluation and referring significance for Sendai's policy:

1. This study had evaluated the hydrological and atmospheric benefits of the urban vegetation under current situation.

2. This study investigated the effects of increasing/decreasing of greening (tree age/ LAI change), especially, the effect of LAI increasing is in accordance with the previous described future greening growing, this had significance of the future scenario estimation and evaluation.

3. Although the Sendai city policy did not emphasize other constructed green infrastructures like green roofs or porous pavement, the study about these GIs could have reference meanings for decision makings in newly constructed areas.

6.4 Discussion

Reasonable urban landscape and drainage design is becoming increasingly important for urban stormwater management, requiring a deeper understanding of the hydrologic performances of imperviousness within small urban drainage catchments. The current study emphasized the effects of TIA and EIA on rainfall-runoff processes in consideration of various storm conditions. Consistent with those of previous research, our results show that increased imperviousness can enhance runoff depth and shorten lag time. Thus, the primary measurement for mitigating runoff risk is to limit the sizes of TIA and EIA. In addition, established quantitative relationships between imperviousness and runoff can help to optimize the impervious arrangement within urban catchments in order to achieve specific runoff control goals. Moreover, variances in imperviousness among subareas were significant in KA, which make the results more valuable for extrapolation. However, limited and high-cost urban land prevents designers from decreasing the sizes of impervious areas without restricting urban landscape planning. Green Infrastructures (GIs) can provide good solutions for urban rainwater regulation because they occupy only a small amount of urban resources but function effectively in runoff mitigation (Dietz, 2007; Walsh et al., 2009). This study also provides an interesting prospect for solving urban runoff issues. Our results show that EIA can alter the runoff hydrograph considerably by altering Qp. By decreasing EIA, such as through the placement of swales/trenches along roads (Dietz and Clausen, 2008), usage of permeable paving materials (Jia et al., 2012), and parcel-based landscape design (Stone, 2004), peak runoff can be reduced and postponed, which can aid rainwater control measures already in place. On this basis, optimizing the imperviousness compositions can reasonably stagger all of the

runoff hydrographs generated from subareas from upper to lower reaches. Therefore, the runoff peak discharge and lag times of the entire catchment can be maintained at acceptable levels for normal operation of urban drainage systems. However, these alternative measures are affected significantly by storm conditions. Moreover, the sensitivity analysis and scale analysis results imply that the effectiveness of imperviousness in predicting runoff variables such as Qp and Qt are sensitive to variations of rainfall pattern and duration. Thus, storm conditions should be treated individually for urban landscape design with distinct stormwater management purposes.

Table 6.2 The performance comparison of SWMM model between this study and previous studies

	Study site and model	Performance	
Krebs et al., 2014	Small urban area, SWMM	$NSE_{calibration}$=0.88	$NSE_{validation}$=0.72
Pertrucci et al., 2014	Medium urban area, SWMM	$NSE_{calibration}$=0.82	$NSE_{validation}$=0.75
Goldstein et al., 2015	Micro urban area, SWMM	$NSE_{calibration}$=0.75	$NSE_{validation}$=0.69
Dongquan et al., 2009	Large urban area, SWMM	$NSE_{calibration}$=0.92	$NSE_{validation}$=0.86
This study	Small urban area, SWMM	$NSE_{calibration}$=0.84	$NSE_{validation}$=0.73

Table 6.2 summarizes several previous studies and the model performance NSE for this study. The research of (Krebs et al., 2014) was based on three small watersheds (5.87 ha, 6.63 ha, and 12.59 ha). The first two regions are highly urbanized, and the third region is urbanized area with large greening. In all the areas the land use type and the direction of water flow on a very small scale had been accurately identified, which means a very fine EIA classification. In addition, both rainfall and outflow were

measured in a very precise manner (0.2mm / 1min for rainfall and 1min step for flow). These factors can play a role in promoting the performance of the model. The study area of (Pertrucci et al., 2014) was a medium-sized urban area (230 ha), with time steps of 5 min for both rainfall and outflow. The size of the area of this study is about 50 ha, and the time step of rainfall outflow is also 5 min. Finally, the model results are similar to those of (Pertrucci et al., 2014). For (Dongquan et al., 2009), a SWMM model was established for a macro urban watershed (1000 ha) and only limited rainfall and runoff data were used for calibration and validation. This model has a slightly higher check performance and a lower verification performance, but it is still within a similar range. From the numerical results, the model of this study performed satisfactorily. The NSE values are located in the midstream of all comparisons. The average NSE in the verification stage is 0.84 and the NSE in the verification stage is 0.73. This means that the hydrological model SWMM already has good simulation and prediction capabilities.

Table 6.3 The average NSE performances of the model before and after incorporating the NDVI data

	Before	After
Mar-May 2018 (calibration)	0.842	0.842
Jun-Jul 2018 (validation)	0.731	0.735
Aug-Nov 2018 (validation)	0.704	0.719

The incorporation of remoted sensed NDVI data had slightly improved the outlet flow performance of the model. The model was initially calibrated using the rainfall-runoff data from Mar to May 2018 and

validated using data from Jun to Jul 2018. Here the extra rainfall runoff data form Aug to Nov 2018 were also used for validation for the purpose of comparison. The NSE values had increased from 0.731 to 0.735 in Jun to Jul period and from 0.704 to 0.719 in Aug to Nov period. When there were no these NDVI data, the interception process were represented using the depression storage values. These kind of parameters were fixed values on certain land use types. The depression storage parameter were calibrated parameters. Even though calibration can help estimate the overall interception depth, the seasonal variations of urban vegetation and the subsequent interception capability change were ignored under this method. The interception abilities were completely same across the year and this may cause the conceptual errors of model. The use of remote sensed data were one way to fetch up these errors. However, the process of conversion of NDVI to LAI and then to canopy storage capacity will possibility introduce new errors and uncertainties and these errors may hamper the model performance. The results in Table 6.3 had proved that the beneficial of remote sensed data outperformed the drawbacks caused by the potential errors. These results were in accordance with (Nourani et al., 2015), who had used NDVI data as indicators of land use variations in a small watershed and found that the model performance at the sub-watershed level were improved. These results had demonstrated the benefits of introducing remote sensed data into hydrological models.

Table 6.4 The interception modeling results of this and previous studies (from Inkiläinen et al., 2013)

Land use (scale)	Climate (species/ type)	LAI	Interception ratio (%)	authers
Urban (stand)	Humid subtropical (broad-leaved deciduous)	1.9	9.1-10.6	Elina N.M. et al. 2013
Urban (stand)	Humid subtropical (broad-leaved deciduous)	1.9	19.9-21.4	Elina N.M. et al. 2013
Urban (stand)	Mediterranean (broad-leaved deciduous)	4.3	18.4	Wang et al. (2008)
Urban (stand)	Mediterranean (broad-leaved evergreen)	na	6.0	Xiao et al. (1998)
Urban (stand)	Mild oceanic (Pseudotsuga menziesii)	na	13.0	Xiao et al. (1998)
Urban (crown)	Mild oceanic (Thuja plicata)	na	49.1	Asadian and Weiler (2009)
Urban (crown)	Mild oceanic (Thuja plicata)	na	60.9	Asadian and Weiler (2009)
Urban (crown)	Semiarid (Ficus benjamina)	na	59.5	Guevara-Escobar et al. (2007)
Urban (crown)	Mediterranean (Pyrus calleryana)	7.0	15.0	Xiao et al. (2000b)
Urban (crown)	Mediterranean (Quercus suber)	3.4	27.0	Xiao et al. (2000b)
Urban (crown)	Mediterranean (Jacaranda mimosifolia)	na	15.3	Xiao and McPherson (2002)
Urban (crown)	Mediterranean (Tristania conferta)	na	66.5	Xiao and McPherson (2002)
Urban (crown)	Mediterranean (Ginkgo biloba)	5.2	25.2	Xiao and McPherson (2011)
Urban (crown)	Mediterranean (Liquidambar styraciflua)	4.7	14.3	Xiao and McPherson (2011)
Urban (crown)	Mediterranean (Citrus limon)	3.0	27.0	Xiao and McPherson (2011)
Rural (stand)	Humid subtropical (mixed hardwood-conifer)	na	18.6	Bryant et al. (2005)
Rural (stand)	Humid subtropical (deciduous broadleaved)	na	17.4	Bryant et al. (2005)
Rural (stand)	Humid subtropical (deciduous broad-leaved)	3.1	16.8	Bryant et al. (2005)
Rural (stand)	Humid subtropical	na	10.0	Lin et al. (2000)

The results listed in Table 6.4 had showed that the interception ratio is ranged from around 6% to 60%. One important reason of this is the different scales of the study: some researches were conducted in the single tree scale while others were conducted on much larger scales. Larger scales will always have more sparse places than the situations under the tree crown, so the stand scale results usually showed less interception ratios than that of the crown scale. Our study scale is a small urban residential catchment, so the results of stand scales were emphasized. In the Mediterranean climate of Sacramento, CA, Xiao et al. (1998) found throughfall percentages between 86.4 and 93.4%. Xiao et al. (1998) noted that less throughfall (86.4%) was generated in the ‘suburban sector’ dominated by broadleaved evergreen trees compared to the ‘city sector’ dominated by broadleaved deciduous trees (93.3%). Apart

from maintaining foliage throughout the rainy winter seasons, evergreen trees also tend to have higher LAI than do deciduous trees (Xiao et al., 1998). Wang et al. (2008) found that rainfall interception in Maryland, USA, accounted for 18.4% of P, resulting in net precipitation, of 81.6%. These results were simulated using the model UFORE-Hydro in an urban watershed dominated by deciduous vegetation (22% of watershed), located in the humid subtropical climate. Our storm-based results from similar climate are comparable with theirs as we found our cumulative yearly interception ratio to be 15%.

Runoff computed with hourly rainfall did not generate a substantial number of flood events in the watershed. Thus, GI practices at various implementation levels were evaluated for mitigating flood volumes. All GI scenarios and the non-GI scenario analyzed in this section were simulated with hourly rainfall data for the year 2018. Implementation of individual GI practices resulted in average annual runoff reduction were ranged from around 11% to 19% (Fig 6.3). Implementation of two or more GI practices indicated a reduction in average annual runoff from around 17% to 28% and 20% to 37% respectively. For the largest ratio, it is the combination of 4 GIs (UC+GR+PP+PT) which was the most effective scenario as expected. The GR included scenario also exhibited large reduction in runoff because of the large impervious surfaces covered by roof top, which represent more than 20% of the total watershed area and more than 50% of total EIA. Treating rooftop runoff with GR was the rather effective scenario due to their large areas. The roadside area and other area treated by PP and PT accounted less than 10% of the watershed area and less than 30% of the total EIA. So the mitigation effect of PP and PT is less effective than GR. Simulation results obtained in this study are consistent with the literature, which showed that runoff volume at the outlet of the watershed was reduced with increasing implementation levels of GI practices (e.g., Walsh et al., 2014; Di Vittorio and Ahiablame,

2015; Ahiablame et al., 2013). In general, individual implementation of GR scenarios for rooftop runoff performed better than other GIs, followed by UC for interception runoff.

Reduction in runoff logically led to reduction in flood events. Nevertheless, even though there are evidence that green infrastructures systems can be used to effectively manage stormwater, they are more credited for controlling small storm events, indicating storm with high peaks (i.e. flood flows) may be too large for these systems to handle, especially when the area treated is relatively small. It is noted that the results achieved in this study are somewhat case specific, and depend on the site characteristics including the distribution of different land use and hydrologic properties. Nevertheless, the concepts and methodologies involving a comprehensive evaluation of different GIs combinations, including their cost and average long-term performance is recommended, as a way of ensuring that the most cost efficient options are ultimately selected for detailed design and implementation.

One of the goals of green infrastructures in this watershed was to ‘maintain base flow’. However, a broader goal of green infrastructure is to maintain the pre-development water balance and flow regime, which was not observed. In our study watershed, the majority of stormwater facilities were underground rather than vegetated and aboveground. Stormwater facilities that are belowground and un-vegetated limit the potential for evapotranspiration of incoming stormwater and more efficiently recharge stormwater compared with a forested landscape, where more diffuse infiltration may have never made it deeper than the root zone. Recent developments in stormwater quantity management are focused primarily on reducing stormwater volume through infiltration, with little sustained consideration given to collecting stormwater for indoor use or increasing evapotranspiration. The harvesting or

evapotranspiration of stormwater in most areas needs to dominate over recharge to maintain pre-development streamflow volumes (Askarizadeh et al., 2015), and these pathways remove flow from the stream altogether rather delaying entry ranging from minutes to years with recharge (Miles and Band, 2015).

Based on a series of explicit or implicit assumptions, SWMM is used for watershed-scale runoff simulations. This paper describes implicit assumptions, some of which are based on subject consensus. Various assumptions about modeling conditions, parameter specifications, and data quality (Aich et al., 2016; Yu and Coulhardhard, 2015) may generate uncertainty. Uncertainties related to parameter specifications and data resolution may introduce inevitable errors in the results obtained. However, deviations from the model output are considered acceptable, and the model is considered satisfactory for scenario analysis. Therefore, uncertainty is not expected to affect the main trends and key insights obtained, and the general results are considered to be related to the design of reasonable strategies for the implementation of geographical indications in the study area.

Uncertainty is inherent in any modeling process, and it originates from multiple sources from model development to the required data collection. Uncertainty cannot be eliminated, so it is necessary to understand its source and the consequences of model results (Beven, 2001).

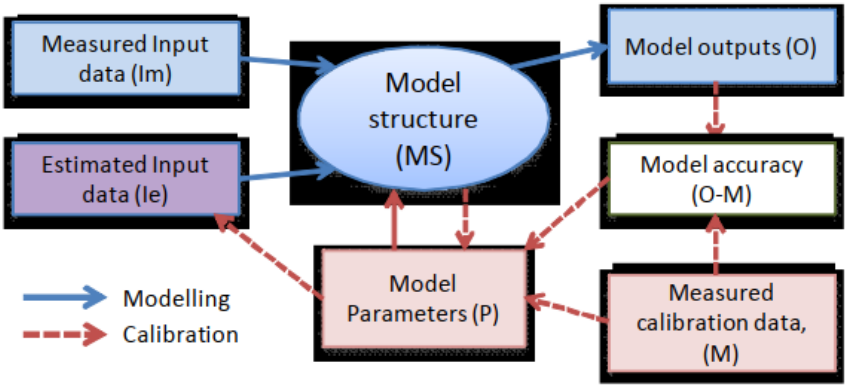

Fig 6.12 General modelling framework (adopted from Deletic et al., 2012).

A common modeling framework is used, which requires the following information (Fig 6.12): model structure (e.g. relationships and numerical methods), measurable input data (e.g. rainfall or evapotranspiration time series), model calibration parameters; (e.g. effective impermeability Area), measured calibration data (e.g. water flow time series), and calibration algorithms (e.g. the sum of squared differences between modeled and measured data) with well-defined objective standards.

According to several previous studies (A. Deletic et al., 2009; Refsgaard et al., 2007; Refsgaard and Keur, 2006; Butts et al., 2004; Engeland et al., 2016), there are several kinds of uncertainties during the urban hydrological modeling and they are listed below. This is a very general and broad classification.

Model input uncertainties:

1. Measured input data– both random and systematic effects that are generated in input data collection process;

2. Model parameters– uncertainty in their calibrated values or estimates (if models are not calibrated, the parameters are ‘guesses’ or ‘defaults’ used).

Calibration uncertainties

3. Measured calibration data uncertainties. Including the data availability, data choices and temporal resolution of the time series;

4. Calibration Algorithms and Criteria Functions which is about assessing the effectiveness of the algorithm in finding a global minima;

Model structure uncertainties:

5. Conceptualisation errors, such as scale-issues or ignoring key processes;

6. Equations and Numerical methods, the former could be ill posed and thus inadequately represent the hydrological process; the latter can be ill defined leading to non-accurate solutions;

7. Integrated modeling Uncertainty. Including the propagation of uncertainty.

Uncertainty cannot be completely eliminated. One must try to reduce uncertainty and improve the situation. Based on current technology and understanding, the best way to discuss uncertainties from 4 to 6 is to compare different methods and models. For monitoring data sets (uncertainty 1 and 3), although there are some numerical methods to estimate uncertainty under certain assumptions, the quality of the data usually depends on the measurement instrument or data provider (Dotto et al., 2012; Pertrucci et al., 2014).

In this study, the conceptual errors, including the scale issues and ignoring key process, were actually one most important topic of the study and had been discussed a lot in Chapter 4. The model parameters

uncertainty were discussed and reduced using sensitivity analysis and model calibration in Chapter 3. There were several research had discussed the uncertainties caused by calibration algorithms, criteria functions and numerical methods (Clark MP et al., 2010; Kavetski et al., 2010; Gan et al., 2018; Hernandez-Suarez et al., 2018). However, these discussions were somehow out of the scope of this study.

This study had conducted a sensitivity analysis which can determine how different values of an independent variable affect a particular dependent variable under a given set of assumptions. Uncertainty analyses study how various sources of uncertainty in a mathematical model contribute to the model's overall uncertainty. The concept are quite similar and related, so ideally, uncertainty and sensitivity analysis should be run in sequence. The fully understanding of the Propagation of Uncertainties through models will need a Total Error Estimation Framework. Due to the large computational burden, here the new uncertainty analysis will not be conducted. The accuracy and uncertainty of different models were discussed independently.

This study had used three models: the hydrological model (SWMM), the interception mode (Rutter model) and the surface energy model. They were integrated in a sequence: firstly only the hydrological model; then the fixed interception parameters were expanded, the interception model were introduced; finally, the calculated evapotranspiration time series and other climate data had created the third model, the energy balance model.

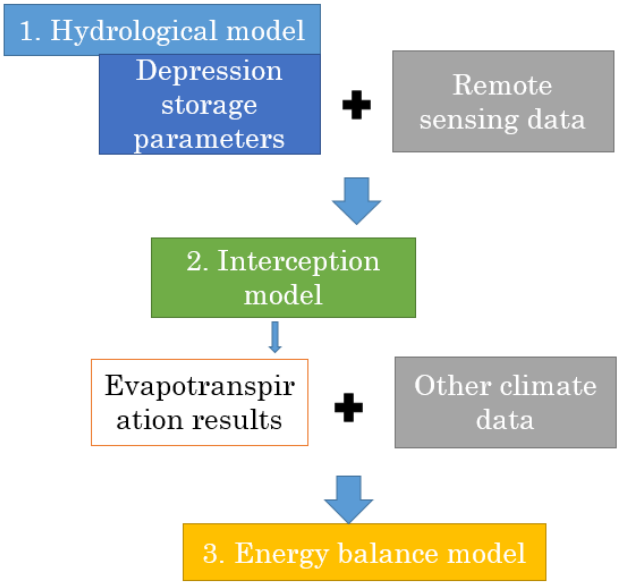

Fig 6.13 The relationship integration of different models.

The storm water management model (SWMM) is a widely used urban hydrology model. Many previous researches had discussed its calibration, validation, uncertainty and parameters. In this study a thoroughly sensitivity analysis were discussed in Chapter 3. Several parameters are quite important: the impervious ratio, roughness parameters and depression storage parameters.

The impervious ratio is the most important parameter. However in this study the value of this parameter is quite well determined: every rooftop foot print, every residential garden and the land use of each urban block are all defined. So in this case, the quite precise impervious ratio values were obtained which largely reduced the space of uncertainty. Thus only the roughness parameters and depression storage parameters were left for calibration.

For the Rutter model, there were previous research which had conducted sensitivity analysis and

uncertainty analysis (Linhoss et al., 2016). The sensitivity analysis results of Rutter model were shown below.

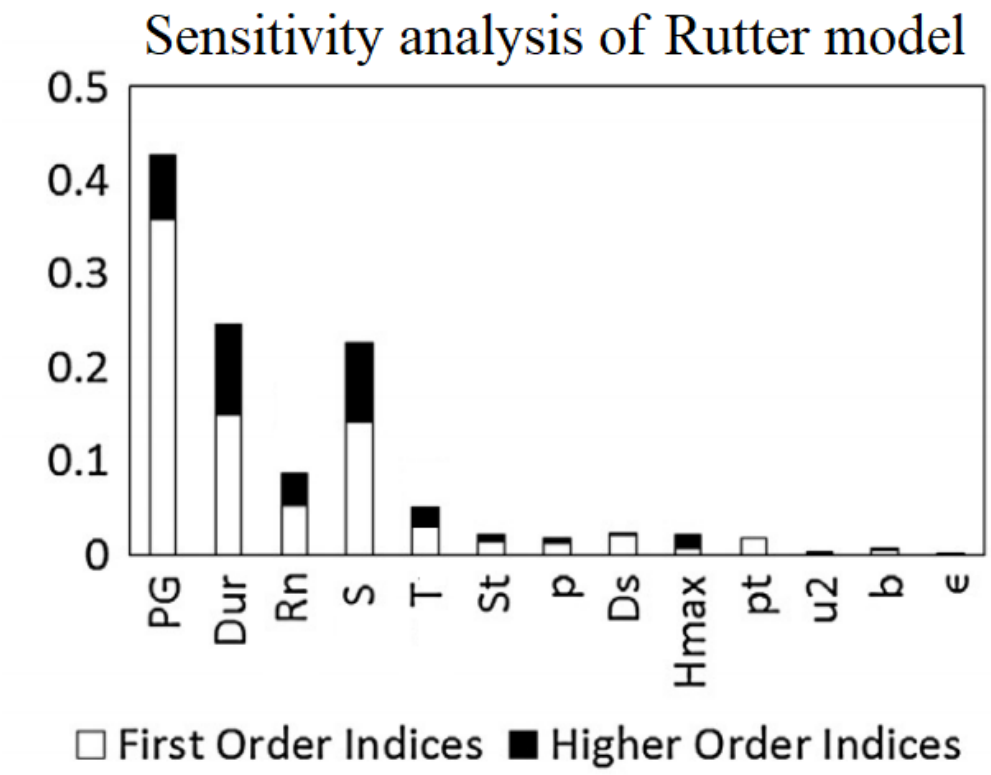

Fig 6.14 Sensitivity analysis of Rutter model (adopted from Linhoss et al, 2016).

It is clear that there were several important parameters: PG (gross precipitation), Dur (rainfall duration), Rn (net radiation), S (Canopy Storage Capacity) and T (air temperature). Among these parameters, PG, Dur, Rn and T are actually data obtained from Japan Meteorological Agency. For the S parameter, the values were obtained from NDVI values from Landsat 8. The equations that convert NDVI to LAI and then to canopy storage were widely used equations and the LAI value were measured at the site. So the LAI equations were validated using these data and had a satisfied performance. So, based on these analysis, it could suggest that the interception model had relatively low errors. The largest error source

might be from the estimation of canopy storage capacity. But the overall uncertainty is limited (with 50% to 150% error range, the variation of results is around 15% (the first order indices)).

6.5 Brief summary

Tree species also have a significant impact on the interception process. Four tree species scenarios were discussed in this study: all deciduous scenario; all evergreen scenario; current scenario and mixed forest scenario. All deciduous scenarios have the highest interception ratio from a year-round perspective, but the seasonality is more pronounced. In the leafed period, the interception ratio is large, and in the leafless period, this ratio is rather small. The all evergreen scenario is the opposite situation: the interception ratio for different seasons remains stable, and the annual interception ratio is lower. The current and mixed scenarios are between the two scenarios mentioned above. Because the all deciduous scenario has a long leafless season, from the perspective of interception and environmental comfort, the recommended choice for tree species is a large proportion of deciduous trees with a small proportion of evergreen trees.

The effects of several different green infrastructures (GIs) are also discussed in the study. As a green infrastructure based on interception, UC (urban canopy) is more effective in reducing flooding in small rainfall events and weaker in heavy rain. For a single GI facility, GR (green roof) has better overall flow and peak flow reduction. The combination of green roof and urban canopy is a more effective response to flood reduction. The increase of vegetation in the urban area can have both the flood and heat reduction effects in the catchment. This had proved and estimated the potential beneficial of the greening policies of the city.

Chapter 7. General summary and conclusions

7.1 Conclusions

This research attempted to analyze how the scales and vegetation affected urban hydrological processes and modeling. The performances of models with different resolution were compared. The parameterization and prediction capacities were discussed during and after the calibration. Spatially distributed values for interception storage capacity was obtained from the NDVI data and field LAI (leaf area index) measurements. The flood mitigation effect with some other green infrastructures as well as the impact of tree species were also discussed. The conclusions are generalized as follows:

1. Although weighted average method was used, there were obvious scale effect across models due to the non-linearity nature of model structure. With the coarsening of grid, both the total and peak runoff tend to decrease while the variations of peak runoff rate was quite obvious while the relative differences can be larger than 30%. The effect of spatial resolution on simulated peak flows is also influenced by storm characteristics. The impact of these factors was quantified by dimensional analysis and a exponent function was fitted to the resulting scatter plots. This provide useful insights into the impact and interaction of spatial resolutions and other factors as well as a practical estimation of the performance that can be expected for a given model input resolution.

2. After independent calibration, all the models showed satisfying performances. The performance of the calibrated models were similar to the S1 model (NSES2=0.837, NSES3=0.836 and NSES4=0.841).

This meant that calibration could completely compensate models' scale effect. When EIA was considered as a calibrated parameter, the NSE value of S2, S3 and S4 model during calibrated period were 0.859, 0.863 and 0.845, while the performance of validation period hold the line or decreased (NSES2=0.744, NSES3=0.685 and NSES4=0.613). The objective function surface of the models were analyzed. It could be found that the grid resolution led to the change of the overall shape of the surface and deviation of the best performance area.

3. The use of NDVI data is helpful in obtaining distributed vegetation information, and the interception process is simulated separately, making the model more process-based. Due to the seasonality of the vegetation, interception, as a hydrological process, also has a strong seasonality. The interception ratio during the leafed season is more than 85% of the annual interception. This is mainly due to the increase in the degree of vegetation and the intensity of rainfall during this season. At the same time, the rainfall characteristics have a greater impact on the interception process. The smaller the rainfall is, the greater the rate of interception.

4. Tree species also have a significant impact on the interception process. Four tree species scenarios were discussed in this study: all deciduous scenario; all evergreen scenario; current scenario and mixed forest scenario. All deciduous scenarios have the highest interception ratio from a year-round perspective, but the seasonality is more pronounced. In the leaded period, the interception ratio is large, and in the leafless period, this ratio is rather small. The all evergreen scenario is the opposite situation: the interception ratio for different seasons remains stable, and the annual interception ratio is lower. The current and mixed scenarios are between the two scenarios mentioned above. Because the all deciduous

scenario has a long leafless season, from the perspective of interception and environmental comfort, the recommended choice for tree species is a large proportion of deciduous trees with a small proportion of evergreen trees.

5. The effects of several different green infrastructures (GIs) are also discussed in the study. As a green infrastructure based on interception, UC (urban canopy) is more effective in reducing flooding in small rainfall events and weaker in heavy rain. For a single GI facility, GR (green roof) has better overall flow and peak flow reduction. In the combined GIs, the combination of UC and GR has the best flood-reduction effect.

7.2 Recommendations for future studies

The study on effects of spatial resolution could be extended to determine a threshold or optimum resolution, beyond which subdivision produces little or no effect on peak flow predictions. Identifying such a threshold level is of particular interest to modelers to address the appropriate level of subdivision. For this threshold analysis, models would have to be developed for a large number of spatial resolutions, hydrologic simulations performed and peak flows analyzed. Such a study could also be a suitable application of artificial sewer networks, where the modeler can easily generate networks at multiple resolutions without requiring the exact configuration of drainage area, pipes and nodes in the network.

The study of spatial resolution effects was conducted using the model SWMM. Although similar results

are expected from other models, this needs further verification. It would be an important contribution to perform a similar spatial scaling analysis using other urban hydrology models. This would be valuable for model comparisons often done in rural hydrology, but not so common in urban hydrology.

In addition, the relationship and interaction between model scales and hydrological process scales remains a topic worth exploring. The previously mentioned model scale studies are based primarily on the simulated scale of surface runoff. However, the urban hydrological process is very complicated and is divided into many different processes. Each process has its own physical scale. At the time of simulation, the importance of physical scale and model scale is very obvious. The impact of different simulation scales of different hydrological processes on the final results still lacks quantitative research.

The influence of urban vegetation or green infrastructure has been discussed in many aspects. Under the premise of selecting the appropriate simulation scale, this study evaluated the impact of urban vegetation. However, this process is related before and after. The result of the previous process is used for the input of the latter process, and the transmission and transfer of errors occur during the coupling process. For such a process, uncertainty analysis should be necessary.

References

Aboelnour, M., Gitau, M. W., & Engel, B. A. (2019). Hydrologic response in an urban watershed as affected by climate and land-use change. Water, 11(8), 1603.

Ahiablame, L. M., Engel, B. A., & Chaubey, I. (2013). Effectiveness of low impact development practices in two urbanized watersheds: Retrofitting with rain barrel/cistern and porous pavement. Journal of environmental management, 119, 151-161.

Aich, V., Liersch, S., Vetter, T., Fournet, S., Andersson, J. C., Calmanti, S., ... & Paton, E. N. (2016). Flood projections within the Niger River Basin under future land use and climate change. Science of the Total Environment, 562, 666-677.

Amaguchi, H. and Kawamura, A. (2016) "Evaluation of Climate Change Impacts on Urban Drainage Systems by a Storm Runoff Model with a Vector-Based Catchment Delineation" in World Environmental and Water Resources Congress 2016. Reston, VA, American Society of Civil Engineers, 597–606. [online] http://ascelibrary.org/doi/10.1061/9780784479872.061.

Armson, D., Stringer, P., and Ennos, A. R. (2013) The effect of street trees and amenity grass on urban surface water runoff in Manchester, UK. Urban Forestry and Urban Greening, **12**(3), 282–286. [online] http://dx.doi.org/10.1016/j.ufug.2013.04.001.

Asadian, Y. and Weiler, M. (2009) A new approach in measuring rainfall interception by urban trees in coastal British Columbia. Water Quality Research Journal of Canada, **44**(1), 16–25. [online] https://doi.org/10.2166/wqrj.2009.003.

Bach, P. M., Rauch, W., Mikkelsen, P. S., Mccarthy, D. T., & Deletic, A. (2014). A critical review of integrated urban water modelling–Urban drainage and beyond. Environmental modelling & software, 54, 88-107.

Balacco, G., Figorito, B., Tarantino, E., Gioia, A., & Iacobellis, V. (2015). Space–time LAI variability in Northern Puglia (Italy) from SPOT VGT data. Environmental monitoring and assessment, 187(7), 434.

Beniston, M., Stephenson, D. B., Christensen, O. B., Ferro, C. A., Frei, C., Goyette, S., ... & Palutikof, J. (2007). Future extreme events in European climate: an exploration of regional climate model projections. Climatic change, 81(1), 71-95.

Beven, K., & Freer, J. (2001). Equifinality, data assimilation, and uncertainty estimation in mechanistic modelling of complex environmental systems using the GLUE methodology. Journal of hydrology, 249(1-4), 11-29.

Berland, A., Shiflett, S. A., Shuster, W. D., Garmestani, A. S., Goddard, H. C., Herrmann, D. L., and Hopton, M. E. (2017) The role of trees in urban stormwater management. Landscape and Urban Planning, **162**, 167–177. [online] http://dx.doi.org/10.1016/j.landurbplan.2017.02.017.

Bhaskar, A. S., Hogan, D. M., & Archfield, S. A. (2016). Urban base flow with low impact development. Hydrological Processes, 30(18), 3156-3171.

Braud, I., Vich, A. I. J., Zuluaga, J., Fornero, L., & Pedrani, A. (2001). Vegetation influence on runoff and sediment yield in the Andes region: observation and modelling. Journal of Hydrology, 254(1-4), 124-144.

Brauman, K. A., Freyberg, D. L., & Daily, G. C. (2010). Forest structure influences on rainfall partitioning and cloud interception: A comparison of native forest sites in Kona, Hawai'i. Agricultural and Forest Meteorology, 150(2), 265-275.

Bryant, M. L., Bhat, S., and Jacobs, J. M. (2005) Measurements and modeling of throughfall variability for five forest communities in the southeastern US. Journal of Hydrology, **312**(1–4), 95–108.

Bulcock, H. H. and Jewitt, G. P. W. (2012) Modelling canopy and litter interception in commercial forest plantations in South Africa using the Variable Storage Gash model and idealised drying curves. Hydrology and Earth System Sciences, **16**(12), 4693–4705.

Butts, M. B., Payne, J. T., Kristensen, M., & Madsen, H. (2004). An evaluation of the impact of model structure on hydrological modelling uncertainty for streamflow simulation. Journal of hydrology, 298(1-4), 242-266.

Carlson, T. N., & Ripley, D. A. (1997). On the relation between NDVI, fractional vegetation cover, and leaf area index. Remote sensing of Environment, 62(3), 241-252.

Chang, T. J., Wang, C. H., and Chen, A. S. (2015) A novel approach to model dynamic flow interactions between storm sewer system and overland surface for different land covers in urban areas. Journal of Hydrology, **524**, 662–679. [online] http://dx.doi.org/10.1016/j.jhydrol.2015.03.014.

Chang, T. J., Wang, C. H., Chen, A. S., and Djordjević, S. (2018) The effect of inclusion of inlets in dual drainage modelling. Journal of Hydrology, **559**, 541–555.

Chen, J., Hill, A. A., & Urbano, L. D. (2009). A GIS-based model for urban flood inundation. Journal of Hydrology, 373(1-2), 184-192.

Chen, W., Huang, G., Zhang, H., and Wang, W. (2018) Urban inundation response to rainstorm patterns with a coupled hydrodynamic model: A case study in Haidian Island, China. Journal of Hydrology, **564**, 1022–1035.

Clark, M. P., & Kavetski, D. (2010). Ancient numerical daemons of conceptual hydrological modeling: 1. Fidelity and efficiency of time stepping schemes. Water Resources Research, 46(10).

Cronin, A. A., Breslin, N., Gibson, J., & Pedley, S. (2006). Monitoring source and domestic water quality in parallel with sanitary risk identification in Northern Mozambique to prioritise protection interventions.

Journal of Water and Health, 4(3), 333-345.

Damodaram, C., Giacomoni, M. H., Prakash Khedun, C., Holmes, H., Ryan, A., Saour, W., & Zechman, E. M. (2010). Simulation of Combined Best Management Practices and Low Impact Development for Sustainable Stormwater Management 1. JAWRA Journal of the American Water Resources Association, 46(5), 907-918.

Deguchi, A., Hattori, S., and Park, H. T. (2006) The influence of seasonal changes in canopy structure on interception loss: Application of the revised Gash model. Journal of Hydrology, **318**(1–4), 80–102.

Deletic, A., Dotto, C. B. S., McCarthy, D. T., Kleidorfer, M., Freni, G., Mannina, G., ... & Bertrand-Krajewski, J. L. (2012). Assessing uncertainties in urban drainage models. Physics and Chemistry of the Earth, Parts A/B/C, 42, 3-10.

Dietz, J., Hölscher, D., & Leuschner, C. (2006). Rainfall partitioning in relation to forest structure in differently managed montane forest stands in Central Sulawesi, Indonesia. Forest Ecology and Management, 237(1-3), 170-178.

Dietz, M. E., & Clausen, J. C. (2008). Stormwater runoff and export changes with development in a traditional and low impact subdivision. Journal of Environmental Management, 87(4), 560-566.

Di Vittorio, D., & Ahiablame, L. (2015). Spatial translation and scaling up of low impact development designs in an urban watershed. Journal of Water Management Modeling.

Dongquan, Z., Jining, C., Haozheng, W., Qingyuan, T., Shangbing, C., & Zheng, S. (2009). GIS-based urban rainfall-runoff modeling using an automatic catchment-discretization approach: a case study in Macau. Environmental Earth Sciences, 59(2), 465.

Dotto, C. B., Mannina, G., Kleidorfer, M., Vezzaro, L., Henrichs, M., McCarthy, D. T., ... & Deletic, A. (2012). Comparison of different uncertainty techniques in urban stormwater quantity and quality modelling.

Water research, 46(8), 2545-2558.

Elhag, M. (2014) Sensitivity analysis assessment of remotely based vegetation indices to improve water resources management. Environment, Development and Sustainability, **16**(6), 1209–1222.

Elliott, A. H., & Trowsdale, S. A. (2007). A review of models for low impact urban stormwater drainage. Environmental modelling & software, 22(3), 394-405.

Endreny, T. (2008). Naturalizing urban watershed hydrology to mitigate urban heat‐island effects. Hydrological Processes: An International Journal, 22(3), 461-463.

Engeland, K., Steinsland, I., Johansen, S. S., Petersen-Øverleir, A., & Kolberg, S. (2016). Effects of uncertainties in hydrological modelling. A case study of a mountainous catchment in Southern Norway. Journal of hydrology, 536, 147-160.

Fan, L. Y., Gao, Y. Z., Brück, H. E. B. C., & Bernhofer, C. (2009). Investigating the relationship between NDVI and LAI in semi-arid grassland in Inner Mongolia using in-situ measurements. Theoretical and applied climatology, 95(1-2), 151-156.

Fewtrell, T. J., Duncan, A., Sampson, C. C., Neal, J. C., and Bates, P. D. (2011) Benchmarking urban flood models of varying complexity and scale using high resolution terrestrial LiDAR data. Physics and Chemistry of the Earth, Parts A/B/C, **36**(7–8), 281–291. [online] https://linkinghub.elsevier.com/retrieve/pii/S1474706510002184.

Fletcher, T. D., Vietz, G., and Walsh, C. J. (2014) Protection of stream ecosystems from urban stormwater runoff: The multiple benefits of an ecohydrological approach. Progress in Physical Geography, **38**(5), 543–555.

Flynn, K. M., & Traver, P. R. G. (2011). Evaluation of Green Infrastructure Practices Using Life Cycle Asessment (Doctoral dissertation, Villanova University).

Flynn, K. M., & Traver, R. G. (2013). Green infrastructure life cycle assessment: A bio-infiltration case study. Ecological engineering, 55, 9-22.

Gan, Y., Liang, X. Z., Duan, Q., Ye, A., Di, Z., Hong, Y., & Li, J. (2018). A systematic assessment and reduction of parametric uncertainties for a distributed hydrological model. Journal of hydrology, 564, 697-711.

Gash, J. H. C. (1979). An analytical model of rainfall interception by forests. Quarterly Journal of the Royal Meteorological Society, 105(443), 43-55.

Ghosh, I. and Hellweger, F. L. (2012) Effects of Spatial Resolution in Urban Hydrologic Simulations. Journal of Hydrologic Engineering, **17**(1), 129–137. [online] https://ascelibrary.org/doi/10.1061/%28ASCE%29HE.1943-5584.0000405.

Goldstein, a, DiGiovanni, K., and Montalto, F. a. (2010) Resolution and Sensitivity Analysis of a Block-Scale Urban Drainage Model. World Environmental and Water Resources Congress 2010, 4720–4729. [online] http://dx.doi.org/10.1061/41114(371)479.

Goldstein, A., Foti, R., and Montalto, F. (2016) Effect of Spatial Resolution in Modeling Stormwater Runoff for an Urban Block. Journal of Hydrologic Engineering, **21**(11), 06016009. [online] http://ascelibrary.org/doi/10.1061/%28ASCE%29HE.1943-5584.0001377.

Goyen, A. G., & O'Loughlin, G. G. (1999, August). Examining the basic building blocks of urban runoff. In 8th International Urban Storm Drainage Conference, Sydney, Australia (Vol. 30).

Granger, R. J. and Carey, S. K. (2007) The cold regions hydrological model : a platform for basing evidence. Hydrological Processes, **2667**(November 2007), 2650–2667.

Guan, M., Sillanpää, N., and Koivusalo, H. (2015a) Modelling and assessment of hydrological changes in a developing urban catchment. Hydrological Processes, **29**(13), 2880–2894. [online] http://doi.wiley.com/10.1002/hyp.10410.

Guan, M., Sillanpää, N., and Koivusalo, H. (2015b) Storm runoff response to rainfall pattern, magnitude and urbanization in a developing urban catchment. Hydrological Processes, n/a-n/a. [online] http://doi.wiley.com/10.1002/hyp.10624.

Guevara-Escobar, A., González-Sosa, E., Véliz-Chávez, C., Ventura-Ramos, E., and Ramos-Salinas, M. (2007) Rainfall interception and distribution patterns of gross precipitation around an isolated Ficus benjamina tree in an urban area. Journal of Hydrology, **333**(2–4), 532–541.

Guo, Y., & Adams, B. J. (1998). Hydrologic analysis of urban catchments with event‐based probabilistic models: 1. Runoff volume. Water Resources Research, 34(12), 3421-3431.

Guo, J. C. Y., Cheng, J. C. Y., and Wright, L. (2011) Field Test on Conversion of Natural Watershed into Kinematic Wave Rectangular Plane. Journal of Hydrologic Engineering, **17**(8), 944–951.

Goswami, S., Gamon, J., Vargas, S., & Tweedie, C. (2015). Relationships of NDVI, Biomass, and Leaf Area Index (LAI) for six key plant species in Barrow, Alaska (No. e1127). PeerJ PrePrints.

Guevara-Escobar, A., González-Sosa, E., Véliz-Chávez, C., Ventura-Ramos, E., & Ramos-Salinas, M. (2007). Rainfall interception and distribution patterns of gross precipitation around an isolated Ficus benjamina tree in an urban area. Journal of Hydrology, 333(2-4), 532-541.

Herbst, M., Roberts, J. M., Rosier, P. T. W., and Gowing, D. J. (2006) Measuring and modelling the rainfall interception loss by hedgerows in southern England. Agricultural and Forest Meteorology, **141**(2–4), 244–256.

Hernandez-Suarez, J. S., Nejadhashemi, A. P., Kropp, I. M., Abouali, M., Zhang, Z., & Deb, K. (2018). Evaluation of the impacts of hydrologic model calibration methods on predictability of ecologically-relevant hydrologic indices. Journal of hydrology, 564, 758-772.

Houborg, R., & McCabe, M. (2018). Daily Retrieval of NDVI and LAI at 3 m Resolution via the Fusion of CubeSat,

Landsat, and MODIS Data. Remote Sensing, 10(6), 890.

Huang, J. Y., Black, T. A., Jassal, R. S., and Lavkulich, L. M. L. (2017) Modelling rainfall interception by urban trees. Canadian Water Resources Journal, **42**(4), 336–348. [online] http://doi.org/10.1080/07011784.2017.1375865.

Inkiläinen, E. N., McHale, M. R., Blank, G. B., James, A. L., & Nikinmaa, E. (2013). The role of the residential urban forest in regulating throughfall: A case study in Raleigh, North Carolina, USA. Landscape and urban planning, 119, 91-103.

Jang, J. H., Chang, T. H., and Chen, W. B. (2018) Effect of inlet modelling on surface drainage in coupled urban flood simulation. Journal of Hydrology, **562**, 168–180.

Jayawardena, A. W. (2013). Environmental and hydrological systems modelling. CRC Press.

Jia, H., Lu, Y., Shaw, L. Y., & Chen, Y. (2012). Planning of LID–BMPs for urban runoff control: The case of Beijing Olympic Village. Separation and Purification Technology, 84, 112-119.

Jin, M., & Zhang, D. L. (2002). Observed variations of leaf area index and its relationship with surface temperatures during warm seasons. Meteorology and Atmospheric Physics, 80(1-4), 117-129.

Jonkman, S. N., & Vrijling, J. K. (2008). Loss of life due to floods. Journal of Flood Risk Management, 1(1), 43-56.

Kavetski, D., & Clark, M. P. (2010). Ancient numerical daemons of conceptual hydrological modeling: 2. Impact of time stepping schemes on model analysis and prediction. Water Resources Research, 46(10).

Khader, O., & Montalto, F. A. (2009). Development and calibration of a high resolution SWMM model for simulating the effects of LID retrofits on the outflow hydrograph of a dense urban watershed. In Low Impact Development for Urban Ecosystem and Habitat Protection (pp. 1-9).

Kepner, W. G., Ramsey, M. M., Brown, E. S., Jarchow, M. E., Dickinson, K. J., & Mark, A. F. (2012). Hydrologic futures: using scenario analysis to evaluate impacts of forecasted land use change on hydrologic services.

Ecosphere, 3(7), 1-25.

Khader, O., & Montalto, F. A. (2009). Development and calibration of a high resolution SWMM model for simulating the effects of LID retrofits on the outflow hydrograph of a dense urban watershed. In Low Impact Development for Urban Ecosystem and Habitat Protection (pp. 1-9).

Kirnbauer, M. C., Baetz, B. W., & Kenney, W. A. (2013). Estimating the stormwater attenuation benefits derived from planting four monoculture species of deciduous trees on vacant and underutilized urban land parcels. Urban forestry & urban greening, 12(3), 401-407.

Kleidorfer, M., Möderl, M., Fach, S., and Rauch, W. (2009) Optimization of measurement campaigns for calibration of a conceptual sewer model. Water Science and Technology, **59**(8), 1523–1530.

Kong, F., Ban, Y., Yin, H., James, P., and Dronova, I. (2017) Modeling stormwater management at the city district level in response to changes in land use and low impact development. Environmental Modelling and Software, **95**, 132–142.

Krebs, G., Kokkonen, T., Valtanen, M., Setälä, H., and Koivusalo, H. (2014) Spatial resolution considerations for urban hydrological modelling. Journal of Hydrology, **512**, 482–497. [online] https://linkinghub.elsevier.com/retrieve/pii/S0022169414001875.

Kumar, D. (2015) Remote Sensing Based Vegetation Indices Analysis to Improve Water Resources Management in Urban Environment. Aquatic Procedia, **4**(Icwrcoe), 1374–1380. [online] http://dx.doi.org/10.1016/j.aqpro.2015.02.178.

Leandro, J., Schumann, A., and Pfister, A. (2016) A step towards considering the spatial heterogeneity of urban key features in urban hydrology flood modelling. Journal of Hydrology, **535**, 356–365.

Legendre, P., & Legendre, L. F. (2012). Numerical ecology (Vol. 24). Elsevier.

Leitão, J. P., Simões, N. E., Maksimović, Č., Ferreira, F., Prodanović, D., Matos, J. S., and Sá Marques, A. (2010)

Real-time forecasting urban drainage models: Full or simplified networks? Water Science and Technology, **62**(9), 2106–2114.

Lin, T. C., Hamburg, S. P., King, H. B., & Hsia, Y. J. (2000). Throughfall patterns in a subtropical rain forest of northeastern Taiwan. Journal of Environmental Quality, 29(4), 1186-1193.

Linhoss, A. C., & Siegert, C. M. (2016). A comparison of five forest interception models using global sensitivity and uncertainty analysis. Journal of Hydrology, 538, 109-116.

Livesley, S. J., Baudinette, B., and Glover, D. (2014) Rainfall interception and stem flow by eucalypt street trees - The impacts of canopy density and bark type. Urban Forestry and Urban Greening, **13**(1), 192–197. [online] http://dx.doi.org/10.1016/j.ufug.2013.09.001.

Machac, D., Reichert, P., Rieckermann, J., and Albert, C. (2016) Fast mechanism-based emulator of a slow urban hydrodynamic drainage simulator. Environmental Modelling & Software, **78**, 54–67. [online] https://linkinghub.elsevier.com/retrieve/pii/S1364815215301213.

Machac, D., Reichert, P., Rieckermann, J., Del Giudice, D., and Albert, C. (2018) Accelerating Bayesian inference in hydrological modeling with a mechanistic emulator. Environmental Modelling and Software, **109**, 66–79.

Magliano, P. N., Whitworth-Hulse, J. I., and Baldi, G. (2019) Interception, throughfall and stemflow partition in drylands: Global synthesis and meta-analysis. Journal of Hydrology, **568**(October 2018), 638–645.

Mannina, G. and Viviani, G. (2010) Receiving water quality assessment: Comparison between simplified and detailed integrated urban modelling approaches. Water Science and Technology, **62**(10), 2301–2312.

McPherson, E. G. (1998) Structure and sustainability of Sacramento's urban forest. Journal of Arboriculture, **24**(4), 174–189.

McPherson, E. G., van Doorn, N., and de Goede, J. (2016) Structure, function and value of street trees in

California, USA. Urban Forestry and Urban Greening, **17**, 104–115. [online] http://dx.doi.org/10.1016/j.ufug.2016.03.013.

Mejía, A. I., & Moglen, G. E. (2010). Spatial distribution of imperviousness and the space‐time variability of rainfall, runoff generation, and routing. Water Resources Research, 46(7).

Merz, R., Parajka, J., and Blöschl, G. (2009) Scale effects in conceptual hydrological modeling. Water Resources Research, **45**(9).

Mitchell, V. G., McMahon, T. A., and Mein, R. G. (2003) Components of the Total Water Balance of an Urban Catchment. Environmental Management, **32**(6), 735–746.

Mullaney, J., Lucke, T., and Trueman, S. J. (2015) A review of benefits and challenges in growing street trees in paved urban environments. Landscape and Urban Planning, **134**, 157–166. [online] http://dx.doi.org/10.1016/j.landurbplan.2014.10.013.

Muzylo, A., Llorens, P., Valente, F., Keizer, J. J., Domingo, F., and Gash, J. H. C. (2009) A review of rainfall interception modelling. Journal of Hydrology, **370**(1–4), 191–206. [online] http://dx.doi.org/10.1016/j.jhydrol.2009.02.058.

Nassauer, J. I., Wang, Z., and Dayrell, E. (2009) What will the neighbors think? Cultural norms and ecological design. Landscape and Urban Planning, **92**(3–4), 282–292.

Noh, S. J., Lee, J.-H., Lee, S., Kawaike, K., and Seo, D.-J. (2018) Hyper-resolution 1D-2D urban flood modelling using LiDAR data and hybrid parallelization. Environmental Modelling & Software, **103**, 131–145. [online] https://linkinghub.elsevier.com/retrieve/pii/S1364815217308198.

Nourani, V., Fard, A. F., Niazi, F., Gupta, H. V., Goodrich, D. C., and Kamran, K. V. (2015) Implication of remotely sensed data to incorporate land cover effect into a linear reservoir-based rainfall-runoff model. Journal of Hydrology, **529**(P1), 94–105. [online] http://dx.doi.org/10.1016/j.jhydrol.2015.07.020.

Nowak, D. J., Hirabayashi, S., Doyle, M., McGovern, M., and Pasher, J. (2018) Air pollution removal by urban forests in Canada and its effect on air quality and human health. Urban Forestry and Urban Greening, **29**(November 2017), 40–48. [online] http://dx.doi.org/10.1016/j.ufug.2017.10.019.

Ozdemir, I., & Donoghue, D. N. (2013). Modelling tree size diversity from airborne laser scanning using canopy height models with image texture measures. Forest Ecology and Management, 295, 28-37.

Park, S. Y., Lee, K. W., Park, I. H., and Ha, S. R. (2008) Effect of the aggregation level of surface runoff fields and sewer network for a SWMM simulation. Desalination, **226**(1–3), 328–337. [online] https://linkinghub.elsevier.com/retrieve/pii/S0011916408001653.

Paul, M. J., & Meyer, J. L. (2001). Streams in the urban landscape. Annual review of Ecology and Systematics, 32(1), 333-365.

Petrucci, G. and Bonhomme, C. (2014) The dilemma of spatial representation for urban hydrology semi-distributed modelling: Trade-offs among complexity, calibration and geographical data. Journal of Hydrology, **517**, 997–1007.

Pope, G., & Treitz, P. (2013). Leaf area index (LAI) estimation in boreal mixedwood forest of Ontario, Canada using light detection and ranging (LiDAR) and WorldView-2 imagery. Remote sensing, 5(10), 5040-5063.

Praskievicz, S., & Chang, H. (2009). A review of hydrological modelling of basin-scale climate change and urban development impacts. Progress in Physical Geography, 33(5), 650-671.

Pypker, T. G., Bond, B. J., Link, T. E., Marks, D., and Unsworth, M. H. (2005) The importance of canopy structure in controlling the interception loss of rainfall: Examples from a young and an old-growth Douglas-fir forest. Agricultural and Forest Meteorology, **130**(1–2), 113–129.

Qiao, K., Zhu, W., Xie, Z., & Li, P. (2019). Estimating the seasonal dynamics of the leaf area index using piecewise LAI-VI relationships based on phenophases. Remote Sensing, 11(6), 689.

Querin, C. A. S., Beneditti, C. A., Machado, N. G., da Silva, M. J. G., da Silva Querino, J. K. A., dos Santos Neto, L. A., & Biudes, M. S. (2016). Spatiotemporal NDVI, LAI, albedo, and surface temperature dynamics in the southwest of the Brazilian Amazon forest. Journal of Applied Remote Sensing, 10(2), 026007.

Refsgaard, J. C., Van der Sluijs, J. P., Brown, J., & Van der Keur, P. (2006). A framework for dealing with uncertainty due to model structure error. Advances in water resources, 29(11), 1586-1597.

Refsgaard, J. C., van der Sluijs, J. P., Højberg, A. L., & Vanrolleghem, P. A. (2007). Uncertainty in the environmental modelling process–a framework and guidance. Environmental modelling & software, 22(11), 1543-1556.

Rian, S., Xue, Y., MacDonald, G. M., Touré, M. B., Yu, Y., De Sales, F., ... & Taylor, C. E. (2009). Analysis of climate and vegetation characteristics along the savanna-desert ecotone in mali using modis data. GIScience & Remote Sensing, 46(4), 424-450.

Rodriguez, F., Andrieu, H., and Morena, F. (2008) A distributed hydrological model for urbanized areas – Model development and application to case studies. Journal of Hydrology, **351**(3–4), 268–287. [online] https://linkinghub.elsevier.com/retrieve/pii/S0022169407007299.

Rossman, L. A. (2010). Storm water management model user's manual, version 5.0 (p. 276). Cincinnati: National Risk Management Research Laboratory, Office of Research and Development, US Environmental Protection Agency.

Rutter, A. J., Kershaw, K. A., Robins, P. C., & Morton, A. J. (1971). A predictive model of rainfall interception in forests, 1. Derivation of the model from observations in a plantation of Corsican pine. Agricultural Meteorology, 9, 367-384.

Rutter, A. J., & Morton, A. J. (1977). A predictive model of rainfall interception in forests. III. Sensitivity of the model to stand parameters and meteorological variables. Journal of Applied Ecology, 567-588.

Saito, K., Ogawa, S., Aihara, M., & Otowa, K. (2001, November). Estimates of LAI for forest management in Okutama. In Proceedings of the 22nd Asian Conference on Remote Sensing, Singapore (pp. 5-9).

Saltelli, A. (2004, March). Global sensitivity analysis: an introduction. In Proc. 4th International Conference on Sensitivity Analysis of Model Output (SAMO'04) (pp. 27-43).

Salvadore, E., Bronders, J., and Batelaan, O. (2015) Hydrological modelling of urbanized catchments: A review and future directions. Journal of Hydrology, **529**(P1), 62–81. [online] http://dx.doi.org/10.1016/j.jhydrol.2015.06.028.

Sándor, R., & Fodor, N. (2012). Simulation of soil temperature dynamics with models using different concepts. The Scientific World Journal, 2012.

Sanzana, P., Gironás, J., Braud, I., Branger, F., Rodriguez, F., Vargas, X., Hitschfeld, N., Muñoz, J. F., Vicuña, S., Mejía, A., and Jankowfsky, S. (2017) A GIS-based urban and peri-urban landscape representation toolbox for hydrological distributed modeling. Environmental Modelling and Software, **91**, 168–185.

Schmitt, T. G., Thomas, M., & Ettrich, N. (2004). Analysis and modeling of flooding in urban drainage systems. Journal of hydrology, 299(3-4), 300-311.

Schooling, J. T. and Carlyle-Moses, D. E. (2015) The influence of rainfall depth class and deciduous tree traits on stemflow production in an urban park. Urban Ecosystems, **18**(4), 1261–1284.

Schubert, J. E., Sanders, B. F., Smith, M. J., and Wright, N. G. (2008) Unstructured mesh generation and landcover-based resistance for hydrodynamic modeling of urban flooding. Advances in Water Resources, **31**(12), 1603–1621. [online] https://linkinghub.elsevier.com/retrieve/pii/S0309170808001279.

Singh, V. P. (1997). Effect of spatial and temporal variability in rainfall and watershed characteristics on stream flow hydrograph. Hydrological processes, 11(12), 1649-1669.

Sjöman, H. and Busse Nielsen, A. (2010) Selecting trees for urban paved sites in Scandinavia - A review of

information on stress tolerance and its relation to the requirements of tree planners. Urban Forestry and Urban Greening, **9**(4), 281–293.

Stone Jr, B. (2004). Paving over paradise: how land use regulations promote residential imperviousness. Landscape and urban planning, 69(1), 101-113.

Sobol, I. M. (1993). Sensitivity estimates for nonlinear mathematical models. Mathematical modelling and computational experiments, 1(4), 407-414.

Song, X. P., Tan, P. Y., Edwards, P., and Richards, D. (2018) The economic benefits and costs of trees in urban forest stewardship: A systematic review. Urban Forestry and Urban Greening, **29**(November 2017), 162–170.

Sousa, R., Dias, S., and Antunes, C. (2007) Quantifying the Asian turtle crisis: market survey in Sothern China. Annales Zoologici Fennici, **44**(August), 303–313.

Sriwongsitanon, N., Surakit, K., and Thianpopirug, S. (2011) Influence of atmospheric correction and number of sampling points on the accuracy of water clarity assessment using remote sensing application. Journal of Hydrology, **401**(3–4), 203–220. [online] http://dx.doi.org/10.1016/j.jhydrol.2011.02.023.

Stenberg, P., Rautiainen, M., Manninen, T., Voipio, P., & Smolander, H. (2004). Reduced simple ratio better than NDVI for estimating LAI in Finnish pine and spruce stands.

Stovin, V. (2010) The potential of green roofs to manage urban stormwater. Water and Environment Journal, **24**(3), 192–199.

Sun, G., Noormets, A., Chen, J., & McNulty, S. G. (2008). Evapotranspiration estimates from eddy covariance towers and hydrologic modeling in managed forests in Northern Wisconsin, USA. Agricultural and forest Meteorology, 148(2), 257-267.

Sun, N., Hall, M., Hong, B., and Zhang, L. (2012) Impact of SWMM Catchment Discretization: Case Study in

Syracuse, New York. Journal of Hydrologic Engineering, **19**(1), 223–234. [online] http://ascelibrary.org/doi/10.1061/%28ASCE%29HE.1943-5584.0000777.

Sun, N., Hong, B., and Hall, M. (2014) Assessment of the SWMM model uncertainties within the generalized likelihood uncertainty estimation (GLUE) framework for a high-resolution urban sewershed. Hydrological Processes, **28**(6), 3018–3034.

Toward high-resolution flash flood prediction in large urban.pdf

Udelhoven, T., Stellmes, M., del Barrio, G., and Hill, J. (2009) Assessment of rainfall and NDVI anomalies in Spain (1989-1999) using distributed lag models. International Journal of Remote Sensing, **30**(8), 1961–1976.

Vermuyten, E., Meert, P., Wolfs, V., and Willems, P. (2018) Model uncertainty reduction for real-time flood control by means of a flexible data assimilation approach and reduced conceptual models. Journal of Hydrology, **564**, 490–500.

Walsh, T. C., Pomeroy, C. A., & Burian, S. J. (2014). Hydrologic modeling analysis of a passive, residential rainwater harvesting program in an urbanized, semi-arid watershed. Journal of Hydrology, 508, 240-253.

Wang, B., Zhang, M., Wei, J., Wang, S., Li, S., Ma, Q., ... & Pan, S. (2013). Changes in extreme events of temperature and precipitation over Xinjiang, northwest China, during 1960–2009. Quaternary International, 298, 141-151.

Wang, J., Endreny, T. A., and Nowak, D. J. (2008) Mechanistic simulation of tree effects in an urban water balance model. Journal of the American Water Resources Association, **44**(1), 75–85.

Wang, Q., Adiku, S., Tenhunen, J., & Granier, A. (2005). On the relationship of NDVI with leaf area index in a deciduous forest site. Remote sensing of environment, 94(2), 244-255.

Wang, Y., Chen, A. S., Fu, G., Djordjević, S., Zhang, C., and Savić, D. A. (2018) An integrated framework for high-

resolution urban flood modelling considering multiple information sources and urban features. Environmental Modelling & Software, **107**, 85–95. [online] https://linkinghub.elsevier.com/retrieve/pii/S1364815217307983.

Warsta, L., Niemi, T. J., Taka, M., Krebs, G., Haahti, K., Koivusalo, H., and Kokkonen, T. (2017) Development and application of an automated subcatchment generator for SWMM using open data. Urban Water Journal, **14**(9), 954–963. [online] https://www.tandfonline.com/doi/full/10.1080/1573062X.2017.1325496.

Wildemeersch, S., Goderniaux, P., Orban, P., Brouyère, S., and Dassargues, A. (2014) Assessing the effects of spatial discretization on large-scale flow model performance and prediction uncertainty. Journal of Hydrology, **510**, 10–25.

Xavier, A. C., & Vettorazzi, C. A. (2004). Monitoring leaf area index at watershed level through NDVI from Landsat-7/ETM+ data. Scientia Agricola, 61(3), 243-252.

Xiao, Q., & McPherson, E. G. (2002). Rainfall interception by Santa Monica's municipal urban forest. Urban ecosystems, 6(4), 291-302.

Xiao, Q., McPherson, E. G., Ustin, S. L., Grismer, M. E., and Simpson, J. R. (2000) Winter rainfall interception by two mature open-grown trees in Davis, California. Hydrological Processes, **14**(4), 763–784.

Xiao, Q., & McPherson, E. G. (2011). Rainfall interception of three trees in Oakland, California. Urban Ecosystems, 14(4), 755-769.

Yao, L., Chen, L., and Wei, W. (2016) Assessing the effectiveness of imperviousness on stormwater runoff in micro urban catchments by model simulation. Hydrological Processes, **30**(12), 1836–1848. [online] http://doi.wiley.com/10.1002/hyp.10758.

Yao, L., Wei, W., and Chen, L. (2016) How does imperviousness impact the urban rainfall-runoff process under various storm cases? Ecological Indicators, **60**, 893–905.

Yu, D., & Coulthard, T. J. (2015). Evaluating the importance of catchment hydrological parameters for urban surface water flood modelling using a simple hydro-inundation model. Journal of Hydrology, 524, 385-400.

Zaghloul, N. A. (1981). SWMM model and level of discretization. Journal of the Hydraulics Division, 107(11), 1535-1545.

Zabret, K. and Šraj, M. (2015) Can urban trees reduce the impact of climate change on storm runoff? Urbani Izziv, **26**(2014), S165–S178.

Zhao, N., Yang, Y., & Zhou, X. (2010). Application of geographically weighted regression in estimating the effect of climate and site conditions on vegetation distribution in Haihe Catchment, China. Plant Ecology, 209(2), 349-359.

Zheng, Z., Ren, J., Li, Y., Huang, C., Liu, G., Du, C., and Lyu, H. (2016) Remote sensing of diffuse attenuation coefficient patterns from Landsat 8 OLI imagery of turbid inland waters: A case study of Dongting Lake. Science of the Total Environment, **573**, 39–54. [online] http://dx.doi.org/10.1016/j.scitotenv.2016.08.019.

Zoppou, C. (2001). Review of urban storm water models. Environmental Modelling & Software, 16(3), 195-231.